THE DISSOLUTION EFFECTS OF CARBONATED WATER ON OIL RESERVOIR CARBONATES - A STUDY UNDER HIGH PRESSURE CARBON DIOXIDE FLOOD CONDITIONS

GRAHAM DONALD ROSS

THESIS SUBMITTED FOR THE DEGREE OF DOCTOR OF PHILOSOPHY AT

THE DEPARTMENT OF PETROLEUM ENGINEERING

HERIOT-WATT UNIVERSITY

EDINBURGH

JUNE 1982

PAGE
NUMBERS
CUT OFF
IN
ORIGINAL

THIS MANUSCRIPT IS DEDICATED TO MY PARENTS,

MR. AND MRS. DONALD H. ROSS

TABLE OF CONTENTS

		PAGE
TABLE OF CONTENTS		iii
LIST OF TABLES		v
LIST OF FIGURES		vi
LIST OF PLATES		viii
ACKNOWLEDGEMENTS		xi
ABSTRACT		xiii
NOMENCLATURE		xv
CHAPTER		
I	INTRODUCTION	
	1.1 General Introduction	1
	1.2 Carbonate Dissolution in Reservoir Rock	5
	1.3 Introductory Literature	9
	1.3.1 Laboratory Studies	10
	1.3.2 Field Evidence	11
	1.4 Study Outline	13
II	EXPERIMENTAL FLOW APPARATUS AND OPERATING PROCEDURES	
	2.1 Introduction	15
	2.2 Permeability Determination	15
	2.3 Description of Core Flooding Apparatus	16
	2.3.1 Core Holder	23
	2.3.2 Transfer Barrier	26
	2.3.3 Intensified Carbon Dioxide Supply	27
	2.3.4 Transfer Barrier Rocking Mechanism	28
	2.3.5 Displacement System	28
	2.3.6 Pressure Measurement System	31
	2.3.7 Temperature Control System	32
	2.3.8 Effluent Collection and Measurement System	33
	2.4 Experimental Procedure	34
III	EXPERIMENTAL MATERIALS AND TECHNIQUES OF ANALYSIS	
	3.1 Introduction	35
	3.2 Sandstone Core Material	35
	3.3 Core Preparation	37
	3.4 Sandstone Analysis	38
	3.5 Core Fluids	41
	3.6 Liquid Analysis	41
	3.7 Crude Oil Saturation Apparatus	42

			PAGE
IV	RESULTS AND DISCUSSION OF RESULTS		
	4.1	Introduction	46
	4.2	Yorkshire Jurassic Sandstone	46
	4.3	Fife Carboniferous (A)	64
	4.4	Fife Carboniferous (B)	69
	4.5	Rotliegende Sandstone from Southern North Sea	71
	4.6	Jurassic Sandstone from Northern North Sea	73
	4.7	Rotliegende Sandstone from Indefatigable Field	73
	4.8	Oxfordshire Jurassic Limestone	90
	4.9	Summary of Results	94
V	THEORETICAL CONSIDERATIONS		
	5.1	Introduction	96
	5.2	Schechter-Gidley Model	97
	5.3	Lund-Fogler-McCune Model	99
	5.4	Discussion of the Two Models and Their Applicability to Carbonate Dissolution in Carbonated Water	104
	5.5	Dissolution Rate Data Requirements	107
VI	CONCLUSIONS AND RECOMMENDATIONS		
	6.1	Conclusions	111
	6.2	Recommendations	112
APPENDICES			
1	CARBONATED WATER CORE FLOODING PROCEDURE		114
2	PETROGRAPHIC DESCRIPTIONS AND PHOTOMICROGRAPHS OF ROCKS USED IN CORE TESTS		123
3	STAINING PROCEDURE FOR CARBONATE MINERAL IDENTIFICATION		134
4	DETERMINATION PROCEDURES FOR CALCIUM AND MAGNESIUM ION CONCENTRATIONS BY E.D.T.A. TITRATION		135
5	CORE FLOOD FLOW RATES		138
LIST OF REFERENCES			142

LIST OF TABLES

Table		PAGE
I-1	Effect of CO_2 on pH of Water at 25°C	5
II-1	Transfer Barrier Specifications	27
III-1	Summarised Descriptions of Core Materials	36
A3-1	Carbonate Mineral Stain Colours	134
A5-1	Flow Rates Used in Tests on Yorks Jurassic Sandstone	138
A5-2	Flow Rates Used in Tests on Fife Carboniferous Sandstone (A)	139
A5-3	Flow Rates Used in Tests on Indefatigable Field Sandstone	140
A5-4	Flow Rates Used in Test on Oxfords Jurassic Limestone	141

LIST OF FIGURES

Figure		PAGE
I-1	Schematic Representation of CO_2-Water Slug Process Being Applied to an Oil Reservoir	2
I-2	Solubility of CO_2 in Water as a Function of Temperature and Pressure	7
I-3	Correction Factor for Solubility of CO_2 in Brine	7
I-4	Solubility of Calcite in Fully Carbonated Water as a Function of Temperature and Pressure	8
II-1	Viscosity of Fully Carbonated Water as a Function of Temperature and Pressure	17
II-2	Simplified Schematic Diagram of Carbonated Water Permeameter	20
II-3	Schematic Diagram of Core Holder	24
II-4	Schematic Diagram of Gas Booster	29
III-1	Schematic Diagram of Crude Oil Saturation Apparatus	44
IV-1	Permeability Profile and Effluent Composition for Yorks Jurassic Sandstone (20% Calcite Sandstone; Distilled Water, 1000 psi, 20°C)	47
IV-2	Permeability Profile and Effluent Composition for Yorks Jurassic Sandstone (20% Calcite Sandstone; Brine, 1000 psi, 20°C)	48
IV-3	Permeability Profile and Effluent Composition for Yorks Jurassic Sandstone (20% Calcite Sandstone; 1000 psi Carbonation, 20°C)	50
IV-4	Permeability Profile and Effluent Composition for Yorks Jurassic Sandstone (20% Calcite Sandstone; 1000 psi Carbonation, 80°C)	54
IV-5	Axial Permeability Variations for Flooded Yorks Jurassic Sandstone Cores	56
IV-6	Pore Size Distributions for Yorks Jurassic Sandstone	58
IV-7	Permeability Profile and Effluent Composition for Yorks Jurassic Sandstone (20% Calcite Sandstone; 3000 psi Carbonation, 80°C)	60

		PAGE
IV-8	Permeability Profile and Effluent Composition for Yorks Jurassic Sandstone (20% Calcite Sandstone Containing Oil; 3000 psi Carbonation, 80°C)	61
IV-9	Permeability Profiles for Fife Carboniferous Sandstone (10% Dolomite Sandstone)	66
IV-10	Axial Permeability Variation for Flooded Fife Carboniferous Sandstone Core	67
IV-11	Pore Size Distributions for Fife Carboniferous Sandstone	68
IV-12	Permeability Profile and Effluent Composition for Indefatigable Sandstone (5% Dolomite Sandstone; 1000 psi Carbonation, 80°C)	75
IV-13	Axial Permeability Variation for Flooded Indefatigable Sandstone Core	77
IV-14	Permeability Profile and Effluent Composition for Indefatigable Sandstone (5% Dolomite Sandstone; 2000 psi Carbonation, 80°C)	79
IV-15	Permeability Profile and Effluent Composition for Indefatigable Sandstone (5% Dolomite Sandstone; 3000 psi Carbonation, 80°C)	83
IV-16	Pore Size Distributions for Indefatigable Sandstone	84
IV-17	Permeability Profile and Effluent Composition for Indefatigable Sandstone (5% Dolomite Sandstone; 2000 psi Carbonation, 80°C)	86
IV-18	Permeability Profile and Effluent Composition for Indefatigable Sandstone (5% Dolomite Sandstone Containing Gas Condensate; 2000 psi Carbonation, 80°C)	87
IV-19	Permeability Profile and Effluent Composition for Indefatigable Sandstone (5% Dolomite Sandstone Containing Crude Oil; 2000 psi Carbonation, 80°C)	88
IV-20	Permeability Profile and Effluent Composition for Oxfords Jurassic Limestone (90% Calcite Limestone; 1500 psi Carbonation, 80°C)	91
A1-1	Schematic Diagram of Carbonated Water Permeameter with Valves Numbered	115

LIST OF PLATES

Plate		PAGE
II-1	Front View of Carbonated Water Permeameter	18
II-2	Close-Up of Control Panel	18
II-3	Rear View of Permeameter	19
II-4	Close-Up of Core Holder and Differential Pressure Transducer	19
II-5	Core Holder with Heating Jacket	25
II-6	Disassembled Core Holder	25
II-7	Transfer Barrier Rocking Mechanism	30
II-8	Transfer Barrier Rocking Mechanism	30
III-1	Crude Oil Saturation Apparatus	43
IV-1	Photomicrograph; Crossed Nicols, X2 Magnification. Shows the Apparent Homogeneous Framework of Quartz and Calcite in Yorks Jurassic Sandstone	51
IV-2	Photomicrograph; Crossed Nicols, X2 Magnification. Shows the Dissolved Flow Channel Formed in Yorks Jurassic Sandstone During 1000 psi, 20°C Carbonated Water Flood	51
IV-3	Photomicrograph; Crossed Nicols, X4 Magnification. Close-Up of Flow Channel (Shown in Plate IV-2) Showing Almost Complete Dissolution of Calcite	52
IV-4	Cross-Sectional View of Yorks Jurassic Sandstone Cores Before and After 1000 psi, 80°C Carbonated Water Flood	52
IV-5	Core Segments from 3000 psi, 80°C Carbonated Water Floods on Clean and Oil Containing Yorks Jurassic Sandstone Cores	62
IV-6	Close-Up of Three Segments Shown in Plate IV-5 from 3000 psi, 80°C Carbonated Water Flood on Clean Yorks Jurassic Sandstone Core	62
IV-7	Close-Up of Flow Channel in Core Segment Five from 3000 psi, 80°C Carbonated Water Flood on Clean Yorks Jurassic Sandstone Core	63

Plate		Page
IV-8	Photomicrograph; Crossed Nicols, X2.5 Magnification. Supplementary Flow Channels Formed During 3000 psi, 80°C Carbonated Water Flood on Clean Yorks Jurassic Sandstone Core	63
IV-9	Photomicrograph; Crossed Nicols, X4 Magnification. Fife Carboniferous Sandstone (B)	70
IV-10	Photomicrograph; Crossed Nicols, X4 Magnification. Fife Carboniferous Sandstone (B) After 3500 psi, 80°C Carbonated Water Flood	70
IV-11	Collapsed Rotliegende Sandstone Core with Mudcake on Outlet End Plate of Core Holder	72
IV-12	Photomicrograph; Crossed Nicols, X2.5 Magnification. Indefatigable Sandstone Prior to 1000 psi, 80°C Carbonated Water Flood	76
IV-13	Photomicrograph; Crossed Nicols, X3 Magnification. Indefatigable Sandstone After 1000 psi, 80°C Carbonated Water Flood	76
IV-14	Close-Up of Inlet Core Face Prior to 2000 psi, 80°C Carbonated Water Flood on Interlayered Indefatigable Sandstone	80
IV-15	Inlet Core Face After 2000 psi, 80°C Carbonated Water Flood on Interlayered Indefatigable Sandstone	80
IV-16	Photomicrograph; Crossed Nicols, X4 Magnification. Interlayered Indefatigable Sandstone Prior to 2000 psi, 80°C Carbonated Water Flood	81
IV-17	Photomicrograph; Crossed Nicols, X4 Magnification. Interlayered Indefatigable Sandstone After 2000 psi, 80°C Carbonated Water Flood	81
IV-18	Photomicrograph; Crossed Nicols, X4 Magnification. Cleaned Sandstone from Gas Condensate Zone of Indefatigable Field	89
IV-19	Photomicrograph; Crossed Nicols, X4 Magnification. Cleaned Sandstone from Gas Condensate Zone of Indefatigable Field After 2000 psi, 80°C Carbonated Water Flood	89
IV-20	Unflooded and Flooded Oxfords Jurassic Limestone Cores	92

Plate		Page
IV-21	Close-Up View of Large Wormhole Formed in Oxfords Jurassic Limestone During 1500 psi, 80°C Carbonated Water Flood	93
IV-22	Photomicrograph; Crossed Nicols, X10 Magnification. Well Defined Small Wormhole Formed in Oxfords Jurassic Limestone During 1500 psi, 80°C Carbonated Water Flood	93
A2-1	Photomicrograph; Crossed Nicols, X4 Magnification. Yorks Jurassic Sandstone	124
A2-2	Photomicrograph; Plain Light, X10 Magnification. Yorks Jurassic Sandstone Stained for Calcite Using Alizarin Red S	124
A2-3	S.E.M. View of Yorks Jurassic Sandstone Showing Detrital Quartz Grains with Micritic Pore Fill	125
A2-4	S.E.M. View of Yorks Jurassic Sandstone Showing Micritic Calcite Cement Coating a Quartz Grain	125
A2-5	Photomicrograph; Crossed Nicols, X4 Magnification. Fife Carboniferous Sandstone (A)	127
A2-6	Photomicrograph; Plain Light, X2 Magnification. Fife Carboniferous Sandstone (A) Stained for Dolomite Using Potassium Ferricyanide	127
A2-7	Photomicrograph; Crossed Nicols, X3 Magnification. Rotliegende Sandstone from Southern North Sea	129
A2-8	Photomicrograph; Crossed Nicols, X4 Magnification. Jurassic Sandstone from Northern North Sea	130
A2-9	Photomicrograph; Crossed Nicols, X4 Magnification. Indefatigable Field Sandstone	132
A2-10	Photomicrograph; Crossed Nicols, X2 Magnification. Oxfords Jurassic Limestone	133

ACKNOWLEDGEMENTS

The author takes this opportunity to express his gratitude to the many connected with the production of this thesis.

In particular, I wish to thank Dr. Adrian Todd, the principal project supervisor, for his advice and encouragement, and Charlie McLeod for his enthusiastic and helpful cooperation at all times, but especially for his part in the design and commissioning of the experimental apparatus.

In addition, I would like to thank Andrew Tweedie for his many helpful suggestions, and acknowledge the interest of Professors Jim Brown and George Stewart in my work.

Sincere thanks are extended to all the Technical Staff of the Petroleum Engineering Department for the contributions and friendship:-

Special mention must be given to the workshop team of Alan Brown, George Pratt, Keith Roden, Jonathan Haston and Charles McLeod Jr. for their superb workmanship and unfailing support.

For his advice and often long worked hours carrying out chemical and pore size distribution analyses, Alistair Reid is thanked.

Grateful acknowledgement is made to Clifford Ogle for the photographic work contained herein, but also for his care and assistance with the rock characterisation studies.

Thanks also go to Elaine Blackie, Angela Buchan and Karen McLeod for their valuable assistance with routine experimental work and the preparation of the thesis for typing.

I also thank Ian Simm for performing the many chemical analyses during the final few months of experiments.

I wish to thank the U.K. Department of Energy for generously sponsoring this investigation and the Science Research Council for providing the grant for my post-graduate study.

Finally, thanks are extended to Ken Atkinson for binding the theses copies and to Sheila Mitchell and Carol McDougall for their careful typing.

ABSTRACT

Both formation damage and stimulation effects have been experienced during carbon dioxide field and laboratory tests in the USA. While the stimulation effects have been attributed to dissolution of the reservoir rocks by carbon dioxide enriched flood water (carbonated water), no work has been done to identify and quantify this phenomenon. Nor has any established theory for the formation damage been identified, although it seems likely that in some instances formation damage may be caused by formation fines, released by dissolution and subsequently migrating into pore throats.

The present study was undertaken to investigate the dissolution effect of carbonated water on formation carbonate minerals under CO_2 flood conditions. The design and operation of experimental equipment for flowing CO_2-water solutions through linear rock cores are described, together with the analytical methods used to assess changes in core characteristics.

A series of flow tests were conducted on a variety of sandstones covering a range of permeabilities and carbonate contents. Carbonated water was injected through the cores at constant rate, and the permeability as a function of time together with a chemical analysis of the core effluent monitored to measure the dissolution effect. For the most part, the results indicate that the removal of carbonate mineral gives rise to a dramatic permeability increase, which travels as a front through the linear core. The magnitude of permeability increase and the rate of frontal advance were found to be controlled largely by rock mineralogy and inhomogeneities present.

Allied to the obtained experimental results, predictive mathematical modelling of carbonate dissolution in carbonated floodwater is discussed but concluded difficult for the majority of rock types, owing to the problem of describing inhomogeneous or preferential dissolution effects.

NOMENCLATURE

A	Cross-sectional area of a pore
Ac	Acid capacity number, dimensionless
C	Acid concentration
C_D	Dimensionless acid concentration
C_M	Lumped concentration of all minerals other than quartz in sandstone
C_{MD}	Dimensionless dissolvable mineral concentration
C_{MO}	Initial dissolvable mineral concentration
C_{MI}	Irreducible dissolvable mineral concentration
C_o	Initial acid concentration
Da	Damkohler number, dimensionless
K	Permeability
K_a	Average permeability
K_o	Initial permeability
k_r	Reaction rate constant
L	Core length
l	Mean pore length
N	Number of pores
Q	Flow rate
R_s	Heterogeneous reaction rate of acid with rock
r_a	Reaction rate of lumped dissolvable minerals
t	Time
t_D	Dimensionless time
V	Superficial velocity in core
x	Distance in axial direction
x_D	Dimensionless distance

β	Characteristic constant in permeability - porosity relationship
η	Pore size distribution function
μ	Viscosity
$\Delta \phi$	Porosity change
$\Delta \phi_{max}$	Maximum porosity change
ϕ	Porosity
ϕ_o	Initial porosity
u	Pore growth function
W	Average lumped stoichiometric coefficient

CHAPTER I

INTRODUCTION

1.1 General Introduction

1.2 Carbonate Dissolution in Reservoir Rock

1.3 Introductory Literature

1.3.1 Laboratory Studies

1.3.2 Field Evidence

1.4 Study Outline

1.1 General Introduction

In the past decade carbon dioxide flooding has become recognised as an important enhanced oil recovery technique. Carbon dioxide (CO_2) has several favourable characteristics which enable it to recover oil unrecoverable by conventional methods. Of these perhaps the most important is its ability to extract hydrocarbons from reservoir oils and attain miscibility. In addition, however, it is also highly soluble in crude oil causing large reductions in oil viscosity and appreciable swelling at high pressure.

A principal problem in CO_2 flooding, is the low viscosity of CO_2 compared to that of crude oil. At reservoir conditions CO_2 viscosity is in the order of one tenth that of most low viscosity crude oils (1). At these unfavourable viscosity ratios, CO_2 tends to finger its way through the oil and even ahead of it, thereby reducing volumetric contact of the reservoir. Heterogeneities in the formation accentuate this fingering process. To the extent that fingering occurs, recovery efficiency is reduced, and an economically profitable operation becomes difficult to achieve.

In an effort to reduce fingering, the technique of injecting water in conjunction with CO_2 has been developed (2, 3). The water interferes with the flow of carbon dioxide, causing the CO_2 to behave as if it has a higher viscosity. To date the most satisfactory results have been obtained by alternate injection of slugs of CO_2 and water (Figure I-1) (4).

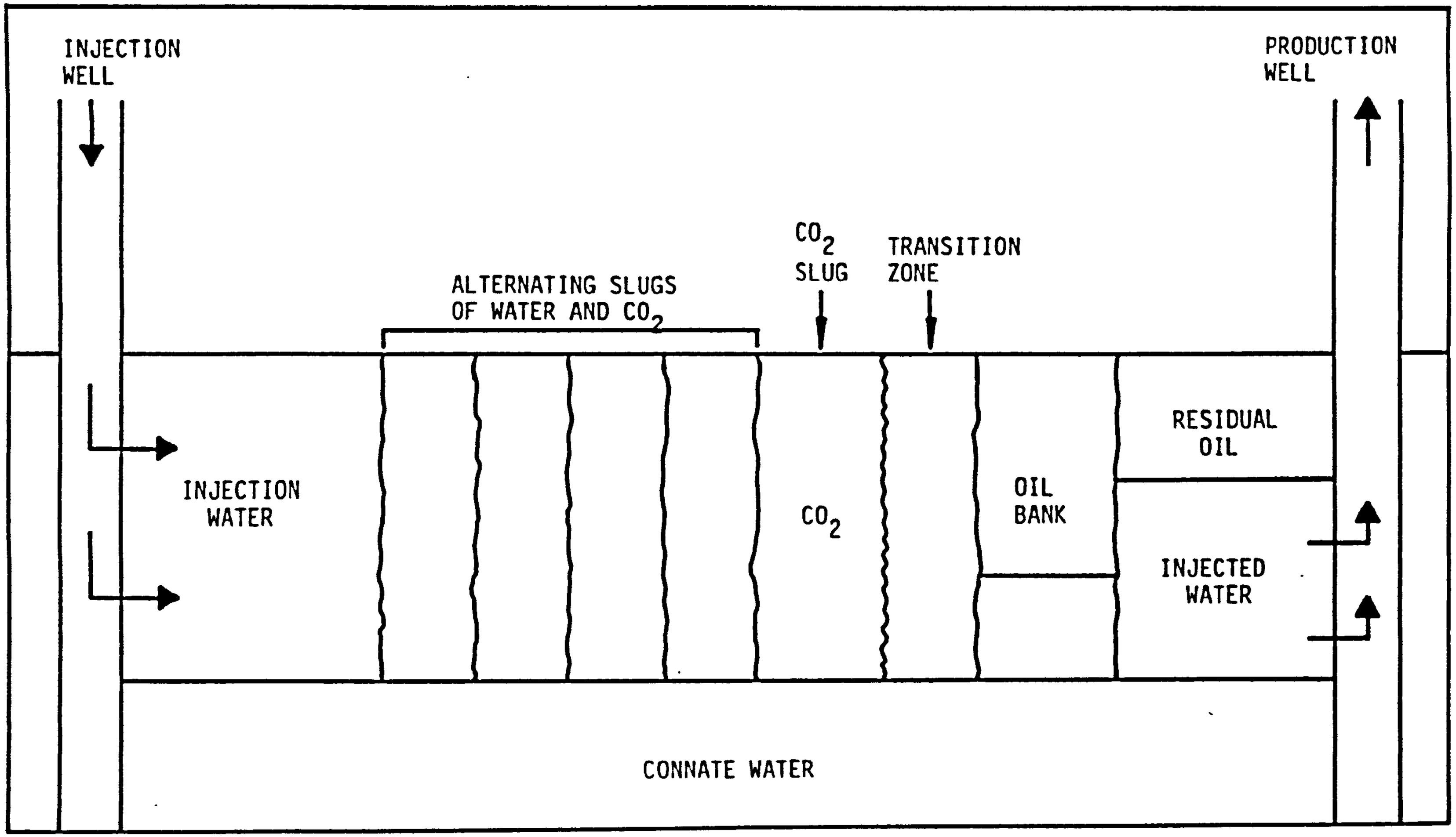

FIGURE I-1. SCHEMATIC REPRESENTATION OF CO_2 - WATER SLUG PROCESS BEING APPLIED TO AN OIL RESERVOIR

Although investigators do not agree completely, it seems that CO_2 slugs between 2% and 5% of the formation pore volume, followed by 0.5% to 3% pore volume slugs of water effect maximum recovery. After 15% to 30% of the pore volume of CO_2 has been injected, normal injection of water is used to drive the slugs through the reservoir. However, where carbon dioxide is expensive and scarce in supply, a CO_2 injection regime may be governed by cost and availability factors.

Besides the problems of viscous fingering, field experience (mostly since 1972 in the United States) has been sufficient to identify a number of other major problems with the carbon dioxide technique. One of the problems is that of reduced injectivity experienced in some reservoirs on injecting carbon dioxide. While many have reported this to be due to the deposition of high molecular weight materials upon mixing of crude and carbon dioxide (5, 6, 7), insitu plugging tests have not proved the occurrence of this type of precipitation (8). Observed reductions in injectivity can probably therefore be attributed to other mechanisms, one of which may be the disintegration of carbonate cements in the reservoir rock, and movement of particulate matter into the throats of interstitial pores.

Conversely, increases in injectivity have also been experienced in the course of carbon dioxide field tests (9). These were in turn attributed to dissolution of carbonate minerals in carbon dioxide enriched flood water (carbonated water), causing increased permeability.

A recent economic feasibility study (10) concludes that carbon dioxide flooding is the most promising enhanced oil recovery technique for many of the fields in the North Sea basin. However, little is known of the conditions required for miscibility, injectivity of carbon dioxide, and total availability of carbon dioxide. Considerable basic study and information is therefore essential if required expertise is to be gained.

In view of the lack of data and uncertainty in the published results relating to carbonate dissolution on carbon dioxide flooding, a research programme has been initiated to study the phenomenon. The objectives of the programme are to evaluate the dissolution effects of carbonated water on formation carbonates, and to determine how formation permeability characteristics are likely to be altered during a carbon dioxide flood. This thesis presents the first phase of the study, the development and operation of apparatus for flowing CO_2-water mixtures through linear rock cores, together with the results of experiments undertaken to establish the mechanism(s) of carbonate dissolution in porous media. It is intended that the experimental results be correlated with mathematical predictions in the next phase of the study.

To test the susceptibility of North Sea reservoir rocks to carbonate dissolution, core material from both the Southern and Northern North Sea areas were included in the study.

1.2 Carbonate Dissolution in Reservoir Rock

Many producing formations contain carbonates in some form. In the case of limestone and dolomite reservoirs, carbonates constitute the bulk of the formation rock. In sandstones, carbonates are commonly found as pore filling and replacement cements consolidating the sand grains, although varying, but usually minor amounts of detrital carbonate grains may also be present. Since the cementing material in sandstone is located between sand grains adjacent to flow channels, a relatively small change in the pore framework due to carbonate dissolution may significantly affect the total permeability.

Upon injection, carbon dioxide, mixing with either injection water or connate water, will form carbonic acid:

$$CO_2 + H_2O \rightleftharpoons H_2CO_3 \rightleftharpoons H^+ + HCO_3^-$$

One characteristic of carbonic acid is that at very low carbon dioxide partial pressure, the pH is reduced considerably (11), as shown in Table I-1. Thus, carbonated water will retain its acid nature with very little carbon dioxide in solution.

CO_2 Pressure (bars)	Solution pH
1	3.7
1.7	3.5
2.5	3.4
5.4	3.3
33.3	3.3

TABLE I-1. EFFECT OF CO_2 ON pH OF WATER AT 25°C

Published data (11, 12) on the solubility of carbon dioxide in water as a function of pressure, temperature and water salinity are presented in Figure I-2 and I-3. In general these results indicate that carbon dioxide solubility decreases with increasing temperature and salt concentration, but increases with increasing pressure, for temperatures to 100°C and pressures to 300 bars.

The carbonates most commonly found in reservoir rocks are those of calcium (calcite), combinations of calcium and magnesium (dolomite), and iron (siderite). These minerals have a low solubility in pure water at atmospheric conditions, but become increasingly soluble with increasing water carbonation (or CO_2 concentration) and pressure. The carbonate form is converted to that of the soluble bicarbonate, the following equation representing the chemical reaction for calcium carbonate:

$$H_2CO_3 + CaCO_3 \rightleftharpoons Ca(HCO_3)_2$$

Similar chemical reactions take place with the other carbonates.

The solubility trends of calcium carbonate in carbonated water as a function or pressure and temperature are presented in Figure I-4. Although no work has been carried out in the 0°C to 100°C temperature range at pressures above 100 bars, indications from other studies (13 - 18) are that calcite solubility:

(1) increases with increasing temperature at constant total pressure and CO_2 concentration,

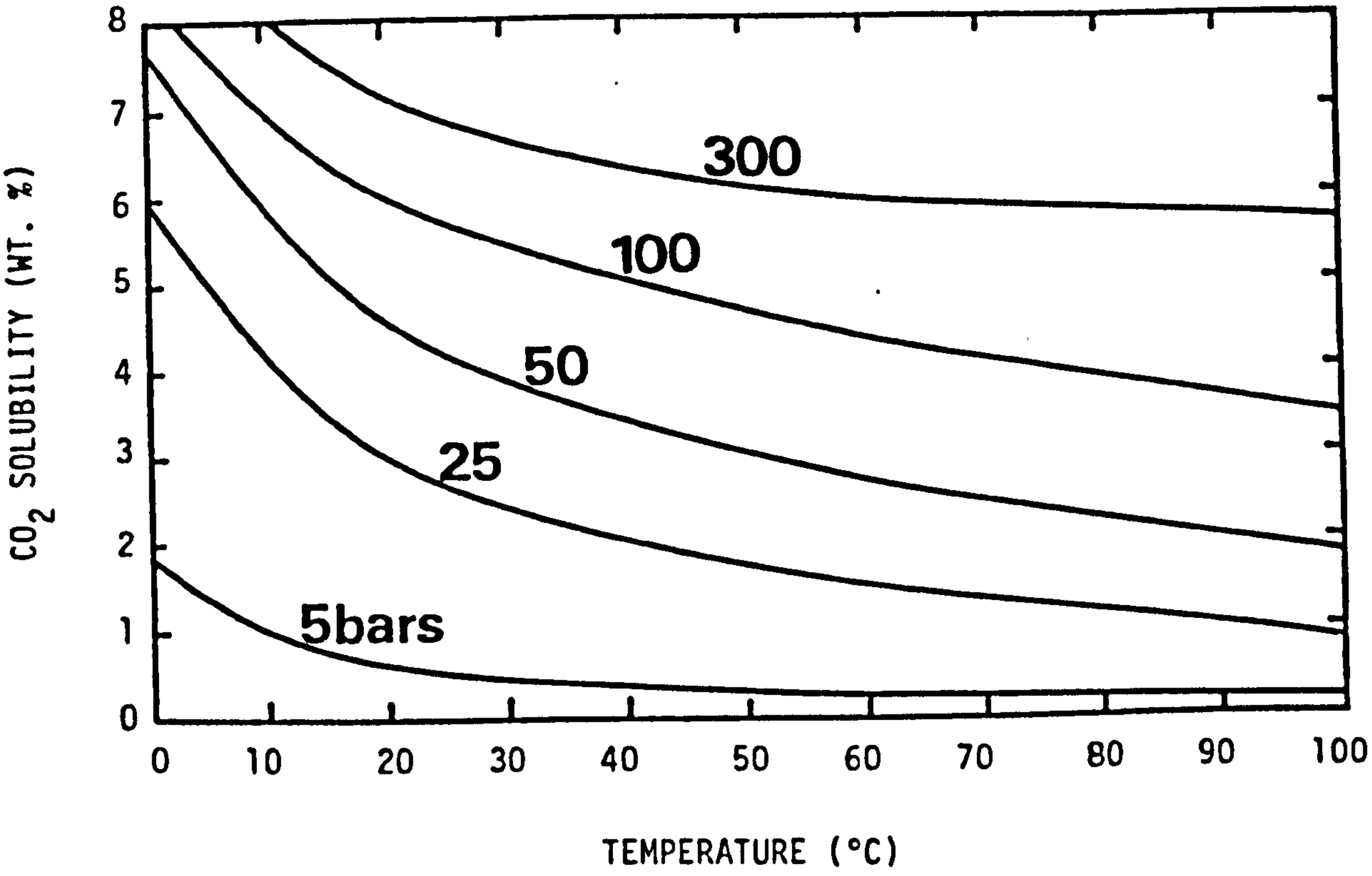

FIGURE I-2. SOLUBILITY OF CO_2 IN WATER AS A FUNCTION OF TEMPERATURE AND PRESSURE

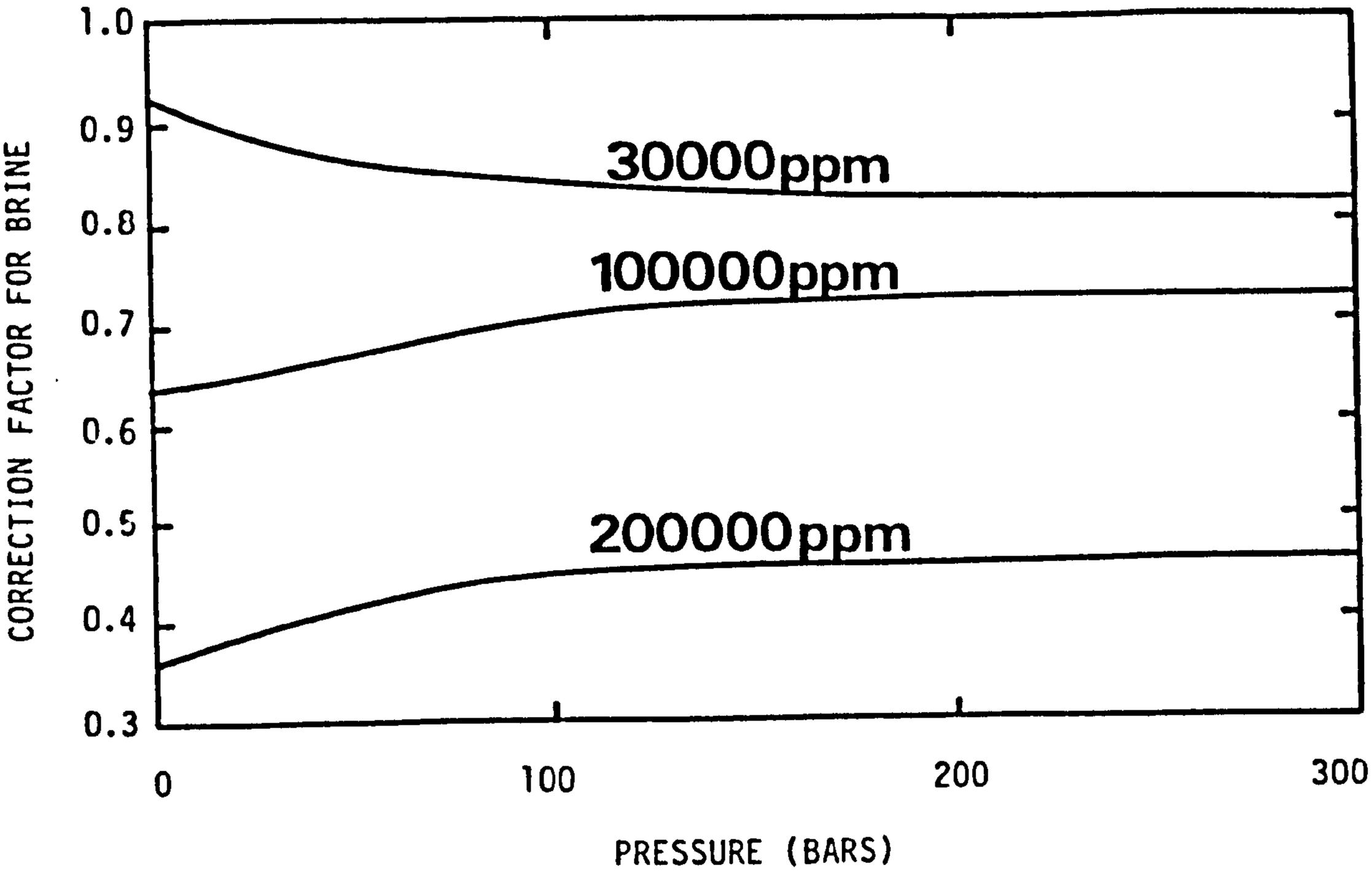

FIGURE I-3. CORRECTION FACTOR FOR SOLUBILITY OF CO_2 IN BRINE.

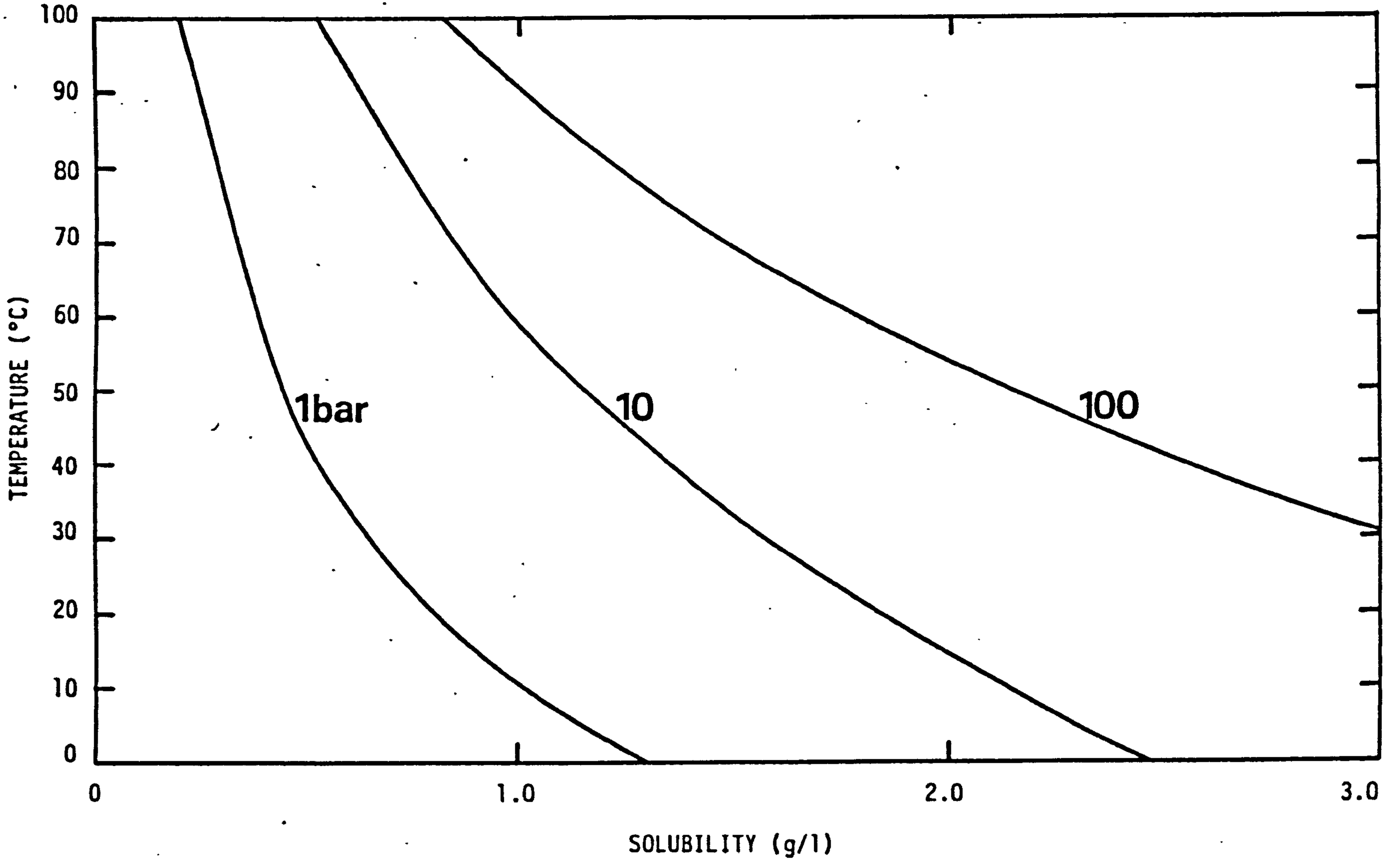

FIGURE I-4. SOLUBILITY OF CALCITE IN FULLY CARBONATED WATER AS A FUNCTION OF TEMPERATURE AND PRESSURE

(2) increases with total pressure at constant temperature and CO_2 concentration,
and

(3) increases up to a maximum at five weight percent CO_2 concentration before gradually falling again at higher CO_2 concentrations, at constant temperature and total pressure.

Carbonated water, formed upon injection of carbon dioxide into a well, will react with the carbonate minerals in the rock and transport the dissolved products through the reservoir. This dissolution effect will be more pronounced in the vicinity of the wellbore since the carbonated water solution will approach total bicarbonate saturation as the water moves away from the well. However, whether the reaction effects a reduction in permeability in the reservoir by releasing particles which then migrate and plug flow channels, or an increase in permeability, is not apparent from tests undertaken to date.

1.3 Introductory Literature

Numerous carbon dioxide flooding review publications have included stimulation by carbonated water as one of the advantages of the CO_2 flood (11, 19-23), yet other authors have attributed injectivity decline problems on carbon dioxide flooding to rock-fluid interaction (8, 24). Certainly, empirical data on the subject is scant to say the least.

Perhaps the issue is best summed by William Conner who concluded in

a report, published after a year of pilot CO_2 injection in the Granny's Creek Field, Appalachia (25), "That much more basic research concerning the interaction of CO_2 and rock characteristics of the reservoir is necessary before accurate predictions as to reservoir response can be made".

1.3.1 Laboratory Studies

J.W. Martin (26) was first to report on the use of carbon dioxide as a recovery agent. He recorded both improved oil recovery and fluid injectivity from carbonated water displacement tests in linear sandstone cores. The increased injectivity was attributed to dissolution of calcium carbonate from passageways between sand grains.

Holm (27) observed through periodic checks during carbon dioxide slug flooding experiments, that the permeability of carbonate containing cores increased with the amount of CO_2 passing through the core. For example, one dolomite core showed a threefold increase in permeability.

Other early workers (28) also observed permeability increases during carbon dioxide core tests, though no quantitative measurements were given.

However, both Reed (29) and Mungan (30) in separate studies, measured significant permeability impairment on flowing salt

solutions through rock cores. In each case plugging by fines, released by dissolution of carbonate cementing material, was shown to be a dominant permeability damage mechanism.

1.3.2 Field Evidence

Following the encouraging results from carbonated water laboratory tests in the early 1950's (26, 28) a number of projects were initiated to determine the effectiveness of carbonated water as a recovery agent in the field (31-33). However, although the ability of carbonated water to dissolve formation carbonates and thereby improve injectivity was clearly established, the oil recovery levels obtained were well below those originally predicted from lab and theoretical data (34, 35). The low recoveries were attributed to 1) unfavourable mobility (viscosity) ratios between the carbonated water and the crudes (36), and 2) poor sweep efficiencies resulting from permeability variations and vertical fissures.

These projects led to the abandoning of carbonated water flooding as a workable, economic enhanced recovery process, and to the emergence of "pure" CO_2 flooding as the principal carbon dioxide type process (37). Successful laboratory tests with CO_2 slugs and continuous CO_2 injection (2, 27, 38-42), in turn led to a series of field trials and commercial floods being started in the early to mid 1970's (43).

However, only a few of these tests have been completed, and these were small-scale pilot projects, thus only limited data as to the success of the carbon dioxide process is currently available.

Evidence of rock-fluid interaction is also somewhat limited, although carbon dioxide-water injection has clearly stimulated injection wells in the SACROC Unit, the major part of the Kelly Snyder Field in Texas (9). Dissolution of the carbonate reservoir rock has increased injectivity by 10% to as much as 50% in some wells.

On the other hand, decreased injectivity was reported in the Crosset flood, Texas, where carbon dioxide was injected continuously (44). One explanation for the declining injectivity was that some type of corrosion inhibitor had been carried into and deposited as a paraffin-like substance in the siliceous carbonate formation. However, Harvey et al (45), whilst examining decreased injectivity (enriched gas miscible flood) in another Texas field with similar lithology, found minute particles of dolomite on the pore surfaces. It is possible, therefore, that the movement of such small particles to pore throats causing plugging, may have accounted significantly for the unforeseen injectivity problems in both projects.

1.4 Study Outline

In view of the lack of data and uncertainty in the published results relating to carbonate dissolution on carbon dioxide flooding, this research programme was undertaken to develop an experimental understanding of the phenomenon. Experimental apparatus was designed and constructed for flowing CO_2-water mixtures through linear rock cores. The apparatus flow system and operating procedures are discussed in Chapter II.

The following were considered important to the apparatus design:

1) The likely pressure range for North Sea crude oil-carbon dioxide miscibility is 2,000 psi to 5,000 psi.
2) The average North Sea reservoir temperature is around 80°C.
3) Average reservoir displacement velocities of around 2 feet per day have been found to maximise CO_2 flood coverage and recovery by restricting viscous fingering (2, 4).
4) Virtually pure CO_2 is used in the miscible displacement process. Relatively small amounts of methane or nitrogen in carbon dioxide can increase substantially the pressure required for miscibility (43).

Consequently, the core flood apparatus was designed to operate at high pressures and temperatures under low flow rate conditions. In addition, only pure carbon dioxide was used for preparation of the carbonated water flooding medium.

To fully evaluate carbonate dissolution effects, a complete series of core floods with simulated carbonated injection water, from initial CO_2 concentration to full CO_2 saturation, were made over a range of pressures and temperatures. A series of sandstone core materials with varying carbonate contents and permeabilities were used in the study.

CHAPTER II

EXPERIMENTAL FLOW APPARATUS AND OPERATING PROCEDURES

2.1 Introduction

2.2 Permeability Determination

2.3 Description of Core Flooding Apparatus

- 2.3.1 Core Holder
- 2.3.2 Transfer Barrier
- 2.3.3 Intensified Carbon Dioxide Supply
- 2.3.4 Transfer Barrier Rocking Mechanism
- 2.3.5 Displacement System
- 2.3.6 Pressure Measurement System
- 2.3.7 Temperature Control System
- 2.3.8 Effluent Collection and Measurement System

2.4 Experimental Procedure

2.1 Introduction

The purpose of this chapter is to present and discuss the carbonated water core flooding apparatus and operating procedures. The permeability determination will also be discussed in this chapter, since the overall core permeabilities were determined as part of the flow experiments.

2.2 Permeability Determination

Core permeability was determined continuously during water and carbonated water flooding by employing Darcy's Law for a linear flow system. To apply Darcy's Law to determine the permeability, the fluid flow rate through the core, the resulting pressure drop across the core, and the viscosity of the fluid flowing through the core must be known.

The fluid flow rate was determined in all cases by employing an Eldex Precision Pump. This positive displacement pump delivers a steady flow that can be varied from 0 to 4.5 cc per minute. The flow rate within this range is adjusted by a micrometer screw on the pump, which sets the length of stroke.

A 0 to 50 psi differential pressure transducer was used to measure the pressure drop across the core. It was connected to strip chart recorder to provide a continuous record of the pressure differential data.

Although required brine viscosity data was obtained from the literature (46), no data on carbonated water is reported. Consequently, an "in-line" capillary tube viscometer was incorporated in the flow apparatus to enable liquid viscosity measurements to be made under test conditions. The general arrangement of the viscometer is shown diagrammatically in Figure II-2. The main elements are:

1) a 20 cm length of 0.2 mm precision bore stainless steel tube (secured by epofix resin inside a length of support tubing)

and

2) a differential pressure transducer.

From the capillary tube dimensions and measurement of the pressure drop across the tube at known constant flow rate, the required carbonated water viscosities were calculated from the Hagen-Poiseuille Equation. The viscosity data as a function of temperature and carbonation pressure are presented in Figure II-1.

2.3 Description of Core Flooding Apparatus

A high pressure, high temperature permeameter was designed and constructed to permit examination of carbonated water dissolution effects. The apparatus shown in Plates II-1, II-2, II-3, and II-4, is capable of operation in moderately corrosive liquid environments under controlled conditions of temperature, pressure and flow rate. The working limits for core overburden/confining pressure and injection pressure are 10,000 psi and 5,000 psi respectively. Those

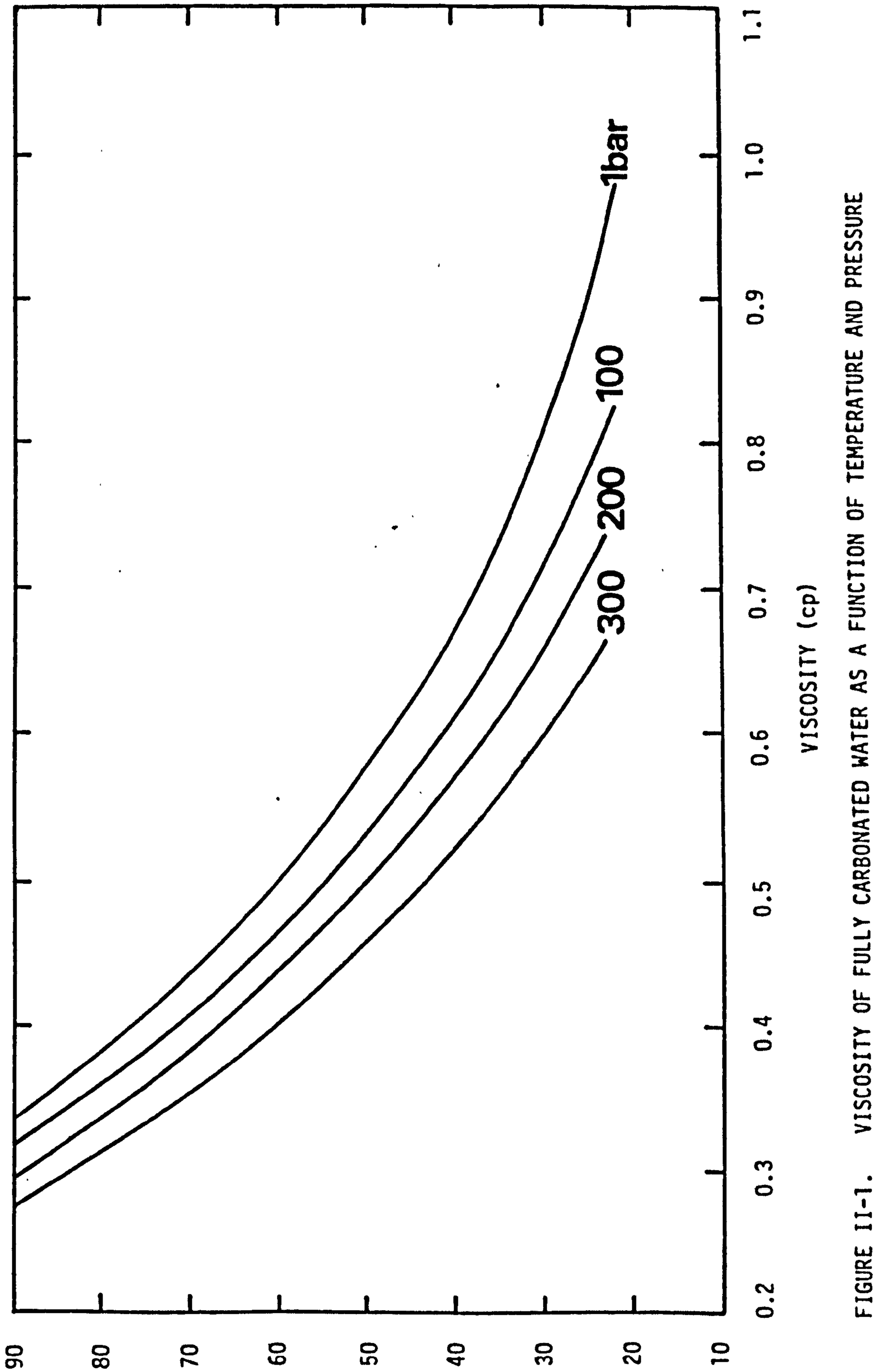

FIGURE II-1. VISCOSITY OF FULLY CARBONATED WATER AS A FUNCTION OF TEMPERATURE AND PRESSURE

PLATE II-1. FRONT VIEW OF CARBONATED WATER PERMEAMETER

PLATE II-2. CLOSE-UP OF CONTROL PANEL

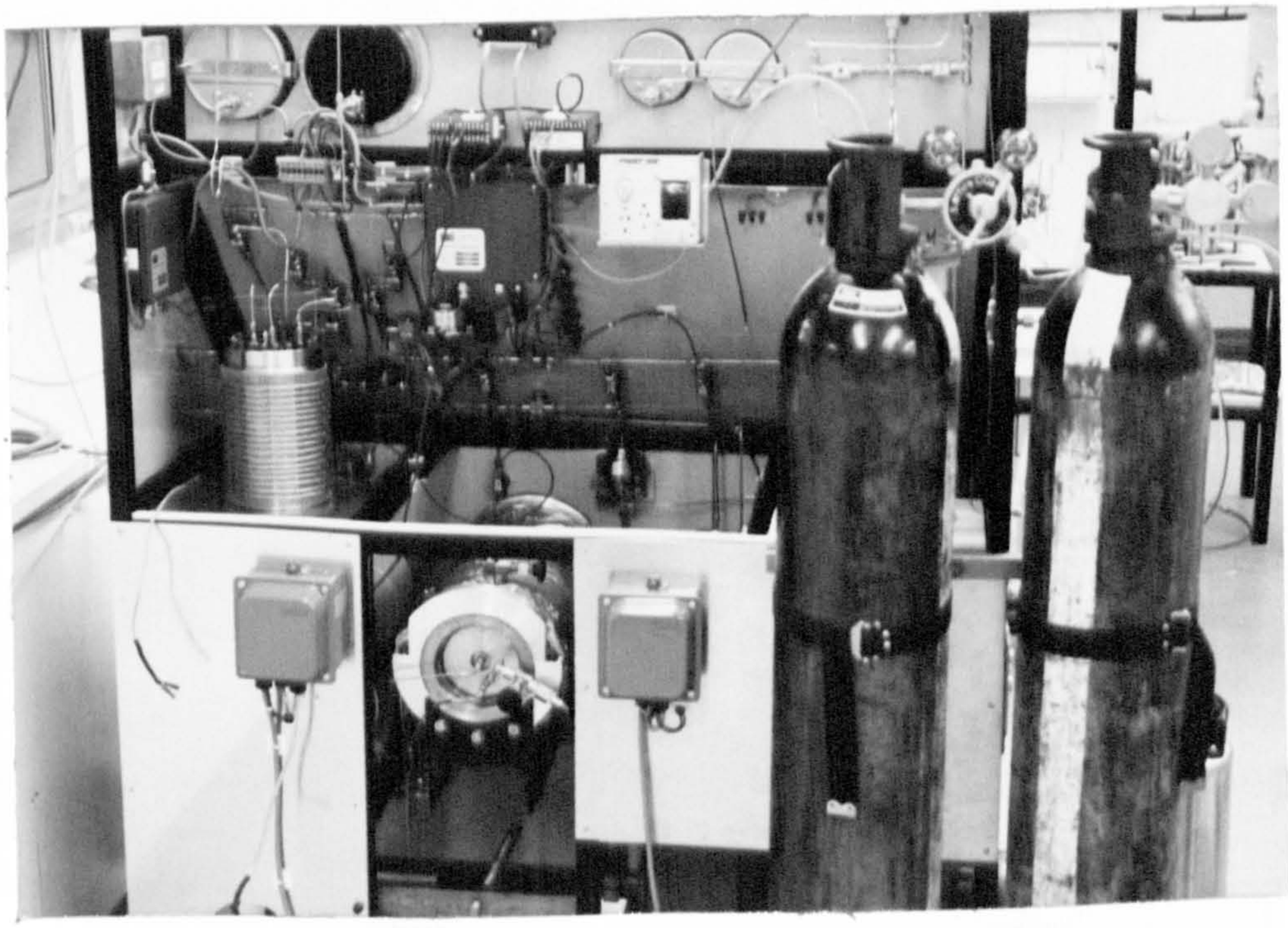

PLATE II-3. REAR VIEW OF PERMEAMETER

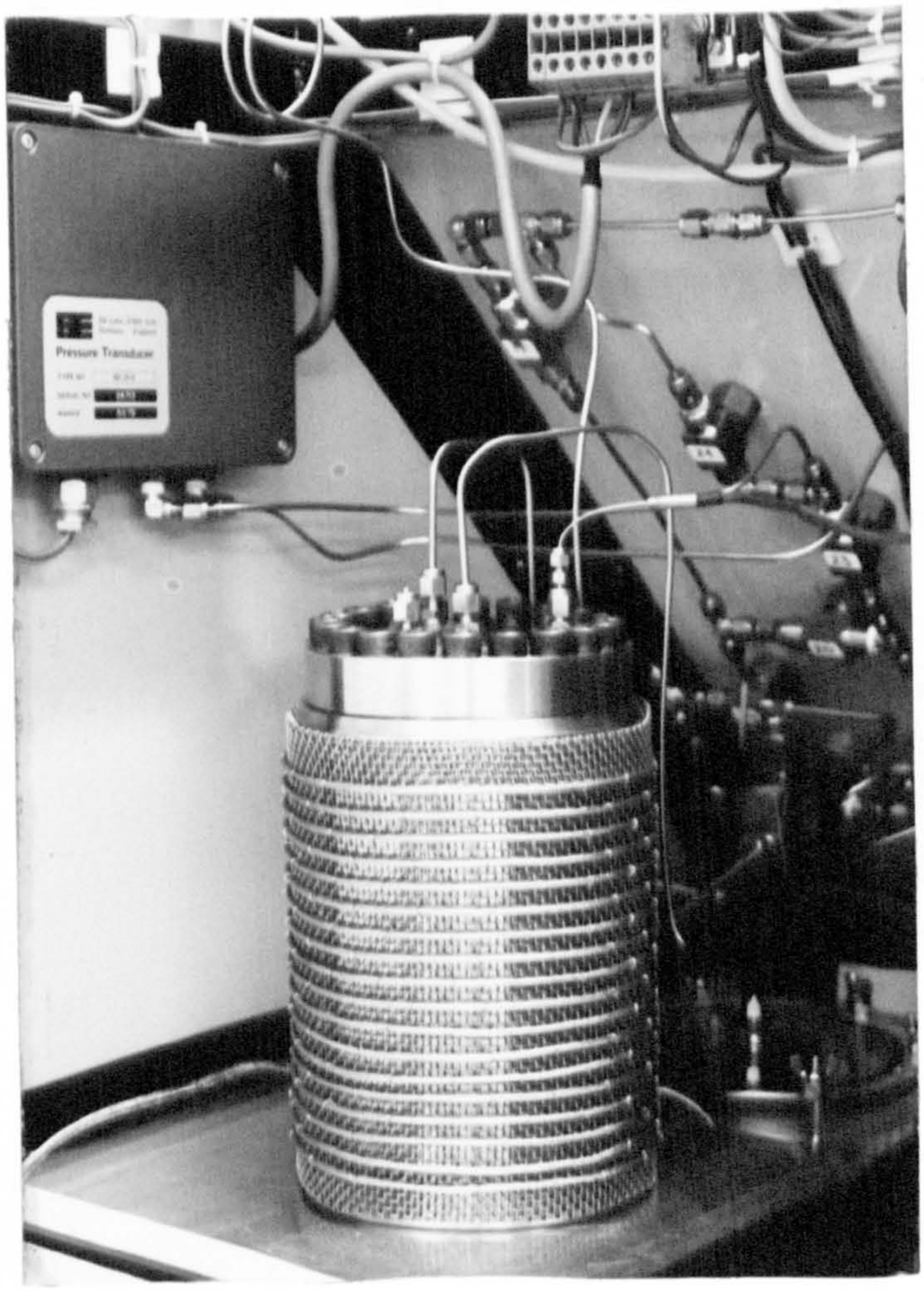

PLATE II-4. CLOSE-UP OF CORE HOLDER AND DIFFERENTIAL PRESSURE TRANSDUCER

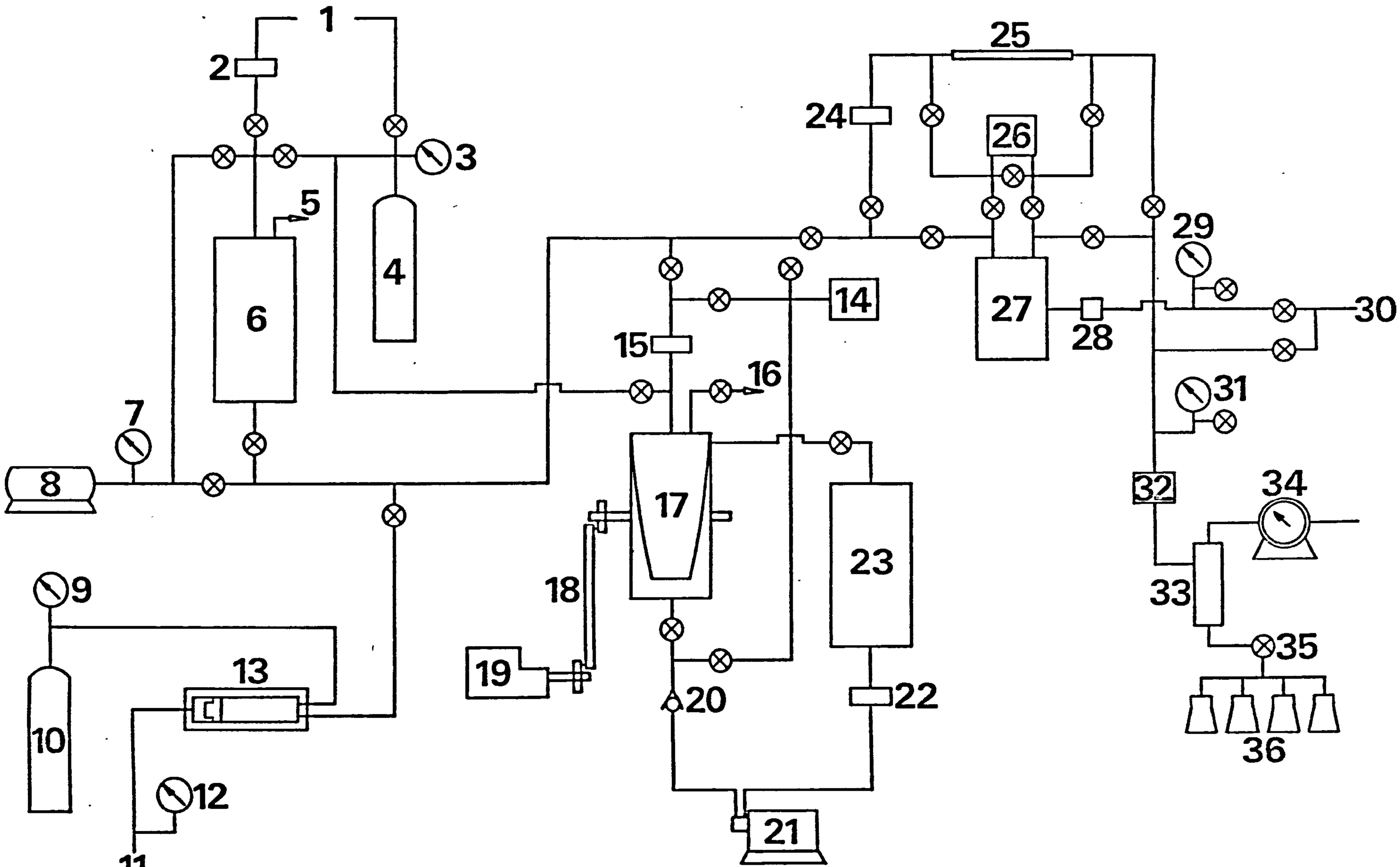

FIGURE II-2. SIMPLIFIED SCHEMATIC OF CARBONATED WATER PERMEAMETER

equipment parts contacted by carbonated water are constructed of 316 stainless steel.

A process flow scheme of the core flooding apparatus is presented in Figure II-2. It consists of:

1) 20 litre capacity, NaCl solution preparation vessel,
2) Millipore filter holder to filter inlet brine,
3) B.O.C. 0 to 150 psi CO_2 regulator,
4) CO_2 cylinder,
5) 20 psi relief valve to protect the perspex brine reservoir,
6) 6 litre capacity, perspex brine reservoir,
7) Budenberg vacuum gauge (-1 to 0 bar),
8) Vacuum system comprising pump, vapour trap and drain,
9) B.O.C. 0 to 2,000 psi CO_2 regulator,
10) CO_2 cylinder,
11) Regulated compressed air supply to drive the gas booster,
12) Budenberg pressure gauge (0 to 10 bar) to monitor the air supply pressure to the gas booster,
13) SC Hydraulic Engineering Corp. high pressure gas booster,
14) SE Labs 0 to 5,000 psi absolute pressure transducer connected to an Analogic digital display unit, to monitor the transfer barrier pressure,
15) Millipore high pressure filter holder to filter the core flood liquid,
16) 10 psi relief valve to enable gas escape whilst filling the transfer barrier,

17) Hydrotrole transfer barrier unit,

18) Rocking assembly for the transfer barrier unit,

19) Kopp variable speed motor to drive the rocking assembly,

20) Whitey non-return valve to protect the Eldex pump,

21) Eldex high pressure precision pump,

22) Nupro in-line filter for filtering the hydraulic oil pump supply liquid,

23) 6 litre capacity, hydraulic oil reservoir,

24) Millipore high pressure filter holder to filter fluid entering the capillary tube viscometer,

25) 20 cm length of capillary tube,

26) SE Labs 0 to 50 psi differential pressure transducer connected to a Bryans strip chart recorder, to measure and record differential pressure across either the core or viscometer,

27) Core holder cell,

28) HIP safety head fitted with rupture disc to prevent over-pressuring of the core holder beyond the designed safety limit,

29) Budenberg pressure gauge (0 to 600 bar) to monitor the core holder pressure,

30) Hydraulic water pump to supply the core pressure and the system back pressure,

31) Wika test pressure gauge (0 to 400 bar) to monitor the system back pressure,

32) Tescom back pressure regulator,

33) Perspex gas-liquid separator,

34) Wet type gas meter to monitor the gas discharge from the core effluent,

35) Five-way ball-valve,

36) Stoppered flasks for effluent liquid collection.

Small bore stainless steel tubing (⅛" O.D., 1/16" I.D.) was used in most of the high pressure flow lines to minimise liquid hold-up. Other lines were ¼" O.D. stainless steel, ½" O.D. copper in the air supply line to the gas booster, and nylon or polythene in low pressure lines where visibility was important. The principal units of the apparatus are:

a) a core holder system,

b) a transfer barrier/mixing vessel,

c) an intensified carbon dioxide source,

d) a mechanism to oscillate the transfer barrier for gas-liquid mixing,

e) a displacement system for the core flood liquids,

f) a pressure measurement and control system,

g) a temperature measurement and control system,

h) an effluent sampling and measurement system.

2.3.1 Core Holder

The core holder cell was designed for high pressure core flooding in corrosive liquid environments. It consists of a thick walled stainless steel outer cylinder with removable lid, fitted internally with a sleeve core holding assembly.

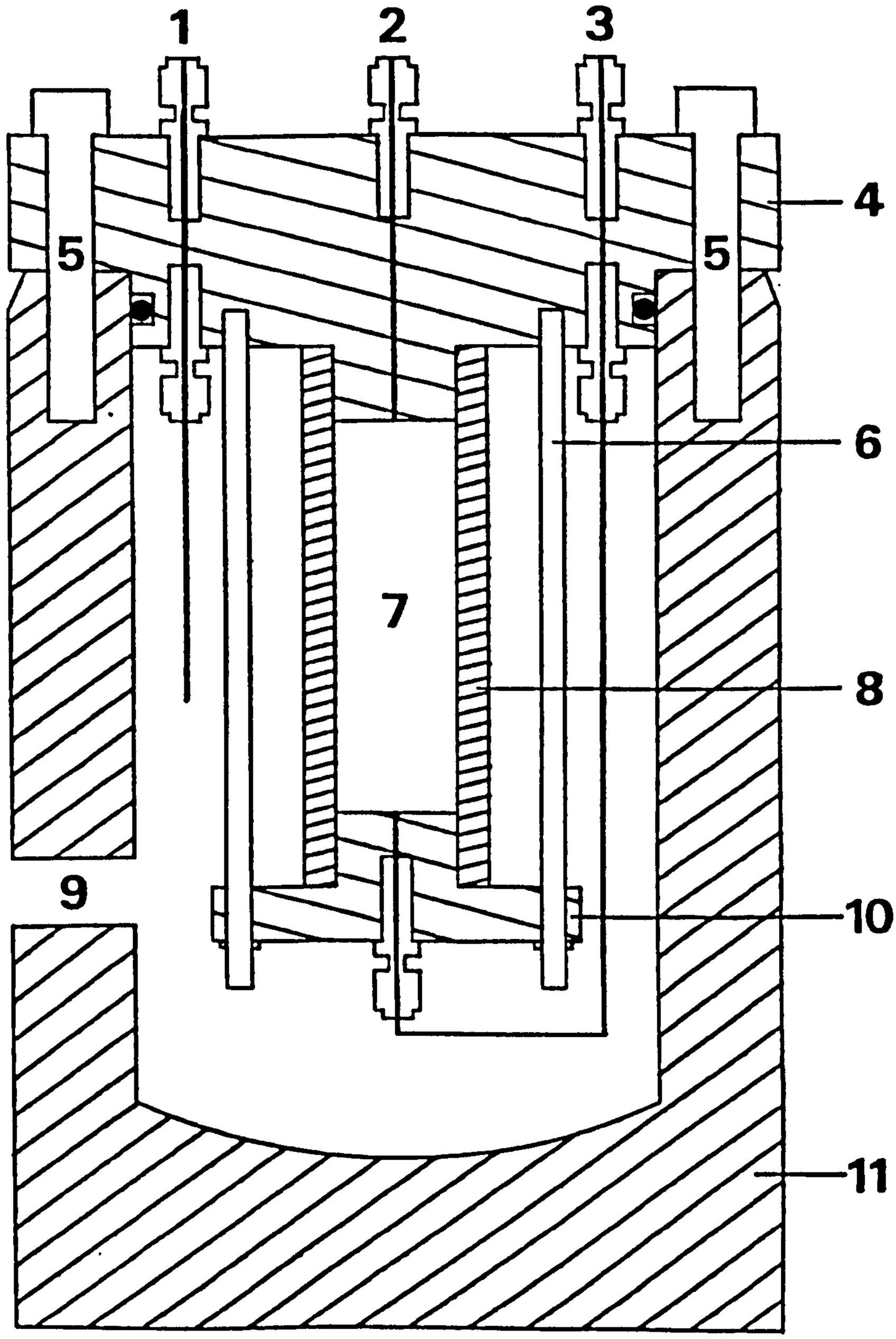

1. Thermocouple Well
2. Fluid Inlet
3. Fluid Outlet
4. Lid/Inlet End Plate
5. High Tensile Bolts
6. Tie Rod
7. Core
8. Rubber Sleeve
9. Sleeve Confining Pressure Inlet
10. Outlet End Plate
11. Cylindrical Shell

FIGURE II-3. SCHEMATIC DIAGRAM OF CORE HOLDER
(⅓ OF ACTUAL SIZE)

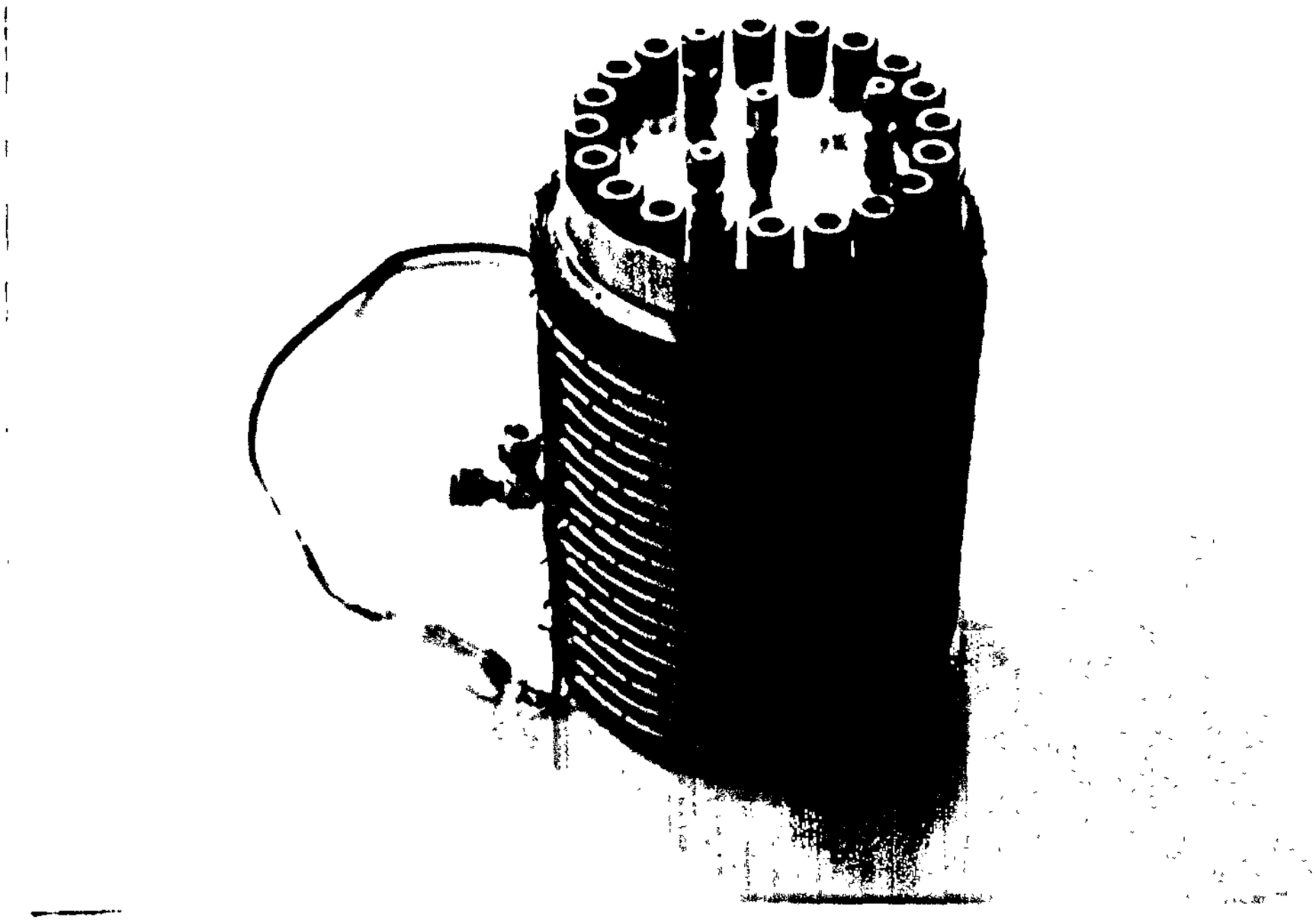

PLATE II-5. CORE HOLDER WITH HEATING JACKET

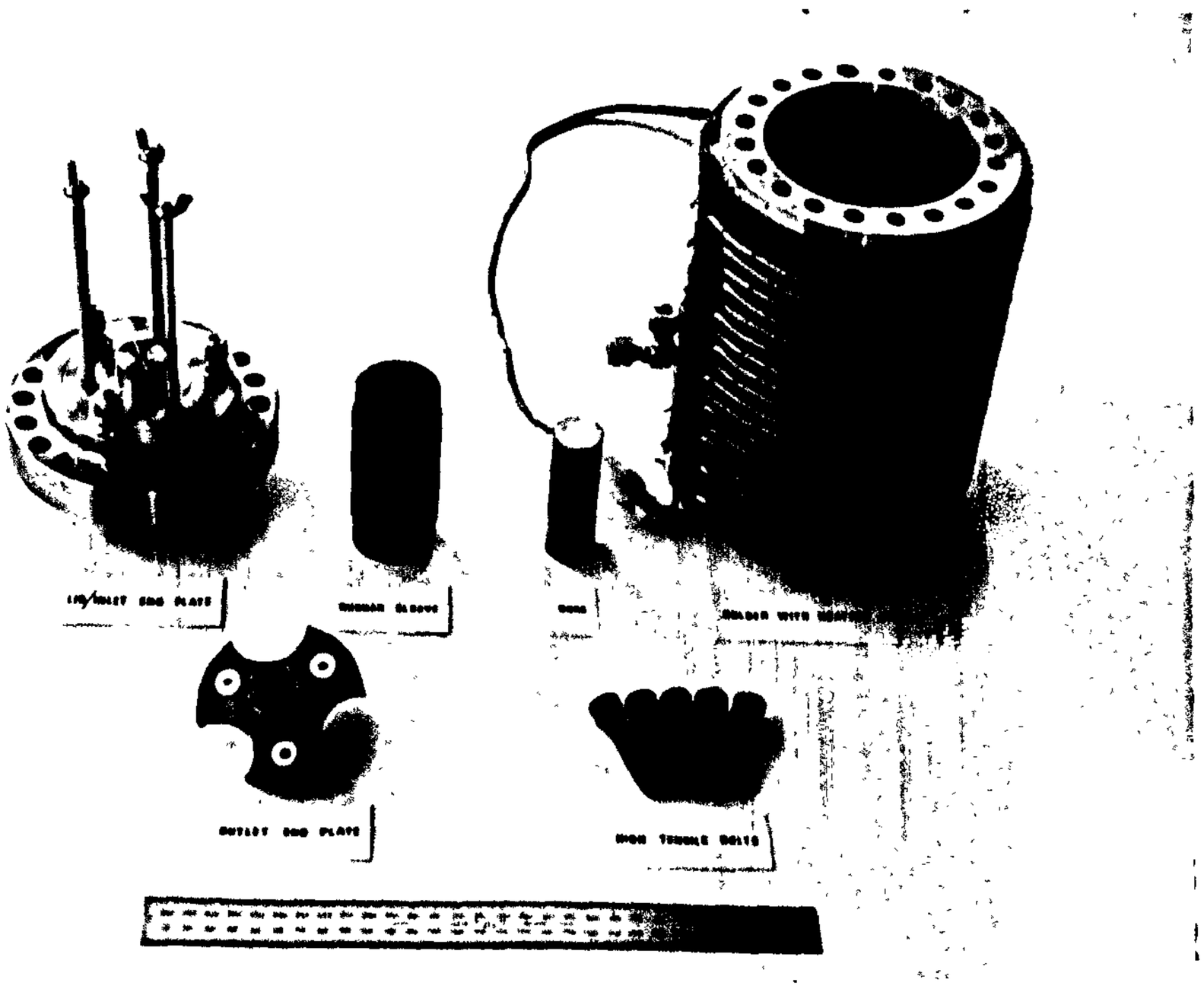

PLATE II-6. DISASSEMBLED CORE HOLDER

It is shown schematically in Figure II-3, and in Plates II-5 and II-6.

The sleeved core is secured between the cell lid/inlet end plate and the outlet end plate by three tie rods. The end plates serve as distributor and receptor respectively for the fluid flowing through the core. Both end plates are scored with lines radiating from the centre and also with concentric circles about the centre. These lines allow even fluid and pressure distribution across the ends of a core. The outlet end plate can be precisely adjusted on the tie rods to enable short cores (down to 1.5 cm long) to be fitted in the cell. The cylindrical shell has four entry ports or taps, one in the side-wall for the core sleeve confining pressure and the others in the lid; one each for the core influent, the core effluent and a thermocouple probe. The cell lid is secured to the base by twenty high tensile bolts and sealed by an O-ring. Water from a hydraulic pump is used to supply the core sleeve confining pressure.

2.3.2 Transfer Barrier

The transfer barrier unit is a fluid pressure transfer device, comprising an open-ended rubber bladder or membrane enclosed in a 5 litre capacity cylindrical steel pressure vessel. It serves as a mixing vessel during carbonated water preparation and as a fluid separator in which pressure and volume changes between the drive fluid (hydraulic oil) and the core

flooding fluid (brine or carbonated brine) are transmitted through the flexible rubber membrane.

The complete design data and dimensions of the vessel are presented in Table II-1.

Dimensions	Length		485 mm
	Outside Diameter		178 mm
	Inside Diameter		127 mm
Capacity	5 litres		
Mass	35 Kg		
Fabrication	a)	CO_2 side of unit	316 stainless steel & nitrile rubber
	b)	oil side of unit	carbon steel & nitrile rubber
Maximum Working Pressure	5,000 psi		
Connections	All $\frac{1}{8}$" NPT		

TABLE II-1 - TRANSFER BARRIER SPECIFICATIONS

2.3.3 Intensified Carbon Dioxide Supply

Carbon dioxide pressures greater than cylinder pressure (830 psi) were obtained using a gas booster. Intensification is obtained by a large area reciprocating piston pushing a small CO_2 compression piston, with a ratio of 100 to 1 between the piston areas. A compressed air drive

hydraulic pump drives the large area piston. A simplified sketch of the apparatus, manufactured by Staffordshire Hydraulic Services, is shown in Figure II-4.

2.3.4 Transfer Barrier Rocking Mechanism

To enable efficient and rapid preparation of equilibrium solutions of carbon dioxide in water, a rocking mechanism was attached to the transfer barrier. The drive for the mechanism is supplied by a Kopp variable speed motor, connected as shown in Plates II-7 and II-8, through a drive arm and couplings to a steel cradle holder bolted to the transfer barrier. The drive arm length was fixed to give a rocking angle of 30 degrees, and the rocking rate from 15 to 90 cycles per minute, was controlled by a remotely controlled adjustor from the variable speed motor.

The fluid lines to and from the transfer barrier are spiralled around the axis of rocking. The spirals help maintain the integrity of the various connections, by offering resistance to the jerks caused by the rocking mechanism.

2.3.5 Displacement System

A non-corrosive fluid (Tellus R10 hydraulic oil) was used as a drive fluid to displace the core flood liquid from the membrane in the transfer barrier. The drive oil was drawn from a perspex reservoir by the Eldex Precision Pump and

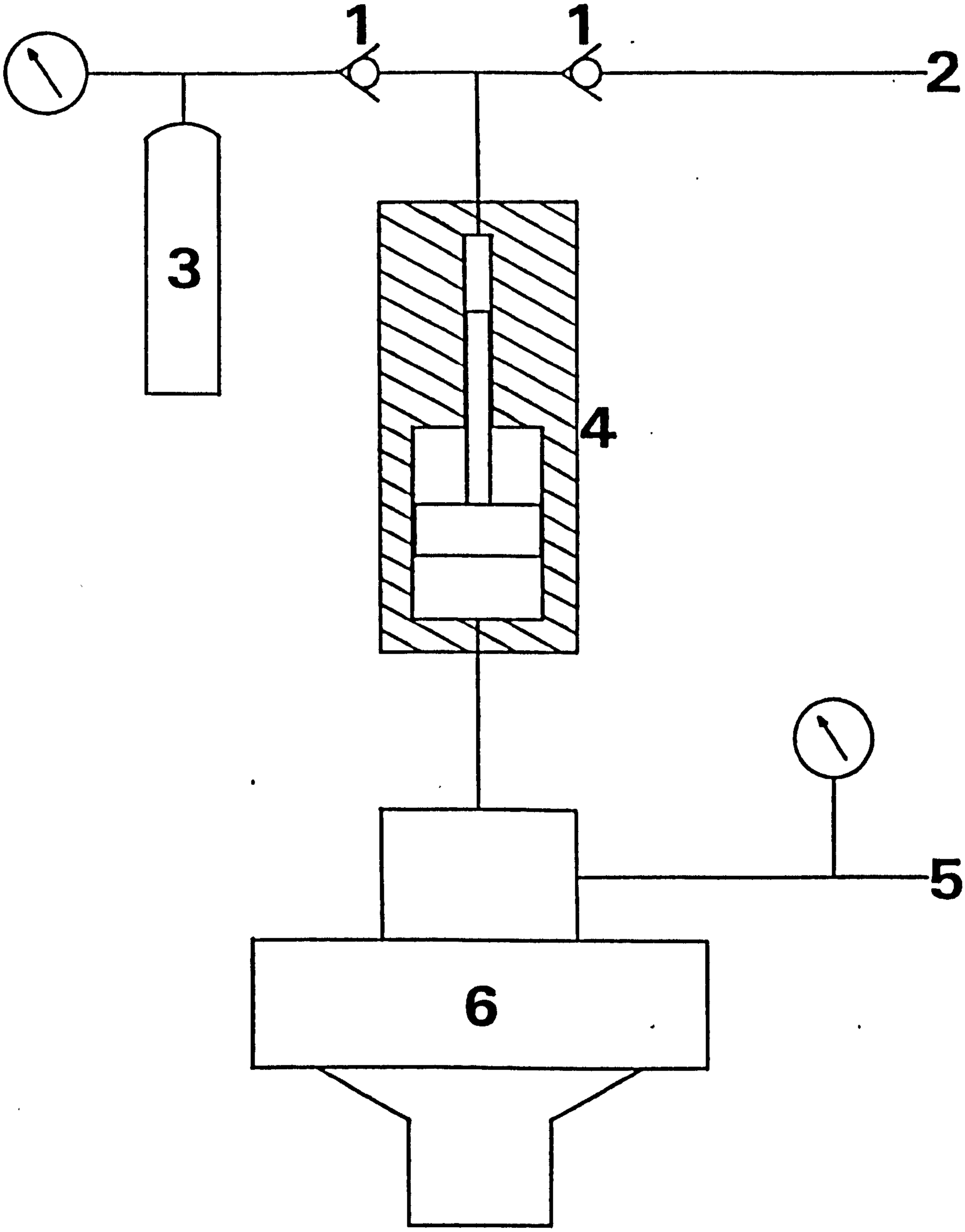

1. Non Return Valves
2. High Pressure CO_2 Outlet
3. Regulated CO_2 Supply
4. Intensifier
5. Regulated Compressed Air Inlet
6. Air Operated Hydraulic Pump

FIGURE II-4. SCHEMATIC DIAGRAM OF GAS BOOSTER

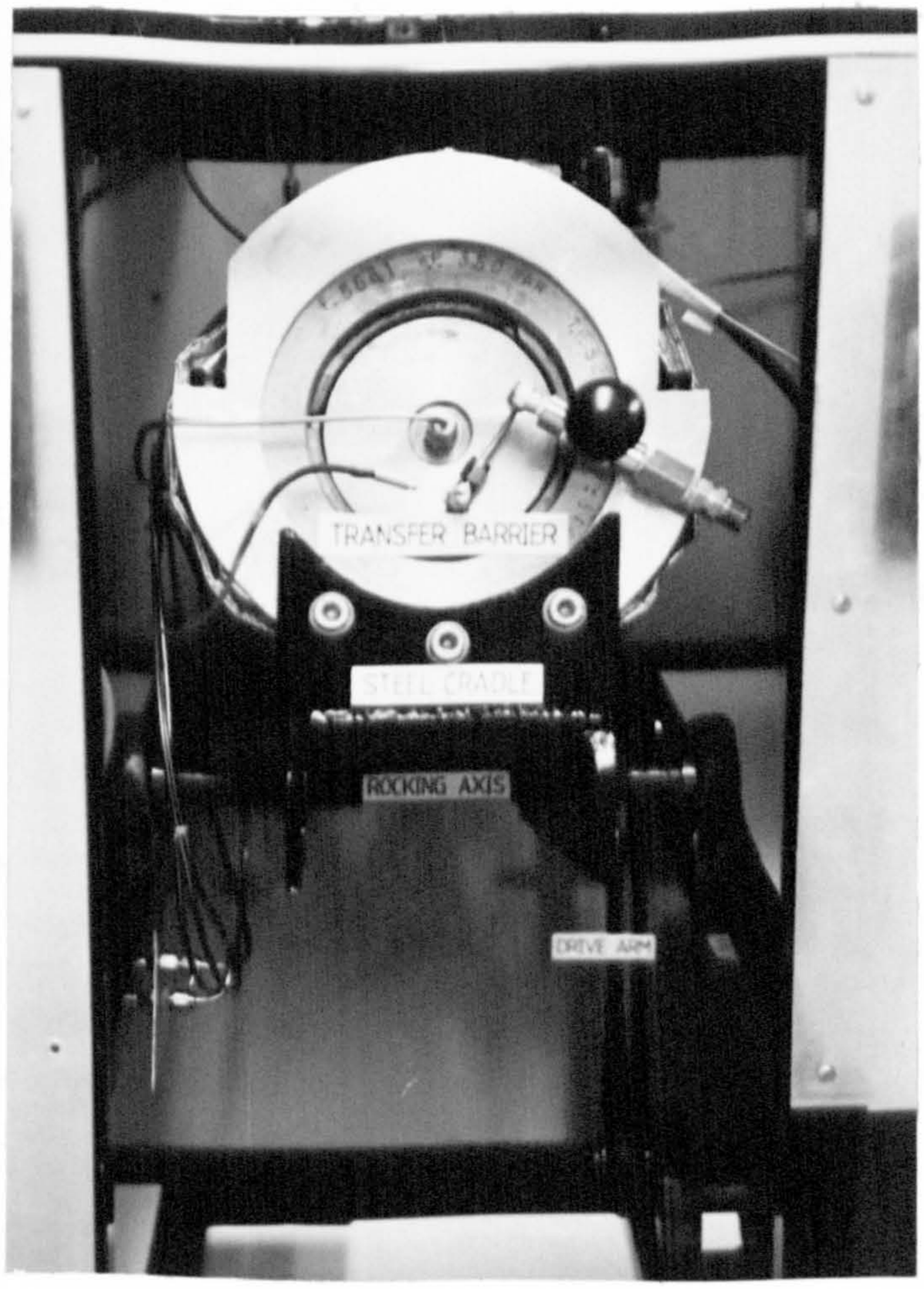

PLATE II-7. TRANSFER BARRIER ROCKING MECHANISM

PLATE II-8. TRANSFER BARRIER ROCKING MECHANISM

pumped at constant volume through a non-return valve into the base of the transfer barrier. The pump is capable of delivery pressures up to 5,000 psi.

As a safety precaution a float switch connected to the pump was fitted in the hydraulic oil reservoir to provide cut-off on delivery of the desired volume of oil to the transfer barrier.

2.3.6 Pressure Measurement System

As shown in Figure II-2, the flow apparatus is equipped with six pressure gauges and two pressure transducers.

A gauge is used to monitor the supply pressure from each of the carbon dioxide cylinders. The other four gauges are as follows:

1) 0 to -1.0 bar vacuum gauge, connected in the line to the vacuum pump - used during initial vessel and pipework evacuation.
2) 0 to 10 bar gauge,connected in the compressed air supply line to the gas booster - to monitor the air pressure to the gas booster and hence the level of gas intensification.
3) 0 to 600 bar gauge, connected to the core sleeve confining pressure line - to monitor core sleeve pressure.

4) 0 to 400 bar precision gauge with a stainless steel measuring element, connected immediately upstream of the back pressure regulator - to monitor system back pressure.

Both pressure transducers are S.E. Labs 21/V models:

1) 0 to 5,000 psi absolute pressure transducer, connected to the transfer barrier to measure the system "upstream" pressure. It is electrically connected to an Analogic digital unit for visual observation.
2) 0 to 50 psi differential pressure transducer, connected across the core holder and viscosity measurement capillary tube. It is linked to a strip chart recorder to provide a continuous record of the pressure differential data.

2.3.7 Temperature Control System

The temperature control system consists of three indpendent sub-systems:

1) to heat the contents of the transfer barrier,
2) to maintain the core and fluids entering the core at the desired temperature level,
3) to maintain the viscometer temperature.

Heat to the transfer barrier and core holder is supplied electrically by close fitting mesh elements and controlled

in each case within ($\pm$ 1°C) by a thermostat/thermocouple controller. Insulation for the vessels is provided by 4 cm thick layers of rock wool encased in aluminised glass cloth jackets. To ensure that all fluid entering the core is at test temperature, the fluid line immediately upstream of the core holder is coiled tightly around the core cell lid. The capillary tube viscometer is enclosed in a water bath where it is maintained at the desired temperature by hot water circulation.

A series of chromel-alumel thermocouples are used to monitor temperature throughout the flow system. These are linked via a selector unit to a digital thermometer for visual display and recording.

2.3.8 Effluent Collection and Measurement System

Core effluent, reduced to atmospheric pressure on discharge from the back pressure regulator, enters the gas/liquid separator. The separator is a sealed perspex cylinder with a capacity of 300 ccs. It has an inlet for the core effluent near the top and outlets in the lid and base for the separated gas and liquid respectively. The volume of carbon dioxide produced is measured by a wet-type volumetric meter connected directly to the gas outlet from the separator. The meter is a precision device provided with a 150 mm dial of 100 divisions and a six digit revolution counter form of

totaliser. Liquid from the base of the separator flows via a five-way selector valve to sealed glass collection vessels for measurement and analysis.

2.4 Experimental Procedure

Initial testing consists of flowing base water (i.e. brine or distilled water) through the core to establish the initial or reference (stabilised) permeability. Subsequently brine, carbonated to the desired level inside the rubber membrane of the mixing vessel, is injected into the core at constant rate by hydraulic oil displacement. The carbonated water and core temperatures are carefully controlled, generally at around 80°C, to represent reservoir conditions. A back pressure above the carbonation pressure is maintained throughout the test to ensure that only liquid phase exists at all points in the flow system.

The permeability of the core is measured as a function of time, and all effluent liquid is collected for chemical analysis. From the permeability profile and ion concentrations in the core effluent, the progress of the core flood can be accurately followed.

Step by step details of the experimental procedure are outlined in Appendix 1.

CHAPTER III

EXPERIMENTAL MATERIALS AND TECHNIQUES OF ANALYSIS

3.1 Introduction

3.2 Sandstone Core Material

3.3 Core Preparation

3.4 Sandstone Analysis

3.5 Core Fluids

3.6 Liquid Analysis

3.7 Crude Oil Saturation Apparatus

3.1 Introduction

The peripheral experimental apparatus, together with the materials used in the flow tests and their methods of analyses are the subject of this chapter.

3.2 Sandstone Core Material

The porous formation rock, sandstone, consists of a compacted mass of mineral grains of widely different size and composition. Quartz is the main mineral constituent of sandstone but considerable amounts of other minerals such as felspars, clays and carbonates may be present.

To enable study of the carbonated water - carbonate mineral reaction without interference from other effects such as clay or mica alteration, it was necessary to choose material with a relatively simple mineralogical composition. Thus a relatively pure quartz-carbonate sandstone, a calcareous grit, was chosen for the initial stage of the study. The selection of this particular sandstone, from a quarry in the Yorkshire Jurassic, was also partly based on its high carbonate content.

However, to gain a more complete understanding of the reaction effect of carbonated water on carbonate mineral in sandstone, a variety of other sandstones, including some specific North Sea reservoir material were also tested in the study. These sandstones, listed in Table III-1, and described more fully in Appendix 2,

FORMATION	ROCK TYPE	DESCRIPTION	MINERAL CONTENT		PHYSICAL PROPERTIES	
Yorkshire Jurassic	Calcarenaceous Sandstone	Subrounded detrital quartz grains and detrital carbonate debris cemented by micritic calcite	Quartz Ferroan Calcite	80% 20%	Permeability Porosity	10-200mD 15-20%
Fife Carboniferous A	Dolomitic Sandstone	Angular to subrounded quartz grains partially cemented by secondary dolomite	Quartz Dolomite	90% 10%	Permeability Porosity	200mD 10%
Fife Carboniferous B	Dolomitic Sandstone	Similar to Fife Carboniferous A but much finer-grained with less dolomite cement	Quartz Dolomite Clay	96% 3% 1%	Permeability Porosity	45mD 20%
Rotliegende Sandstone from Southern North Sea Reservoir	Calcitic Sandstone	Poorly consolidated framework of subrounded to rounded quartz grains with patchy calcite pore fill and clay	Quartz Calcite Felspar and Clay	95% 2-3% 2%	Permeability Porosity	300mD 15%
Jurassic Sandstone from Northern North Sea Reservoir	Dolomitic Sandstone	Loose framework of subangular to subrounded quartz and felspar grains with varying amounts of dolomite cement	Quartz Dolomite Felspar	80% $<$25% $<$15%	Permeability Porosity	250-2000mD 25%
Jurassic Sandstone from Indefatigable Field	Dolomitic Sandstone	Angular to subangular quartz grains with patchy dolomite pore fill	Quartz Dolomite	95-100% 0-5%	Permeability Porosity	1-200mD 9-22%
Oxfordshire Jurassic	Fossiliferous Limestone	Shell fragments and ooliths cemented by micritic calcite	Calcite Quartz	95% 5%	Permeability Porosity	50mD 14%

TABLE III-1. SUMMARISED DESCRIPTIONS OF CORE MATERIALS

generally have much lower carbonate concentrations than the Yorkshire material. Also, during the latter stages of the investigation, a test was carried out on a fossiliferous limestone by way of comparison with the sandstone results.

Considerable time was spent searching for and obtaining the above rock materials. Initially, difficulty was experienced in locating suitable permeable carbonate cemented sandstone from onshore sources, the carbonate cementation almost invariably rendering the materials collected impermeable. This led to an intensive nationwide survey, involving various geological groups, being made before the required materials were obtained. In addition there was difficulty securing valuable reservoir core from operating companies.

3.3 Core Preparation

For each series of experiments a number of 2.5 cm diameter cylindrical cores were diamond drilled, parallel to the bedding from the same block or core of sandstone, so that variation in the properties would be kept to a minimum. As a precaution against collapse on dissolution, the cores were coated on the cylindrical surface with epoxy resin. The cores were then trimmed, generally to a length of 7.5 cm, dried in a humidity controlled oven and stored in a dessicator until required. As the rock materials used were for the most part free from clays, no special coring or cutting fluids were necessary. The core cuttings were used for other phases of the study, including porosity measurement, carbonate staining and the preparation of petrographic thin sections (Section 3.4). Any portion

of the samples left over were stored for future checking and study.

Cores extracted from reservoir material containing crude oil were normally cleaned, prior to epoxy resin coating, in a solvent immersion apparatus. Toluene followed by a chloroform-methanol mixture were used as solvents. As it was found that prolonged cleaning led to a weakening of some cores, the cleaning process was kept as short as possible.

3.4 Sandstone Analysis

Detailed analyses of the sandstone material were made both before and after flow experiments. Analytical procedures used included:

1) Petrographic Analysis. In this form of analysis, the rock was impregnated with epofix resin, slabbed, mounted on a glass slide and ground to a thickness of 30 microns. It was then studied using polarised light on a petrographic microscope. This technique is the best and most accurate way to assess sandstone composition, general aspects of pore geometry and overall mineral distribution.

2) Carbonate Staining. Because of their similar physical characteristics, carbonate minerals such as calcite, ferroan calcite, dolomite and ferroan dolomite are difficult to distinguish under the microscope. Thus a standard differential dye staining procedure (Dickson 1966, 47) was used to establish the identity of the carbonate minerals in the sandstones under study.

The staining technique used was completed in three stages (for details see Appendix 3). First polished thin sections of the sandstones were prepared, washed and partially etched in dilute hydrochloric acid. The sections were then stained in a solution mixture of potassium ferricyanide and alizarin red-S, before immersion in alizarin red-S alone for colour intensification.

Besides their use in identifying carbonate minerals, the stained sections were useful in estimating the percentage of carbonate present in a sandstone and in grain fabric analyses.

3) Scanning Electron Microscope Analysis. This form of analysis was used for determination of the size of pore throats, crystal structure of many fine grained pore-fill cements and details of pore wall geometry. It has advantages over thin section petrography of depth of focus and high magnification, but is generally not as good when used for gross pore geometry studies.

4) Porosity Measurement. Porosity was determined rapidly and accurately from two measurements: 1) the sample bulk volume, and 2) the sample grain volume.

The bulk volume was found by displacement of mercury at atmospheric pressure in a Ruska Universal Porometer, while the grain volume was determined using a helium gas expansion porosimeter. The helium porosimeter utilises the principles

of gas expansion, whereby a known reference volume of helium at known pressure is expanded into an unknown system volume. From measurement of the resultant equilibrium pressure the unknown system volume is calculated from Boyle's Law.

With the bulk volume and the grain volume known, the porosity was determined using the equation:

$$\emptyset = 1 - \frac{V_g}{V_b}$$

where V_g is the sample grain volume and V_b is the sample bulk volume.

5) Permeability Measurement. Routine permeability measurements on core cuttings and segments of flooded core material were made using a precision gas permeameter. Gas permeabilities were then corrected to equivalent liquid permeabilities by applying Klinkenberg factors.

6) Pore Size distribution Analysis. Sample pore size distributions were determined using a Micrometics Mercury Penetration Porosimeter. The measurement technique involved placing the test sample in the porosimeter high pressure cell, evacuating air from the sample and then allowing mercury to cover it by filling the cell. The pressure in the cell was then raised in small increments, and the volume of mercury injected into the sample at each pressure recorded.

Since mercury penetrates the pores in proportion to their size and the pressure applied to the mercury, a pore size

distribution curve is obtained directly from a plot of the applied pressure versus the cumulative volume of mercury which has entered the sample.

3.5 Core Fluids

A 3 weight % sodium chloride solution in distilled water was used as a standard throughout the work. It was used as a core saturation and permeability fluid in the initial stage of core testing, and subsequently with CO_2 gas in the carbonated water preparation stage. The carbon dioxide used was from standard gaseous CO_2 cylinders (British Oxygen Co., commercial grade, 99.9% purity).

In the artificial residual oil saturation of cores, crude oil from Forties Field was used (Section 3.7).

3.6 Liquid Analysis

Analysis of core effluent liquid was governed largely by the mineralogy of the rock under test. Where the only carbonate present was calcite, analyses for calcium were sufficient, but where dolomite was present analyses for both calcium and magnesium were necessary. The required concentrations were determined by EDTA titration (procedures outlined in Appendix 4) and found to be in very close agreement with those obtained using a Techmation plasma emission spectrometer.

In a few cases analyses for iron using a phenanthroline colourometric method (48) were undertaken, but the concentrations found to be sufficiently low to be neglected.

Core effluent analyses also made possible the computation of porosity change in a core during a carbonated water flood. This was achieved simply by recalculating the dissolved mass of carbonate and dividing where appropriate by the average density of calcite (2.71 g/cc) or dolomite (2.8 - 2.9 g/cc), to give the total rock volume change.

3.7 Crude Oil Saturation Apparatus

In addition to carrying out tests on clean and natural oil containing sandstones, a series of experiments (Chapter IV) were also undertaken on core materials containing artificial residual oil saturations. Preparation of the artificially saturated cores was performed in four stages using the specially designed apparatus shown in Plate III-1 and schematically in Figure III-1:

1) A clean, dry core was mounted in the core holder and evacuated.
2) The core was saturated with deaerated brine using gas chromatography pump Number 1.
3) The brine in the core was displaced with crude oil to connate water saturation using gas chromatography pump Number 2. Crude oil was pumped through the core for several days in this stage.
4) Finally, the core was again brine flooded to reduce the oil saturation level.

Although clearly limited in terms of reproducing reservoir rock-fluid equilibrium conditions, using this preparation method it was hoped to approximate within a core, water-wet conditions in a "watered-out" reservoir. To evaluate the water and oil saturation

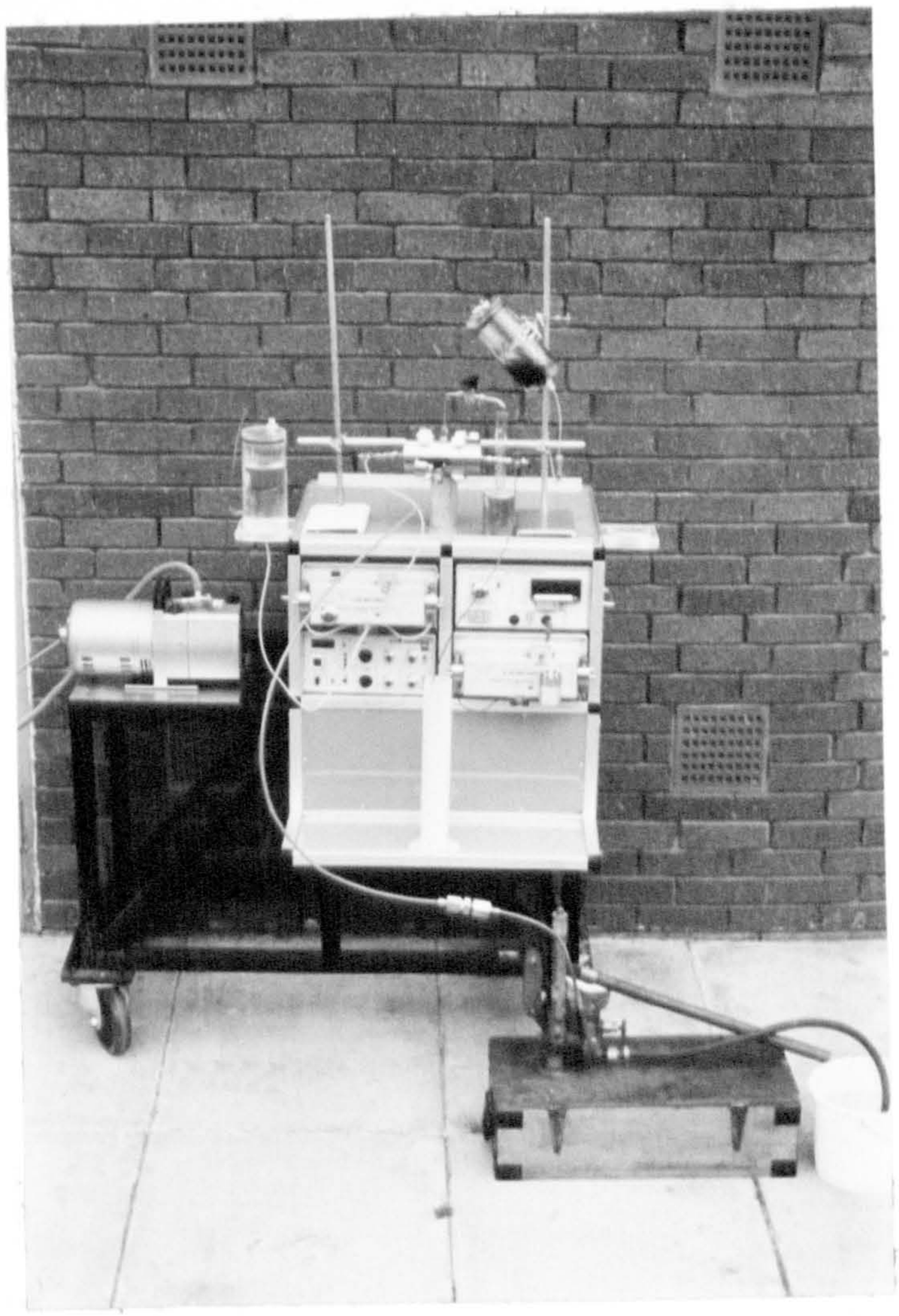

PLATE III-1. CRUDE OIL SATURATION APPARATUS

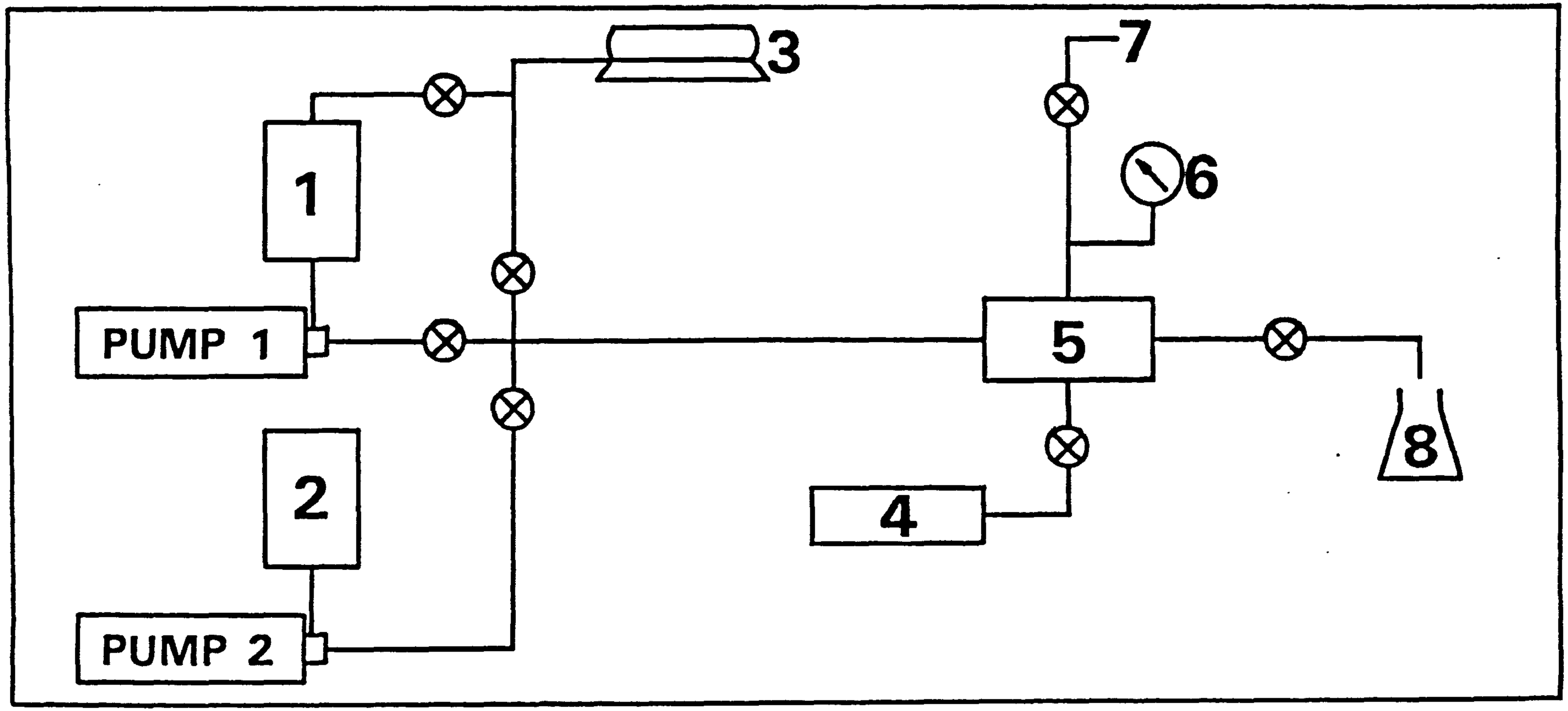

1. Brine Reservoir
2. Crude Oil Reservoir
3. Vacuum System
4. Hydraulic Pump
5. Core Holder
6. Pressure Gauge
7. Air Purge
8. Effluent Collection

FIGURE III-1. SCHEMATIC DIAGRAM OF CRUDE OIL SATURATION APPARATUS

levels through the procedure stages the core was weighed initially and then subsequently following the second, third and last stages. From measurements of the brine and crude oil specific gravities the core saturations were then calculated. Typically, final residual oil saturations of around 20% were obtained.

CHAPTER IV

RESULTS AND DISCUSSION OF RESULTS

4.1 Introduction

4.2 Yorkshire Jurassic Sandstone

4.3 Fife Carboniferous Sandstone (A)

4.4 Fife Carboniferous Sandstone (B)

4.5 Rotliegende Sandstone from Southern North Sea

4.6 Jurassic Sandstone from Northern North Sea

4.7 Rotliegende Sandstone from Indefatigable Field

4.8 Oxfordshire Jurassic Limestone

4.9 Summary of Results

4.1 Introduction

Most of the results of the carbonated water core tests that were performed are presented in this chapter. Of primary interest were the changes in core physical properties and changes in core effluent chemical concentrations. The data collected during the early stages of the investigation, before apparatus and techniques were standardised, have been purposely omitted.

The results are presented, in sequence, under the different rock types used in the study (see Section 3.2). Details of the flow rates used are presented for completeness in Appendix 5.

4.2 Yorkshire Jurassic Sandstone

The initial series of experiments were carried out with distilled water and brine (no carbonation) as core flood liquids. These tests, at 1,000 psi pressure and 20°C temperature, were aimed at establishing a stabilised or reference permeability prior to any carbonated water flood. The results of two such tests are presented in Figures IV-1 and IV-2.

Significant linear increases in permeability were obtained in both tests, with no apparent levelling off in the rate of increase and attainment of a reference value upon injection of 2,100 ccs or 300 pore volumes. Analyses of the core effluents for calcium indicated that the obtained permeability increases were attributable to the dissolution of calcite in the flood liquids. Although

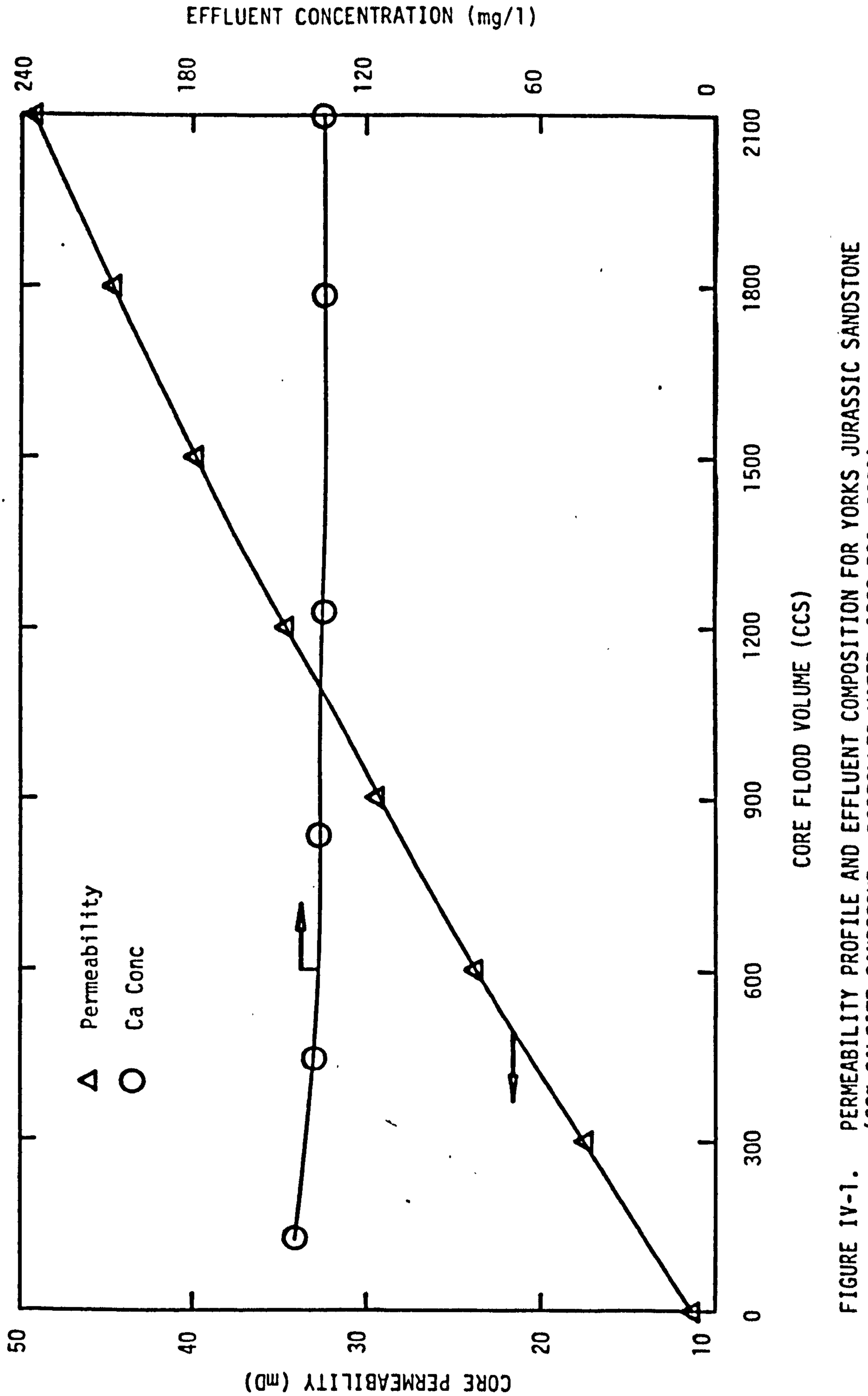

PERMEABILITY PROFILE AND EFFLUENT COMPOSITION FOR YORKS JURASSIC SANDSTONE
(20% CALCITE SANDSTONE; DISTILLED WATER, 1000 PSI, 20°C)

FIGURE IV-1.

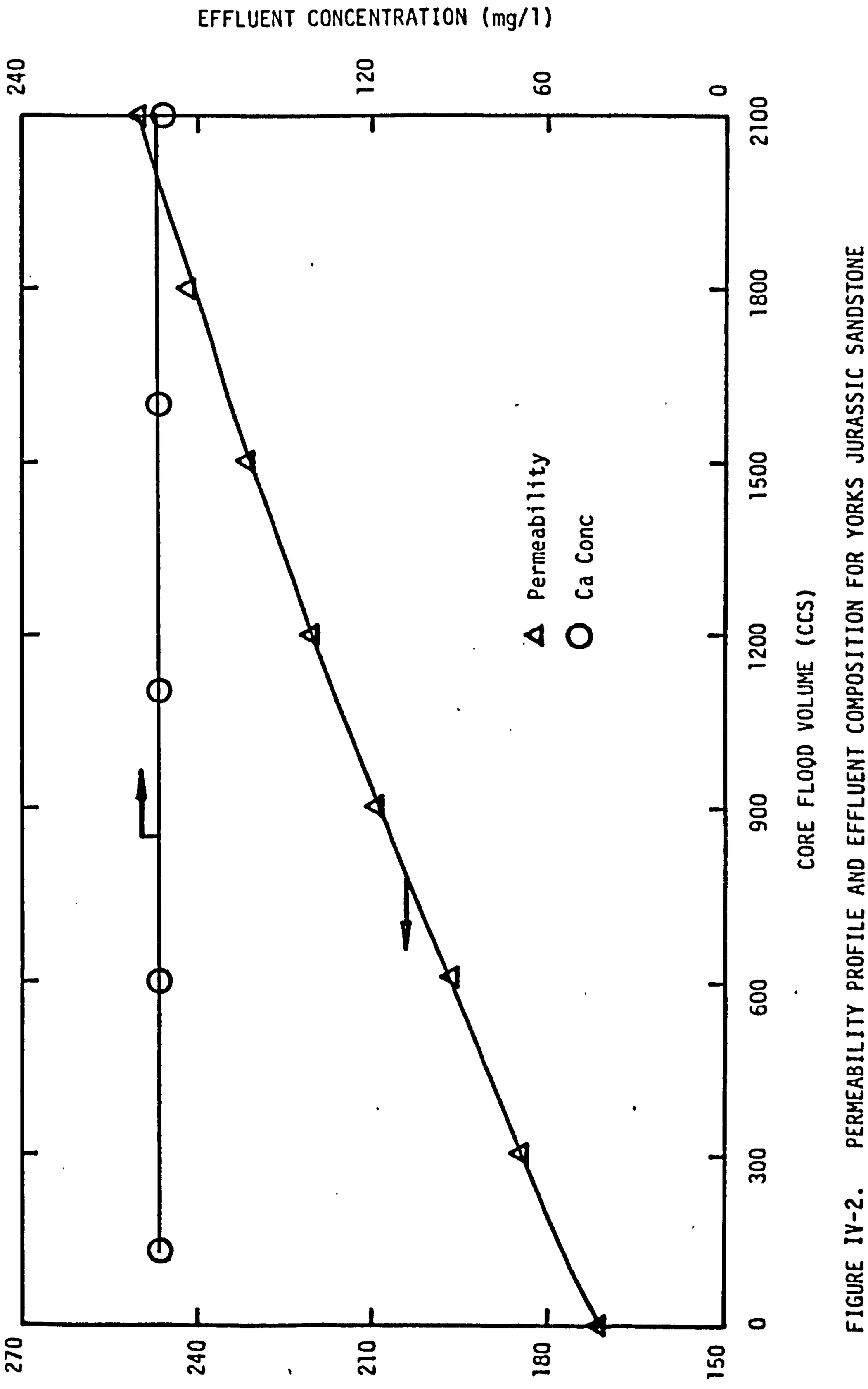

FIGURE IV-2. PERMEABILITY PROFILE AND EFFLUENT COMPOSITION FOR YORKS JURASSIC SANDSTONE (20% CALCITE SANDSTONE; BRINE, 1000 PSI, 20°C)

difficult to compare the order of the permeability increases between the distilled water and brine tests, due to the large difference in initial core permeabilities, comparison of the effluent calcium concentrations showed the volume of calcite dissolved in each test to be similar. That the calcium levels in both tests remained virtually constant throughout, indicates that the calcium bicarbonate concentrations in the flowing liquids had increased to the saturation level within the cores. The higher level of calcium in the brine flood effluent was simply due to the greater solubility of calcite in salt solution than distilled water (13).

As a comparison with the CO_2 free, base liquid experiments, a series of tests were then carried out with fully carbonated water. The result of the first of these, also at 1,000 psi and 20°C, is presented in Figure IV-3. A much greater permeability increase was obtained, from 60 mD to 770 mD, although again there was little indication of any fall in the rate of increase as the test progressed.

Examination of the retrieved, flooded core revealed that a 3 mm thick band had been preferentially dissolved over the length of the core, forming a well defined flow channel. This channel appeared to develop within a poorly cemented, quartz rich (sandy) layer within the sandstone.

Thin section comparisons of the sandstone from before and after the test are presented in Plates IV-1, IV-2 and IV-3. Plate IV-1 shows

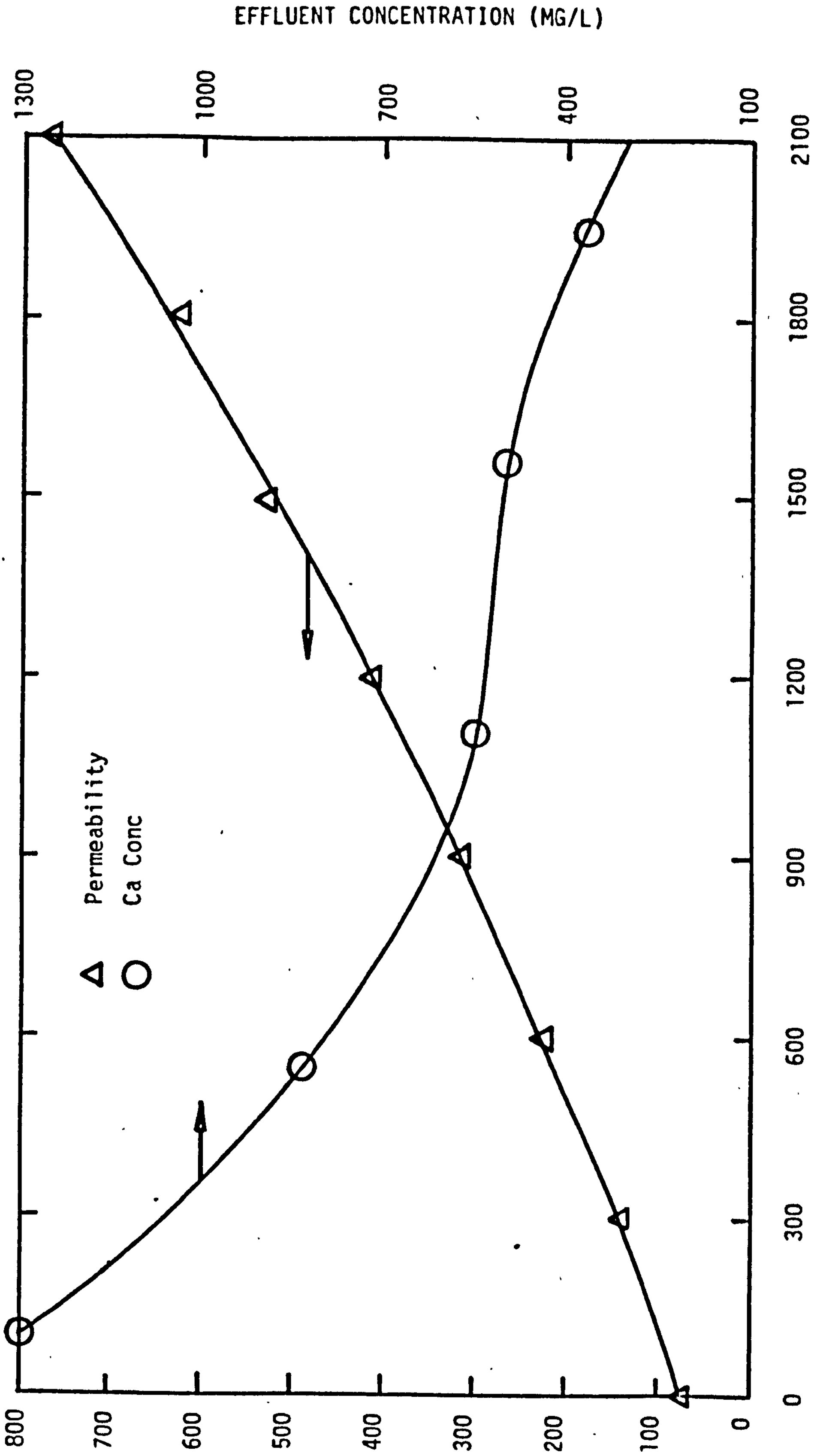

FIGURE IV-3. PERMEABILITY PROFILE AND EFFLUENT COMPOSITION FOR YORKS JURASSIC SANDSTONE (20% CALCITE SANDSTONE; 1000 PSI CARBONATION, 20°C)

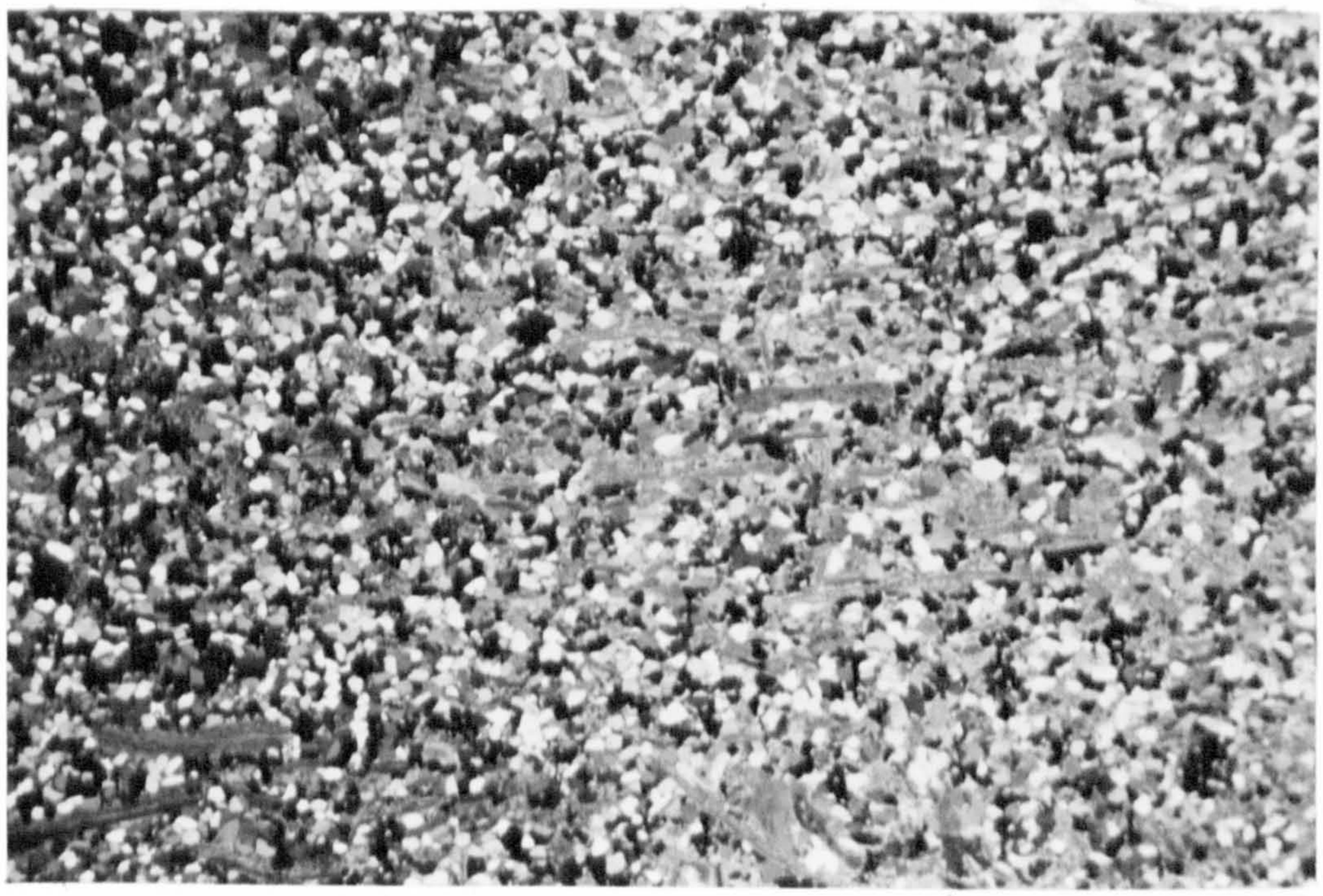

PLATE IV-1. PHOTOMICROGRAPH; CROSSED NICOLS, X2 MAGNIFICATION. SHOWS THE APPARENT HOMOGENEOUS FRAMEWORK OF QUARTZ AND CALCITE IN YORKS JURASSIC SANDSTONE

PLATE IV-2. PHOTOMICROGRAPH; CROSSED NICOLS, X2 MAGNIFICATION. SHOWS THE DISSOLVED FLOW CHANNEL FORMED IN YORKS JURASSIC SANDSTONE DURING 1000 PSI, 20°C CARBONATED WATER FLOOD

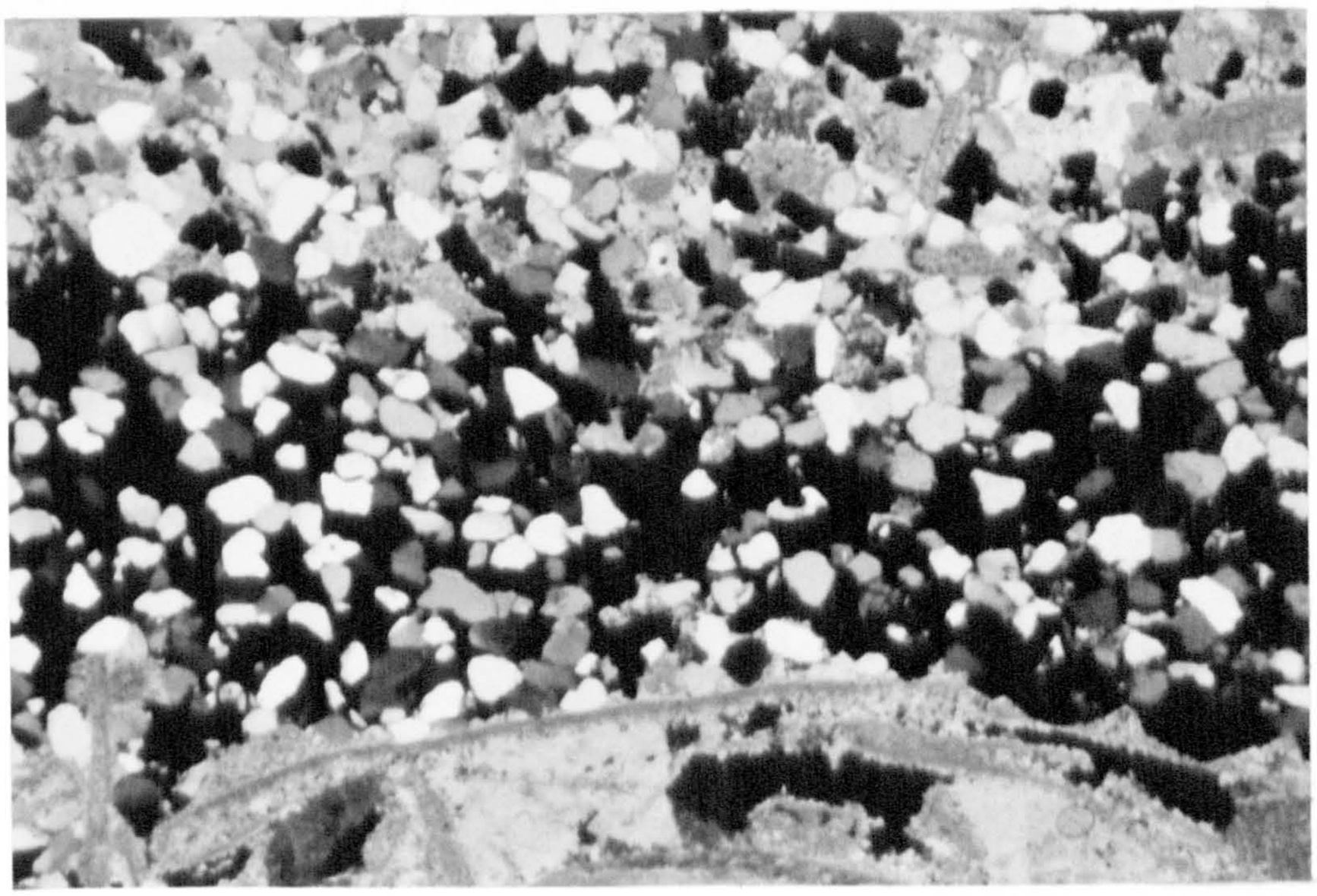

PLATE IV-3. PHOTOMICROGRAPH; CROSSED NICOLS X4 MAGNIFICATION. CLOSE-UP OF FLOW CHANNEL (SHOWN IN PLATE IV-2) SHOWING ALMOST COMPLETE DISSOLUTION OF CALCITE

PLATE IV-4. CROSS-SECTIONAL VIEW OF YORKS JURASSIC SANDSTONE CORES BEFORE (LEFT) AND AFTER (RIGHT) 1000 PSI, 80°C CARBONATED WATER FLOOD. THE FLOODED CORE SHOWS UNIFORM DISSOLUTION OF CARBONATE.

the apparent homogeneous nature of the sandstone prior to the carbonated water flood, while Plates IV-2 and IV-3 show, at different magnifications, the preferentially dissolved flow channel formed during the test.

As expected, the calcium concentration in the core effluent from this test was very much higher than in the base liquid tests, indicating increased calcite dissolution. Initially it was highest as fairly substantial dissolution took place in the early stages of the test, but steadily fell, presumably as the channel formed and the bulk of the liquid flowed through a zone gradually depleted of calcite.

The second carbonated water flood was also carried out at 1,000 psi pressure, but the system temperature raised to 80°C, a more realistic reservoir temperature, to investigate the heating effect on dissolution. The result is presented in Figure IV-4.

Although a similar order of permeability increase to that from the 20°C test was obtained, there was a marked difference in the calcium effluent concentration profile. A lower and far more constant concentration was obtained. Examination of the flooded core showed the constant level of calcium concentration was due to a much more uniform dissolution of carbonate (as shown in Plate IV-4), as opposed to any channel effect, having taken place. The lower level was expected in that calcite solubility decreases with increasing temperature at constant pressure.

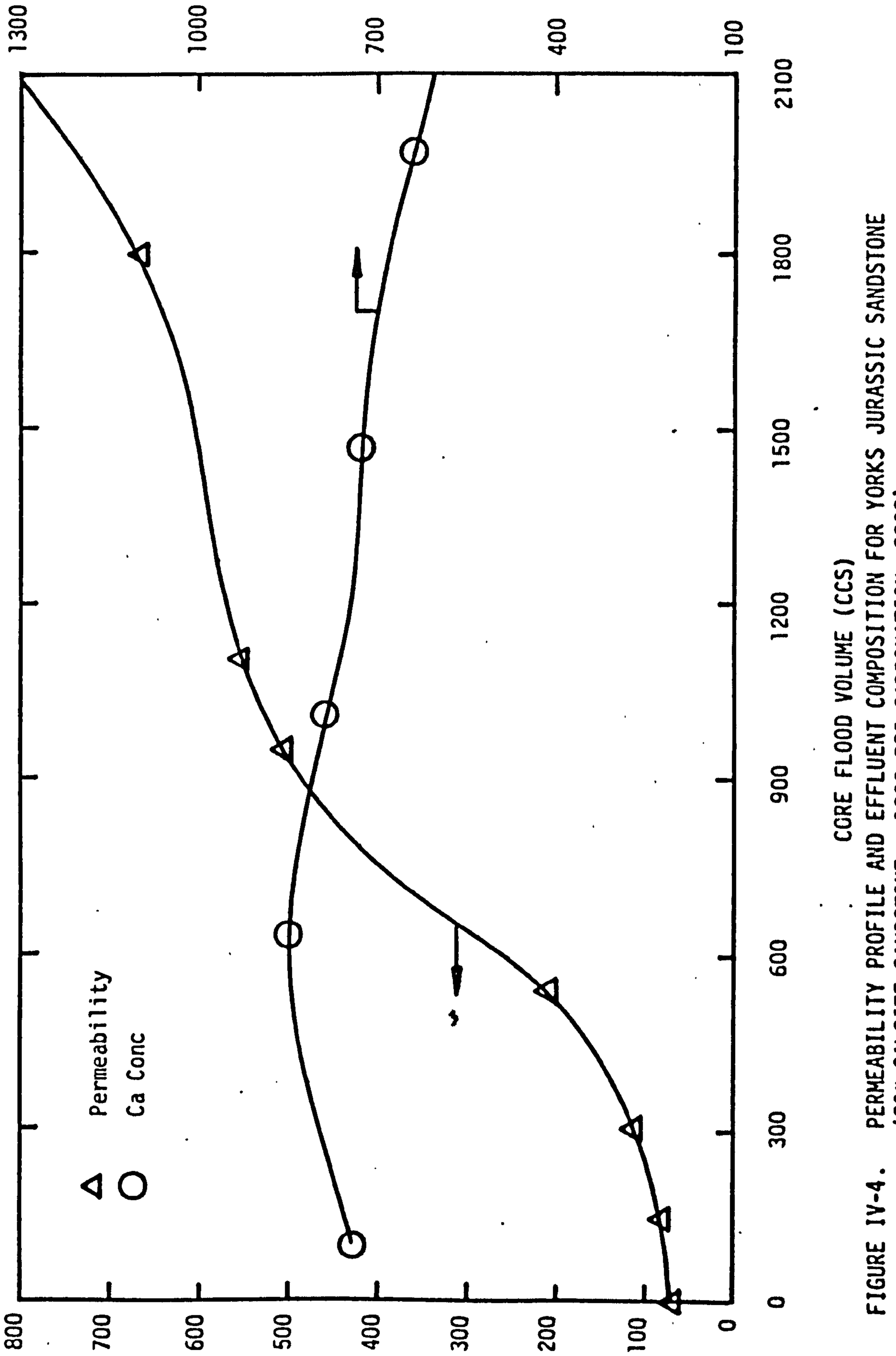

FIGURE IV-4. PERMEABILITY PROFILE AND EFFLUENT COMPOSITION FOR YORKS JURASSIC SANDSTONE (20% CALCITE SANDSTONE; 1000 PSI CARBONATION, 80°C)

At this stage in order to determine whether the flowing carbonated water solution was reaching chemical equilibrium with the calcite in the core, the mass of calcite dissolved in this test was calculated from the calcium effluent concentrations. The mass dissolved per volume of carbonated water injected was found to agree almost identically with published data on calcite solubility in carbonated water (13), thus indicating that complete equilibrium was being maintained at the order of flow rates being used. This result further verifies data published by Sippel and Glover (49), who found equilibrium between calcite and carbonated water to be maintained for flow rates as high as 400 ml/hour. Also, according to Weyl's theory of calcite solution kinetics (50), equilibrium should be attained for flow rates in excess of 760 ml/hour, three times the maximum used in this study.

To gain an understanding of the variation in permeability along the length of core, the cores from the first four tests were retrieved after flooding and cut into three 2.5 cm long segments. The permeability of each segment was then measured and plotted, as a ratio of the original whole-core permeability, against axial position in the core.

The plots for the brine test and the low temperature carbonated brine test are compared in Figure IV-5. The profiles clearly show the effect of carbonation of the brine on the core permeability increases, but more importantly demonstrate the characteristic shape of axial permeability variation profile obtained throughout this investigation.

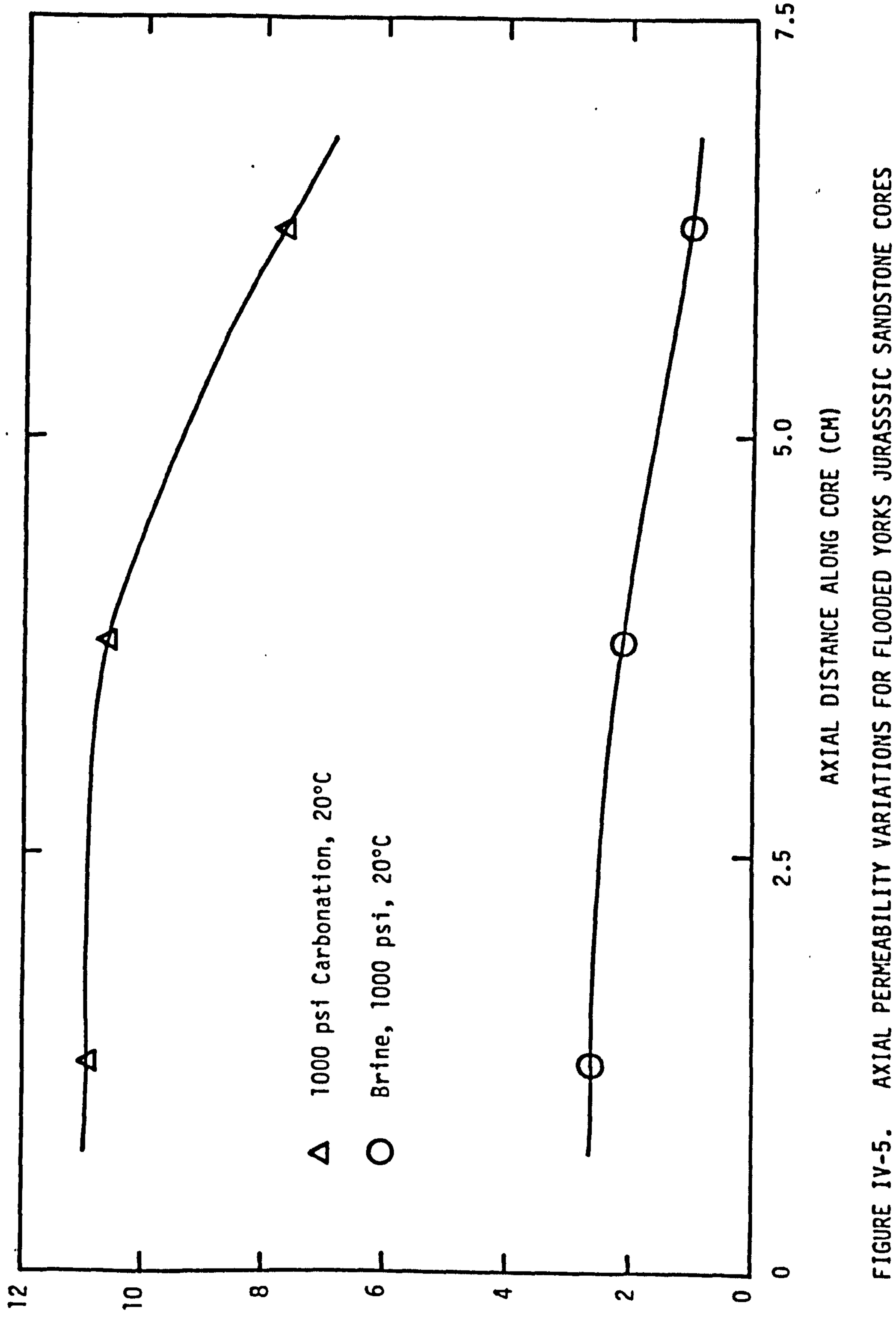

FIGURE IV-5. AXIAL PERMEABILITY VARIATIONS FOR FLOODED YORKS JURASSIC SANDSTONE CORES

The location of a profile is simply determined by the volume of carbonated water injected through a core, or for identical core flood volumes (as in Figure IV-5), by the carbonation level of the brine.

The typical profile shape, indicating a progressively lower stimulation effect from inlet to outlet core faces, implies that a zone or front of increasing permeability was moving through the cores during testing. Similar, though more dramatic results, were obtained by Lund (51) in linear core flood acidisation experiments.

The porosity and pore size distribution of each of the 2.5 cm long core segments were also measured, and compared to initial whole-core values. Generally, it was found that although large increases in the permeability had occurred, the porosity had changed little. This result illustrates that the main mechanism for the increase in permeability was probably not the uniform dissolution of carbonate cement but rather the removal of constrictions between the larger pores. This is confirmed by the mercury porosimeter pore size distribution results, which show that it was primarily the diameters of the larger pores (as shown for the low temperature carbonated water flood in Figure IV-6) that were increased during the tests.

To more realistically evaluate dissolution effects under CO_2 flood conditions two flood tests were then carried out at 3,000 psi carbonation pressure and 80°C. In the first clean core material was used, while in the second the core contained an artificial residual oil

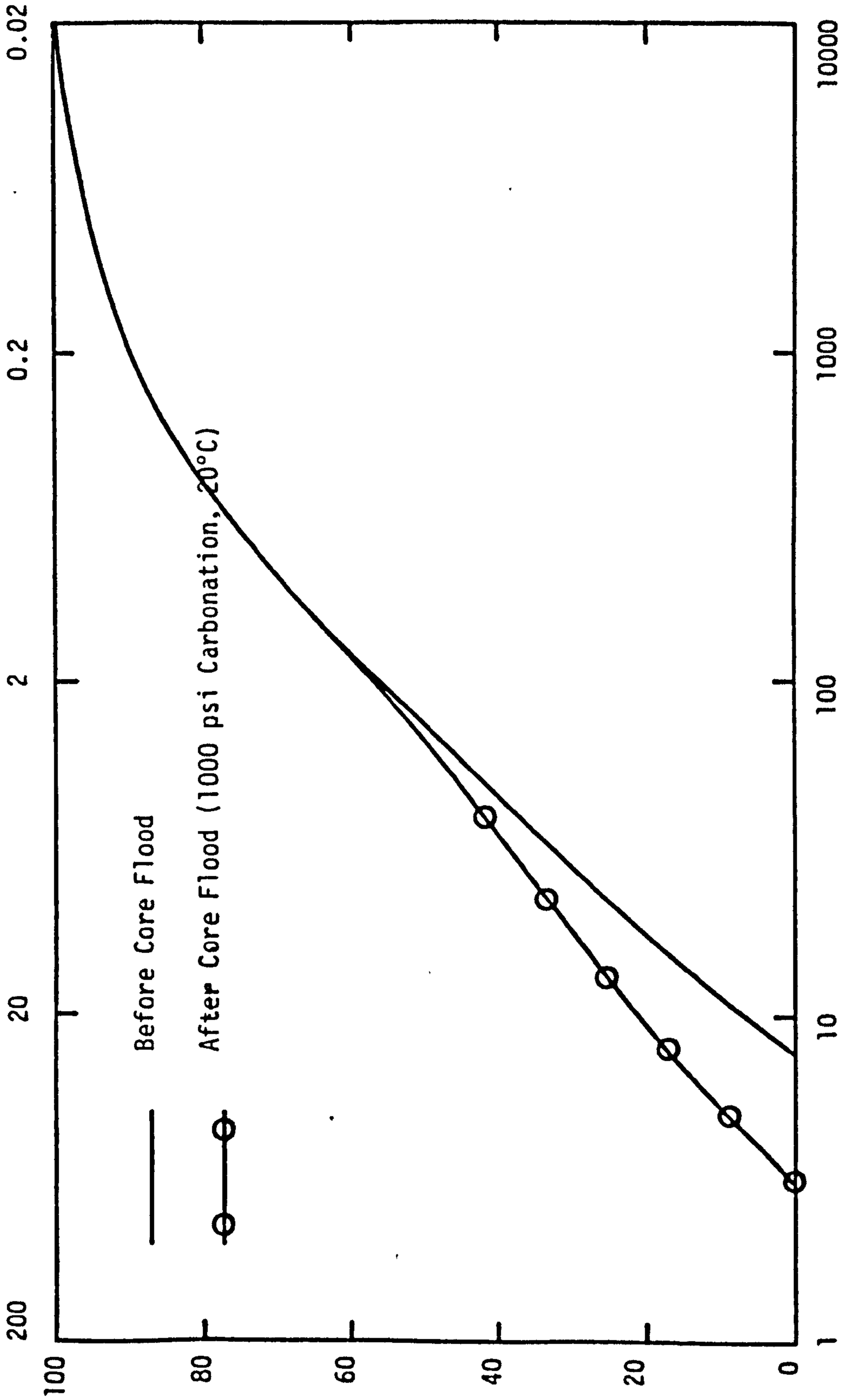

FIGURE IV-6. PORE SIZE DISTRIBUTIONS FOR YORKS JURASSIC SANDSTONE

saturation (Section 3.7). The results are presented in Figures IV-7 and IV-8, an obvious difference from the 1,000 psi results being the levelling off in the rate of permeability increases obtained.

In both Figures the permeability and calcium effluent concentration profiles are seen to be very closely related. The profiles show that in the early stages of the tests, the permeabilities rose gradually as the readily available calcite was dissolved. Then, when the carbonated water had dissolved most of the calcite flow constrictions, the permeabilities increased rapidly. In the latter test stages, there was a fall in the rate of permeability increase as readily dissolvable calcite became less available for extraction, with in the case of the oil containing core, the permeability levelling off completely.

The cores from both tests showed evidence of channel dissolution. In particular one main flow channel was formed over the length of the core in each test, as shown by the divided core segments in Plates IV-5 and IV-6. Although some of the voids in the core segments were formed by disintegration of uncemented material during cutting, they represent areas of preferential dissolution. The uncemented quartz grains around the flow channel are clearly visible in Plate IV-7, a close up of the void and surrounds in the fifth segment from the clean core.

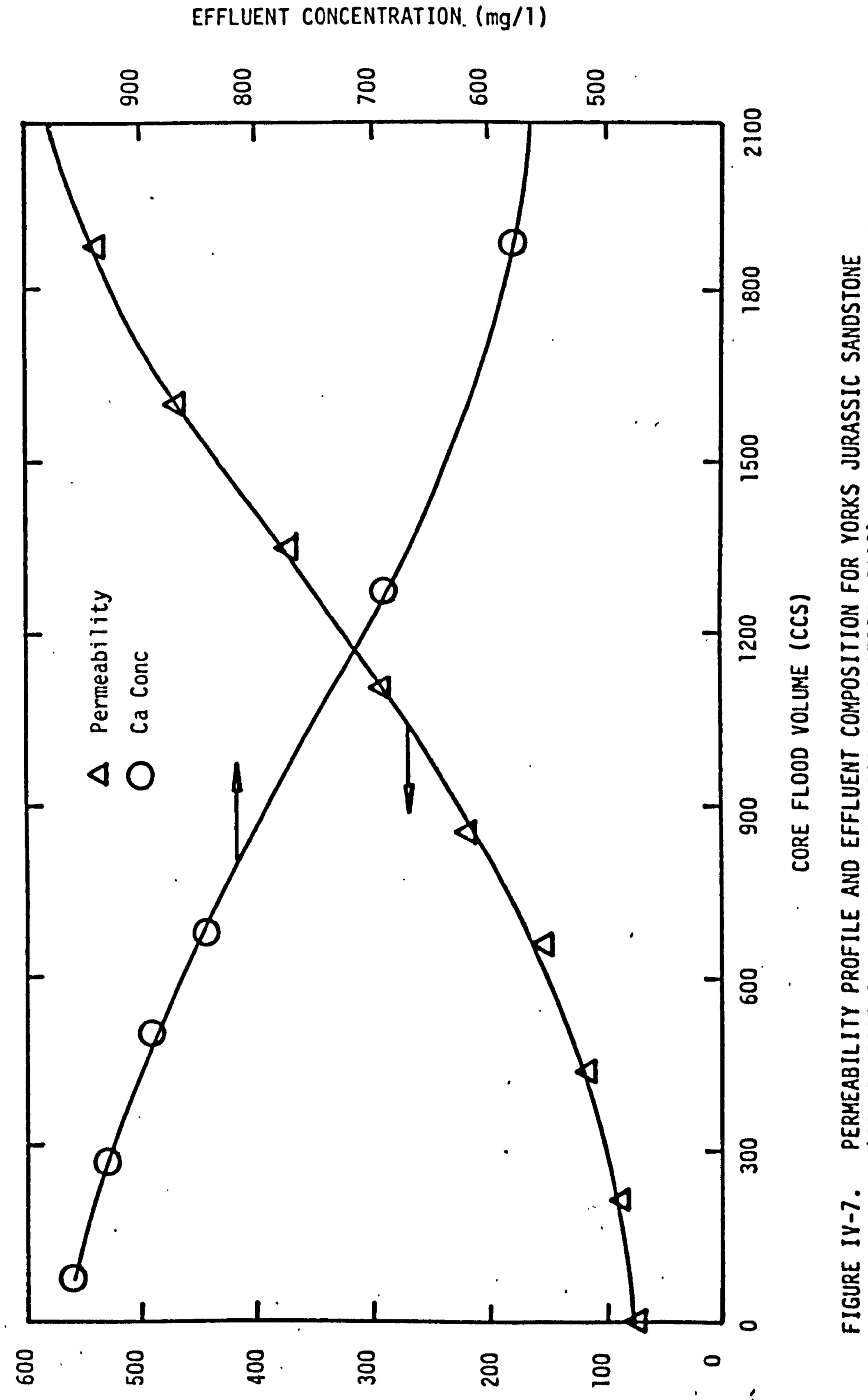

FIGURE IV-7. PERMEABILITY PROFILE AND EFFLUENT COMPOSITION FOR YORKS JURASSIC SANDSTONE (20% CALCITE SANDSTONE; 3000 PSI CARBONATION, 80°C)

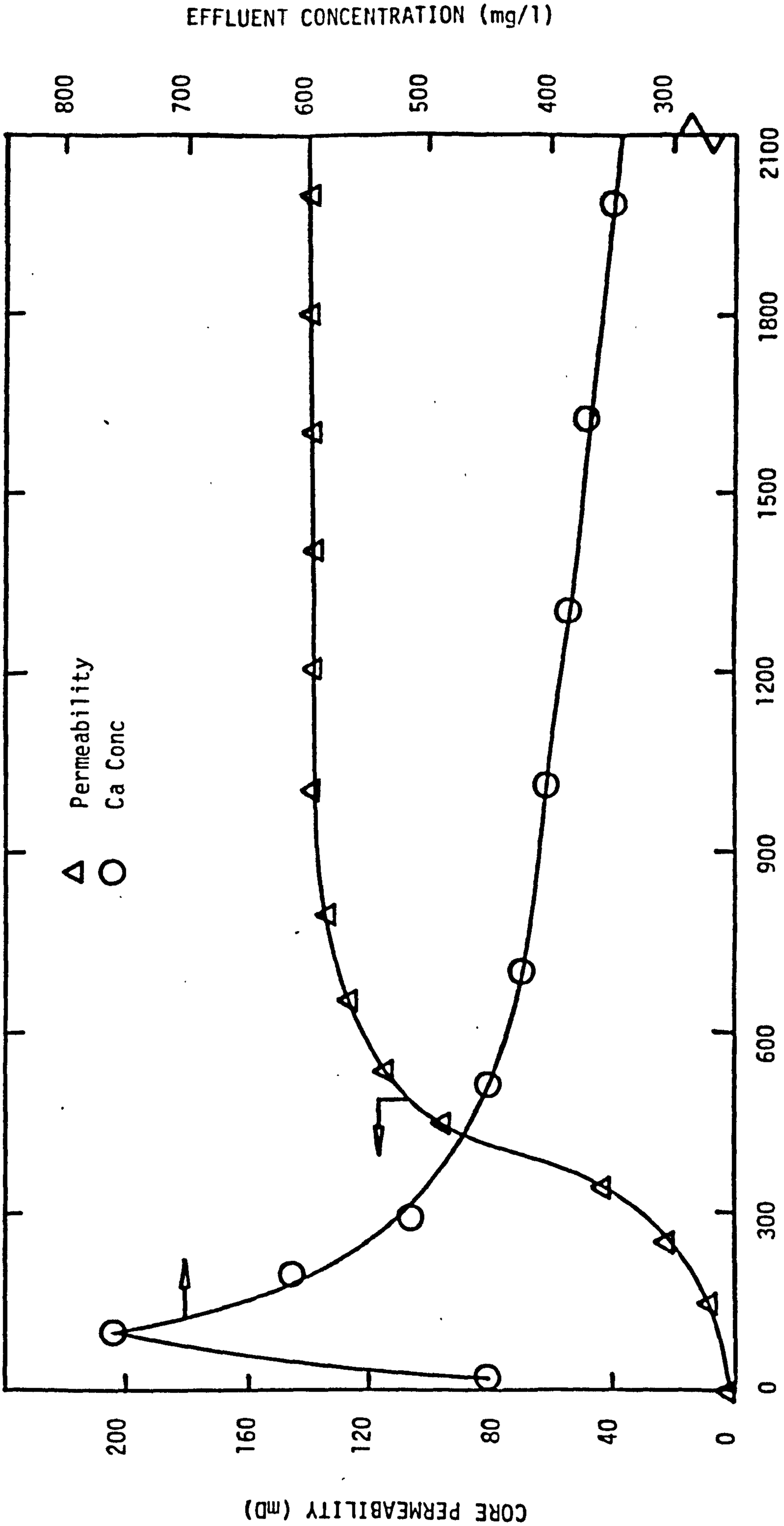

FIGURE IV-8. PERMEABILITY PROFILE AND EFFLUENT COMPOSITION FOR YORKS JURASSIC SANDSTONE (20% CALCITE SANDSTONE CONTAINING OIL; 3000 PSI CARBONATION, 80°C)

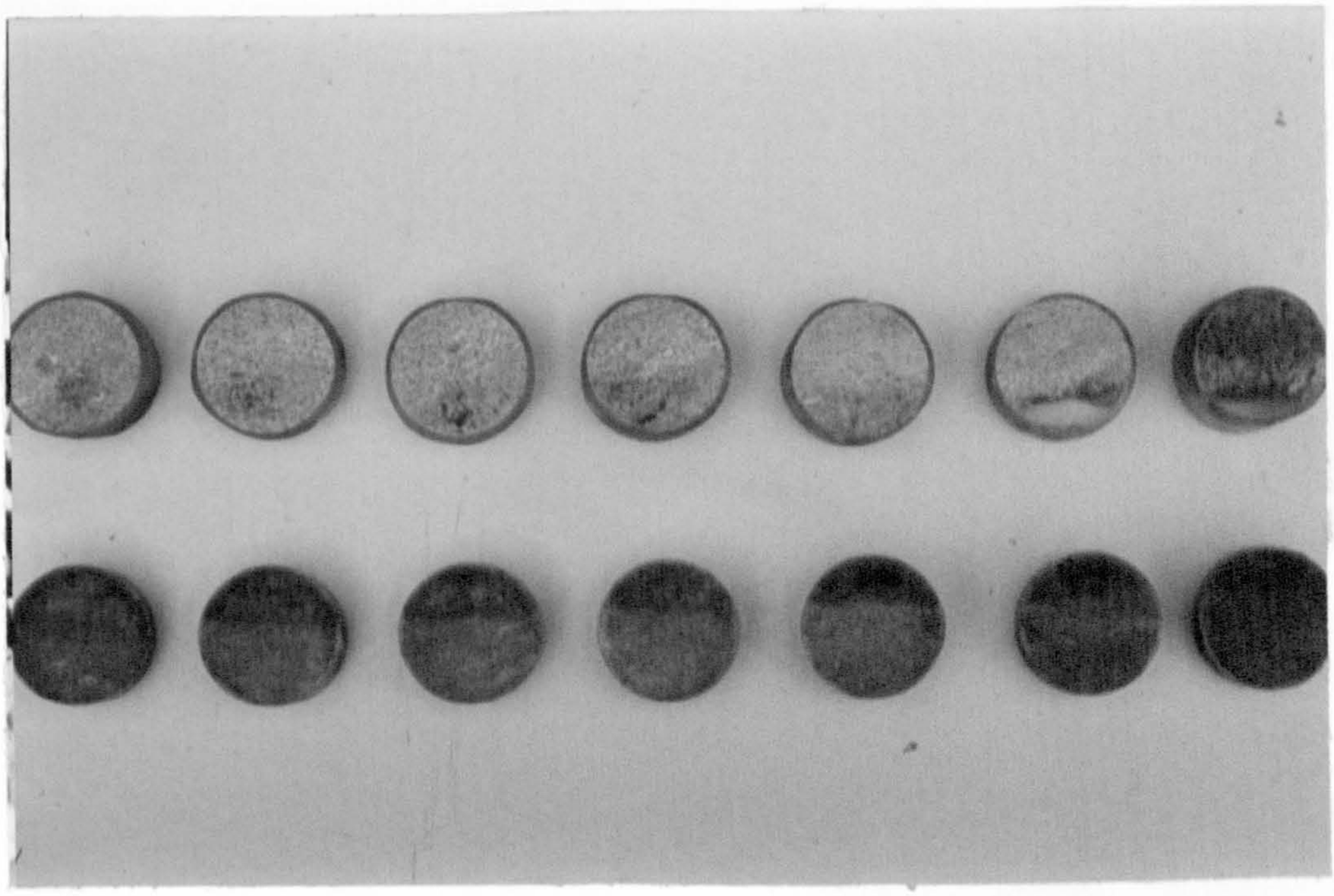

PLATE IV-5. CORE SEGMENTS FROM 3000 PSI, 80°C CARBONATED WATER FLOODS FROM INLET FACE (RIGHT) TO OUTLET FACE (LEFT). THE TOP ROW OF SEGMENTS ARE FROM THE CLEAN CORE AND THE BOTTOM ROW FROM THE OIL CONTAINING CORE

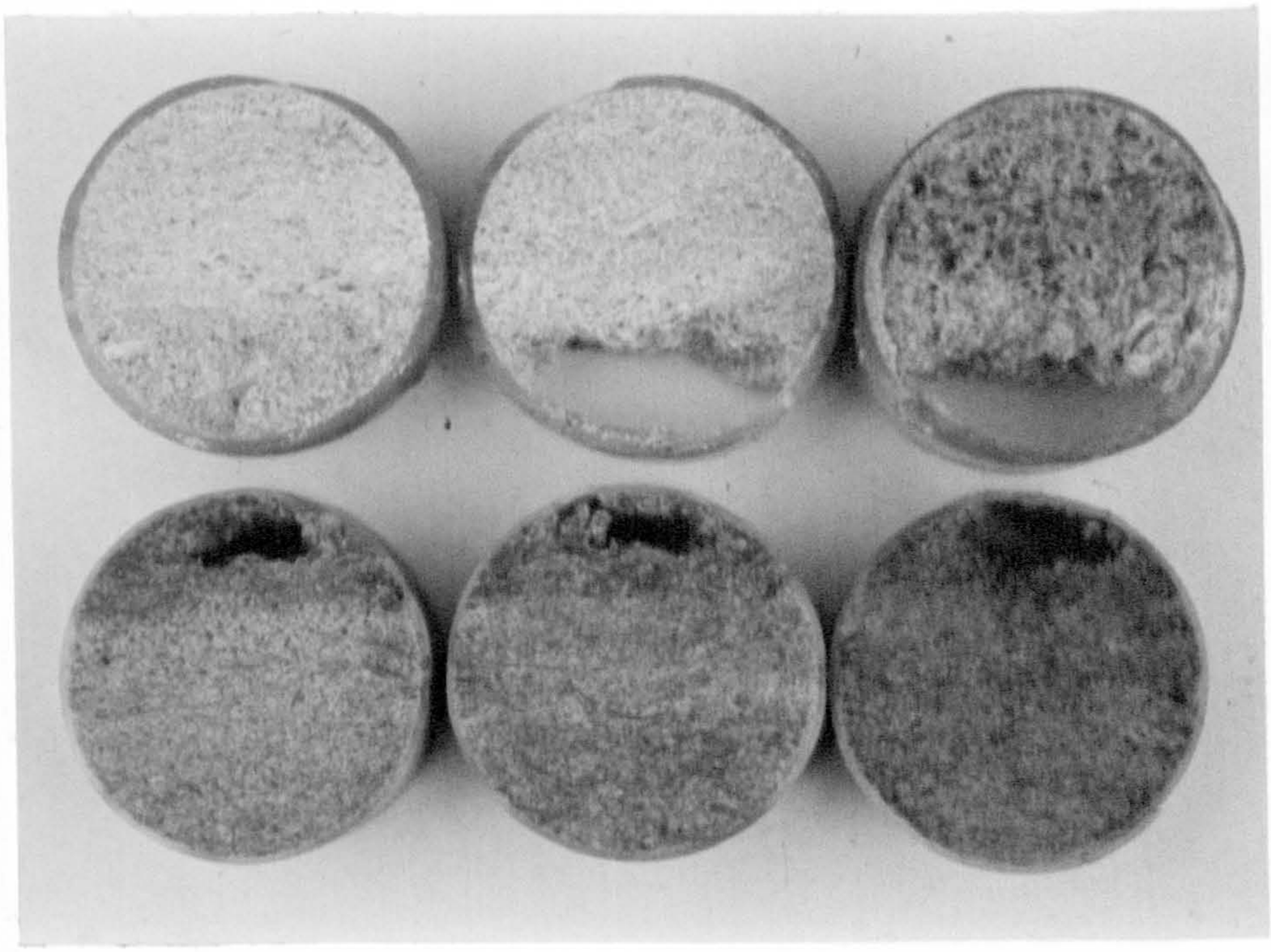

PLATE IV-6. CLOSE-UP OF THE FIRST THREE SEGMENTS FROM THE CLEAN CORE SHOWN IN PLATE IV-5

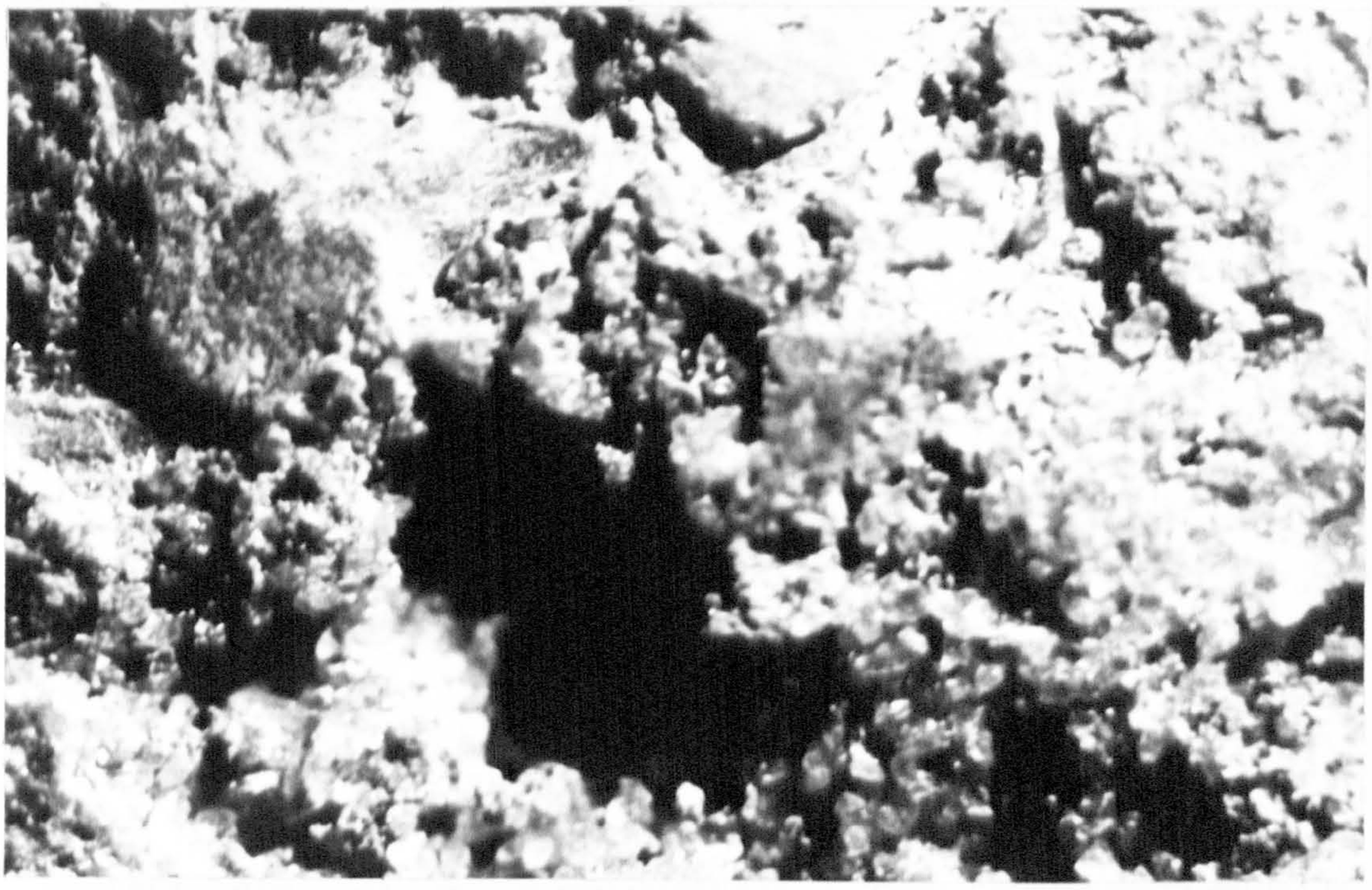

PLATE IV-7. CLOSE-UP OF FLOW CHANNEL IN CORE SEGMENT FIVE FROM 3000 PSI, 80°C CARBONATED WATER FLOOD ON CLEAN YORKS JURASSIC SANDSTONE CORE. THE CHANNEL IS SURROUNDED BY UNCEMENTED QUARTZ GRAINS

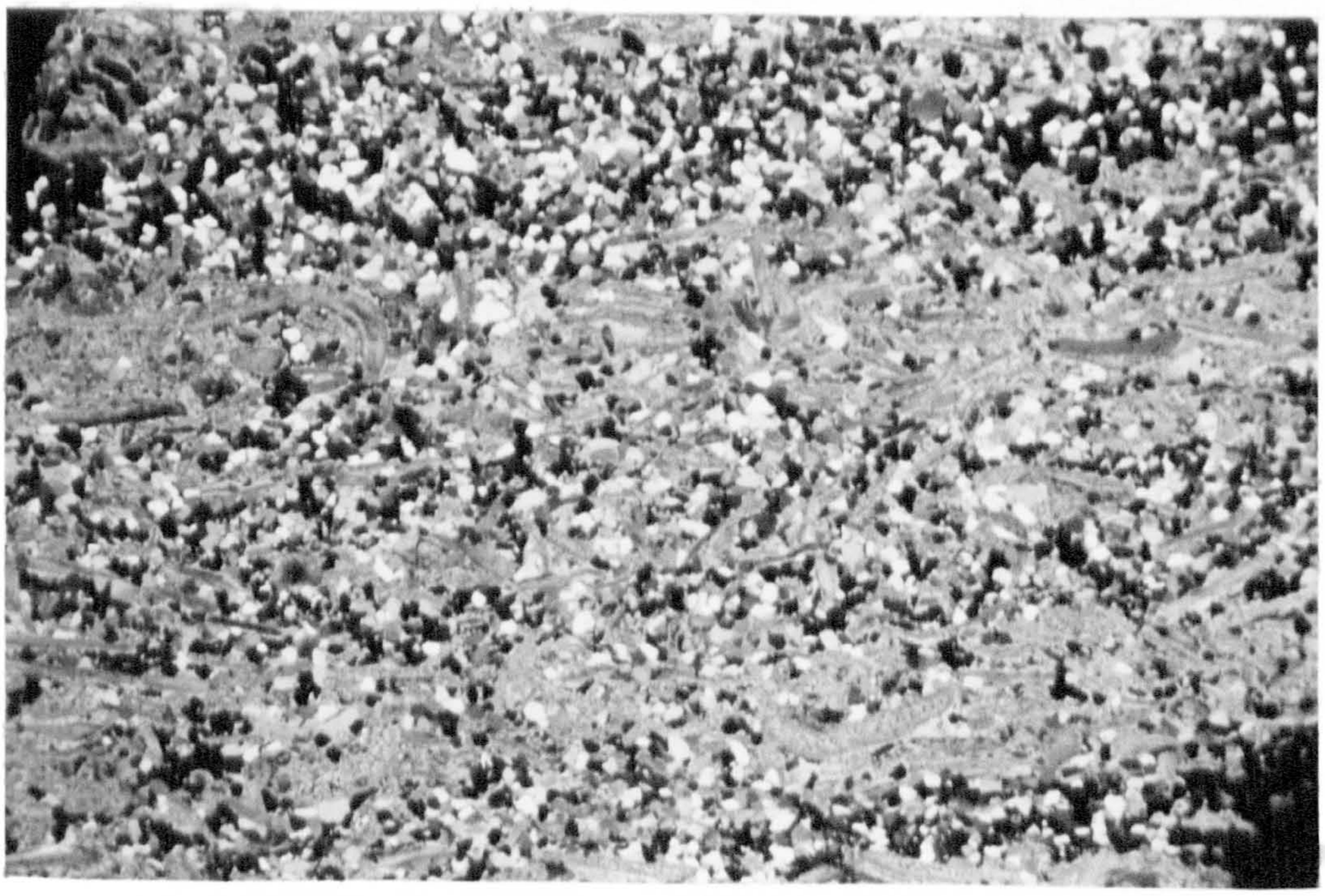

PLATE IV-8. PHOTOMICROGRAPH; CROSSED NICOLS, X 2.5 MAGNIFICATION. SUPPLEMENTARY FLOW CHANNELS FORMED DURING 3000 PSI, 80°C CARBONATED WATER FLOOD ON CLEAN YORKS JURASSIC SANDSTONE CORE

The effluent calcium concentration from the test on the oil containing core was initially very much lower than in the clean core test. This was presumably due to an oil "screening" effect on calcite dissolution. The transfer of CO_2 from the carbonated water to the crude oil, leading to the displacement (by viscosity reduction) of the crude, meant little calcite dissolution occurred in the early test stages. On removal of the crude oil, the channel dissolution mentioned previously took place, leading to attainment of constant permeability upon injection of only 900 ccs of carbonated water.

Further thin section analyses of the flooded cores revealed that in addition to the major channel formed in both experiments, a series of supplementary minor channels had begun to form in the clean core (Plate IV-8) but not in the oil containing core. This suggests that the continuing slow rise in permeability laterally in the clean core test was due to secondary channel formation. Also, in the oil containing core test, the complete levelling off in the permeability indicates that dissolution was effectively complete with the permeability front having "broken-through" to the outlet core face. In the latter stages of the test, the bulk of the flow must have occurred through the formed calcite depleted channel.

4.3 Fife Carboniferous Sandstone (A)

The second series of core flood tests were carried out on a sandstone from the Fife Carboniferous containing 10% dolomite cement. Fully carbonated water was used throughout. The permeability

profiles for two of the tests are presented in Figure IV-9.

The very slow reaction rate of dolomite under ambient temperature conditions meant virtually no dissolution effects were observed in a low temperature run at 1,000 psi pressure. An almost constant permeability was maintained throughout the test. Analyses of the core effluent for calcium and magnesium revealed that only a minimal amount of dolomite had been dissolved.

On the other hand, in a test carried out under more realistic CO_2 flood conditions (2,500 psi, 80°C), a significant permeability increase was obtained. This result was expected in that the rate of dolomite dissolution in carbonated water rapidly increases with increasing temperature.

Evidence for permeability front migration was again obtained from permeability measurements on the flooded core segments (Figure IV-10). However, the continued permeability increase in the latter stages of the test showed that permeability front breakthrough did not occur, and that continued dissolution was taking place. The constant levels of calcium and magnesium in the core effluent, together with microscopic analyses of the flooded core, further indicated that the dolomite dissolution taking place was relatively uniform.

Porosity and pore size distribution analyses of the flooded core segments were again made, and found similar to the results obtained

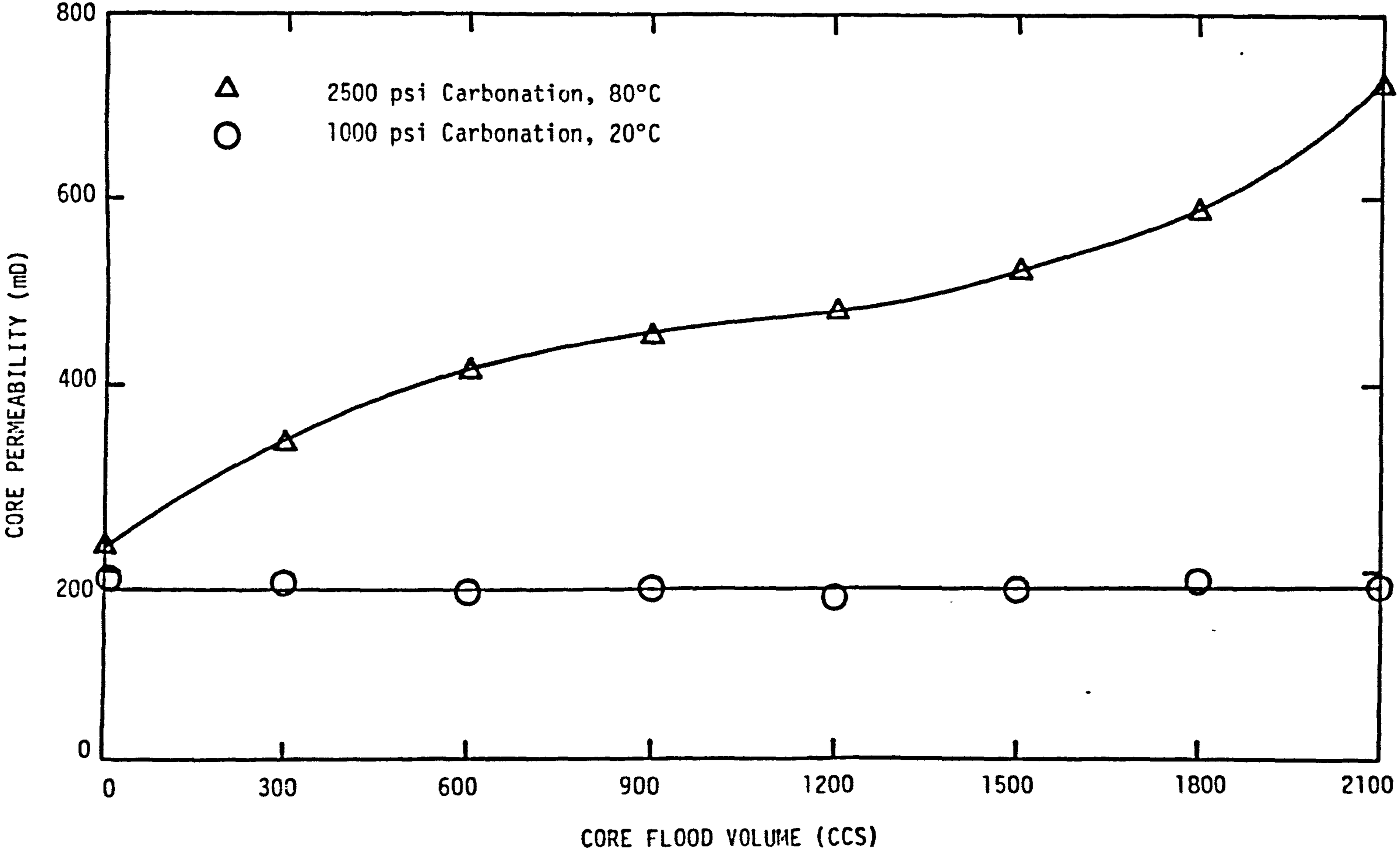

FIGURE IV-9. PERMEABILITY PROFILES FOR FIFE CARBONIFEROUS SANDSTONE (10% DOLOMITE SANDSTONE)

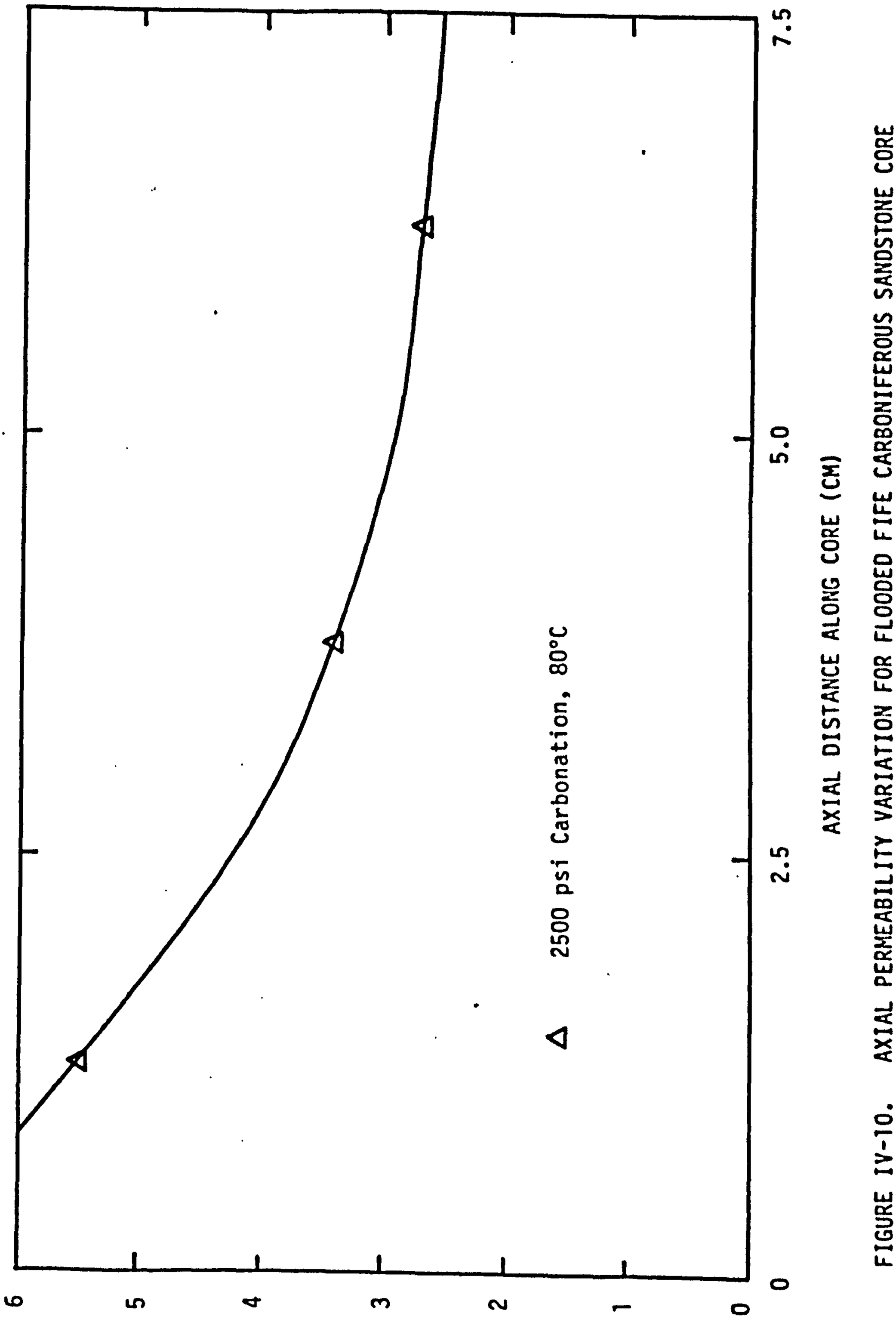

FIGURE IV-10. AXIAL PERMEABILITY VARIATION FOR FLOODED FIFE CARBONIFEROUS SANDSTONE CORE

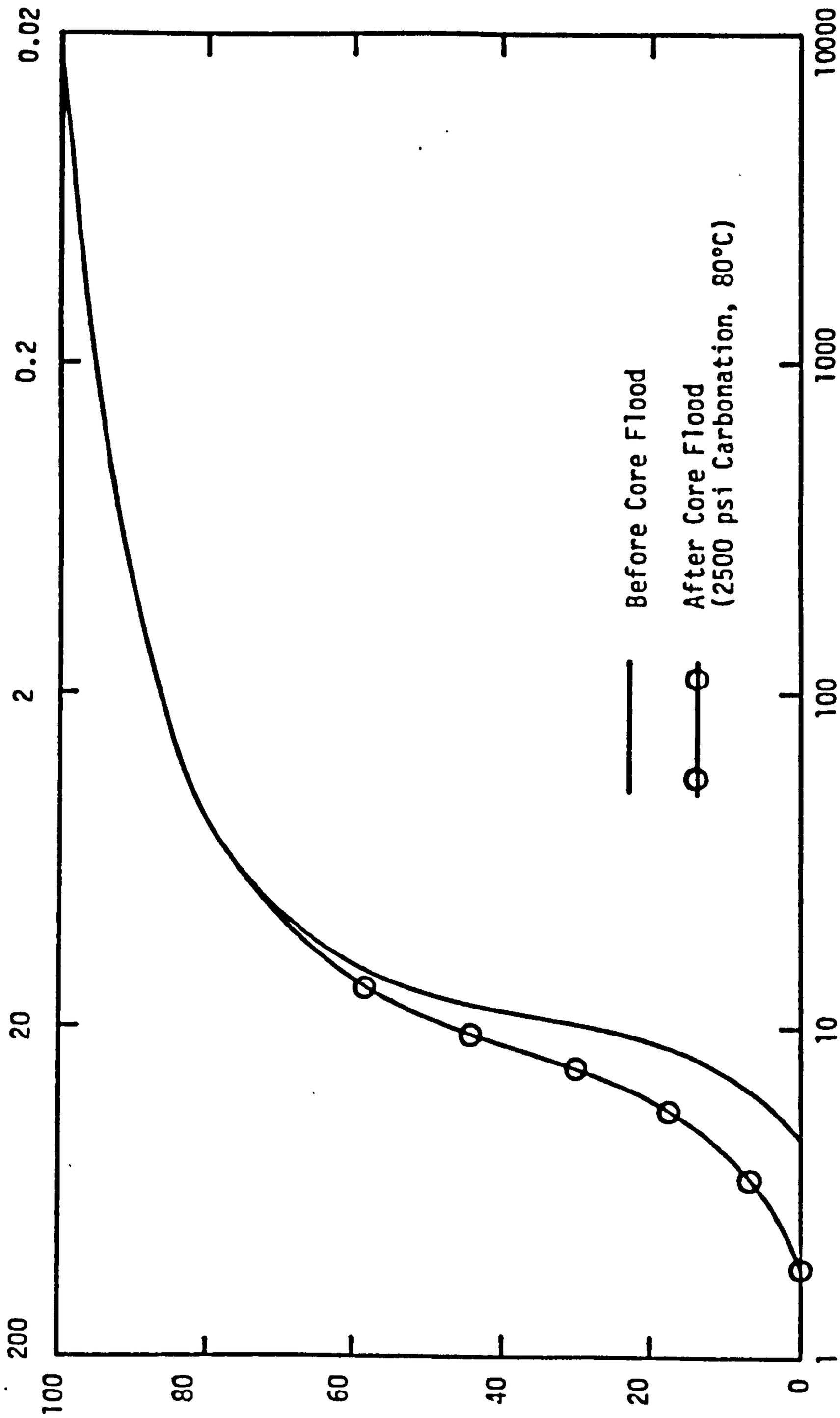

FIGURE IV-11. PORE SIZE DISTRIBUTIONS FOR FIFE CARBONIFEROUS SANDSTONE

from the Yorks Jurassic Sandstone tests. Only small increases in porosity were obtained, while again it was the larger pores that were selectively increased in diameter. The pore size distribution result for the first core segment as compared to that from unflooded material is presented in Figure IV-11.

4.4 Fife Carboniferous Sandstone (B)

A test with fully carbonated water at 3,500 psi and 80°C was carried out on a second sandstone from the Fife Carboniferous. This material, containing 3% dolomite cement, was considered more representative of reservoir sandstone in carbonate content. It was hoped to be possible to dissolve out all of the dolomite and obtain breakthrough of a permeability front.

However, although thin section comparisons of the unflooded and flooded material (Plates IV-9 and IV-10) show that virtually total dissolution of the dolomite took place in the test, the expected increase in permeability was not obtained. Rather a small decrease in permeability, from 17.6 mD to 16.7 mD was measured upon injection of 2,600 ccs or 370 pore volumes. However, this was assumed insignificant as error is often incurred calculating permeabilities from the differential pressure trace on the chart recorder.

Considering the mass of dolomite dissolved this result was somewhat surprising in that no permeability increase at all was obtained. It was probably attributable to the uniformly scattered occurrence

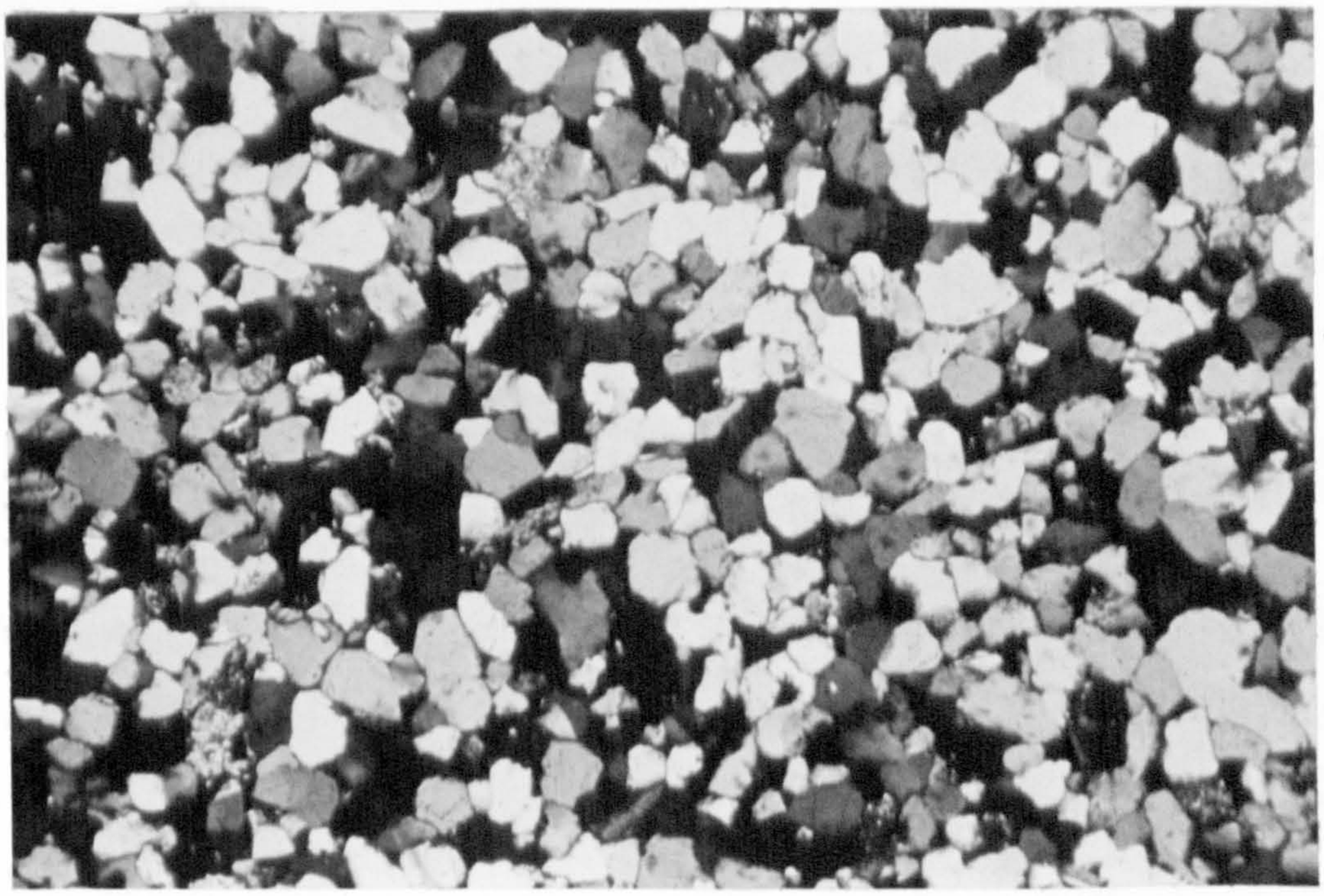

PLATE IV-9. PHOTOMICROGRAPH; CROSSED NICOLS, X4 MAGNIFICATION. FIFE CARBONIFEROUS SANDSTONE (B).

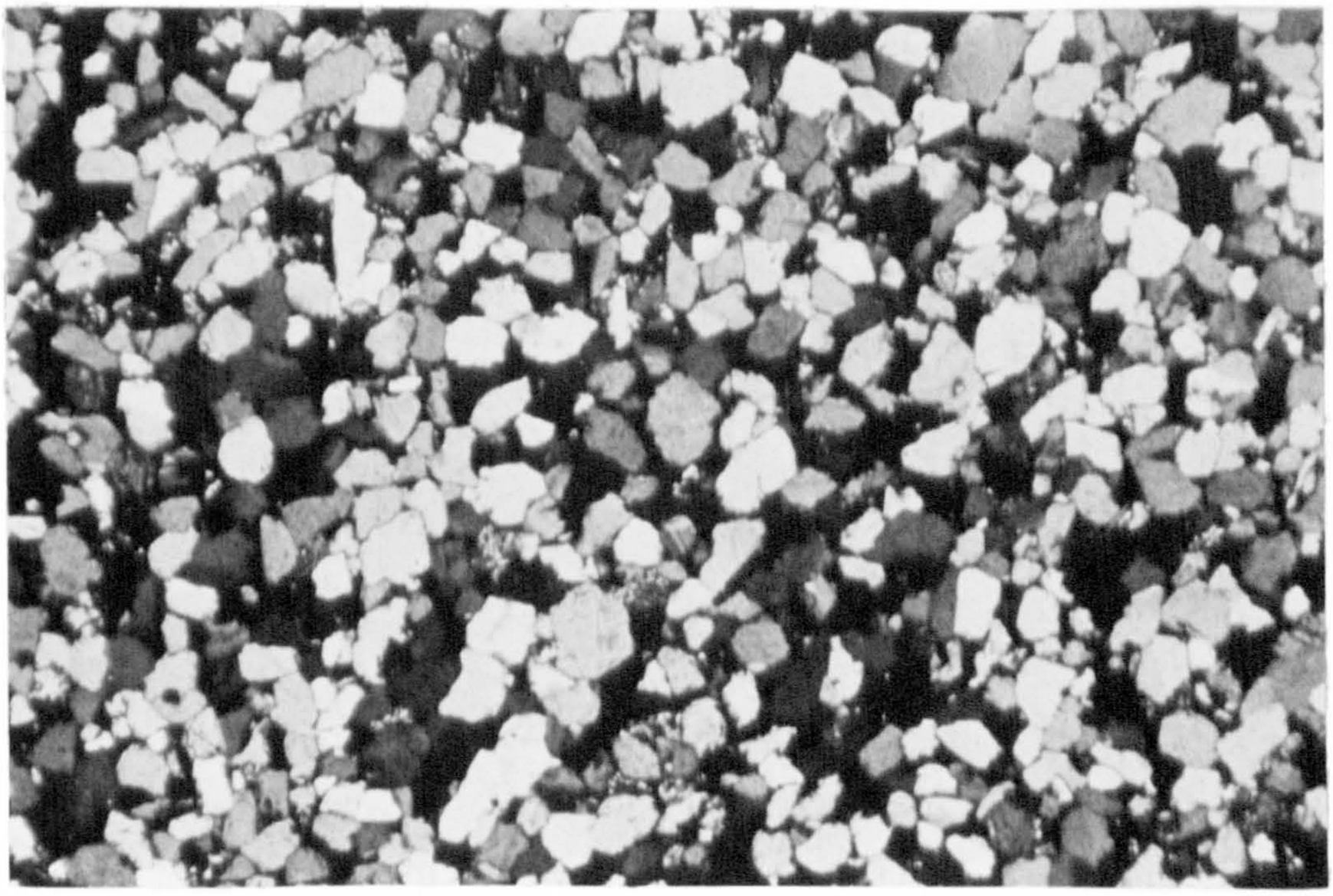

PLATE IV-10. PHOTOMICROGRAPH; CROSSED NICOLS, X4 MAGNIFICATION. FIFE CARBONIFEROUS SANDSTONE (B) AFTER 3500 PSI, 80°C CARBONATED WATER FLOOD

of the dolomite crystals in the sandstone. Had the dolomite been concentrated in a particular band or area, dissolution would have been expected to create additional flow channels and thereby increase permeability. As it was, removal of the scattered crystals had little stimulation effect.

4.5 Rotliegende Sandstone from Southern North Sea

Having obtained a variety of often unpredictable types of dissolution effect from core floods on sandstones collected from outcrop and quarries, a series of experiments were then initiated on reservoir sandstones. For the first of these Rotliegende material from a Southern North Sea gas field was used.

A number of tests over a range of carbonation pressure conditions were undertaken, all with similar results. The poorly consolidated, friable nature of the sandstone caused core disintegration/collapse to occur in each of the tests. Even at low pressure conditions it was impossible to complete a core flood. Core collapse, identified by a sharp rise in differential pressure across the core with a sudden drop in flow rate, was found to cause a complete barrier to flow.

One of the collapsed cores is shown in Plate IV-11, a mudcake blanket of disaggregated sand grains having formed over the outlet end plate of the core holder. The cause of the collapse was uncertain. It may simply have been due to disintegration under confining pressure, or to dissolution of calcite cement causing weakening, but a combination of both effects seems more likely.

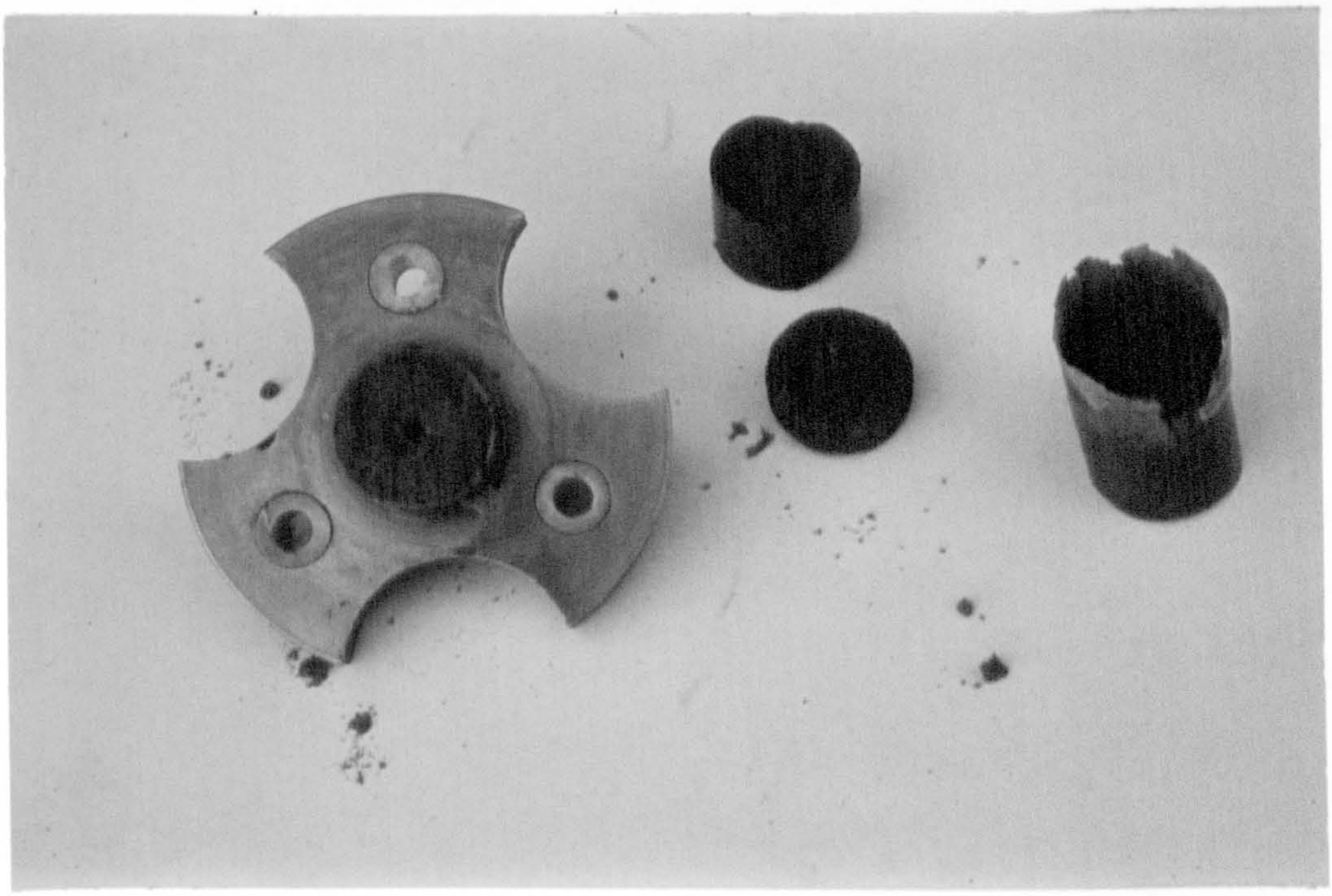

PLATE IV-11. COLLAPSED ROTLIEGENDE SANDSTONE CORE WITH MUDCAKE ON OUTLET END PLATE OF CORE HOLDER

4.6 Jurassic Sandstone from Northern North Sea

Four core tests were carried out on a reservoir sandstone from the Northern North Sea. As with the earlier Rotliegende material, the sandstone was poorly consolidated (Plate A 2-8) and so the test pressures were kept below 1,000 psi in an attempt to avoid core collapse. However, again it was found impossible to prevent collapse, although care was taken in simultaneously increasing the confining pressure and core pressure in a bid to avoid such an occurrence. Each test was abandoned in turn as the differential pressure across the core rose above the range of instrumentation.

4.7 Rotliegende Sandstone from Indefatigable Field

Following the series of core collapses obtained with poorly consolidated reservoir sandstone materials, a hard compact material from Indefatigable Field was obtained for testing. Although it was only possible to drill 5 cm long plugs from the core material, it was found to be much more durable, enabling a series of experiments to be completed. Fully carbonated water at 80°C was used throughout to try and maximise dissolution effects at reservoir temperature conditions.

For the first experiment a core was selected from the gas zone of the reservoir. It did not show any signs of oil presence and therefore was not cleaned. As the cores in previous tests had readily disintegrated, a low carbonation pressure of 1,000 psi was chosen.

The result is presented in Figure IV-12.

A gradual increase in permeability from 4.5 mD to 12.4 mD was obtained in conjunction with a steady fall in effluent calcium and magnesium concentrations. The rate of permeability increase in the latter stages of the test gradually declined, with a constant permeability value being attained upon injection of 2.0 litres. Attainment of constant permeability, together with the rapidly falling effluent ion concentrations, suggested that dissolution was complete either through depletion of dolomite or channel formation.

As shown in Plates IV-12 and IV-13 the former proved to be the case. In Plate IV-12 the sandstone prior to flooding is seen to contain isolated areas fully cemented by large dolomite crystals together with uniformly distributed smaller dolomite crystals. Plate IV-13 shows that on completion of the test the readily dissolvable finer dolomite had been removed while the large crystals remained unaffected. It is also apparent from Plate IV-13 that any further dolomite dissolution would have been very small.

Prior to the preparation of thin sections, the core was divided into three, equal length segments and the permeability of each measured, as before, to examine local permeability variation. From the result in Figure IV-13, it can be seen that the increase in permeability obtained was uniform over the length of the core, indicating that breakthrough of a permeability front had occurred.

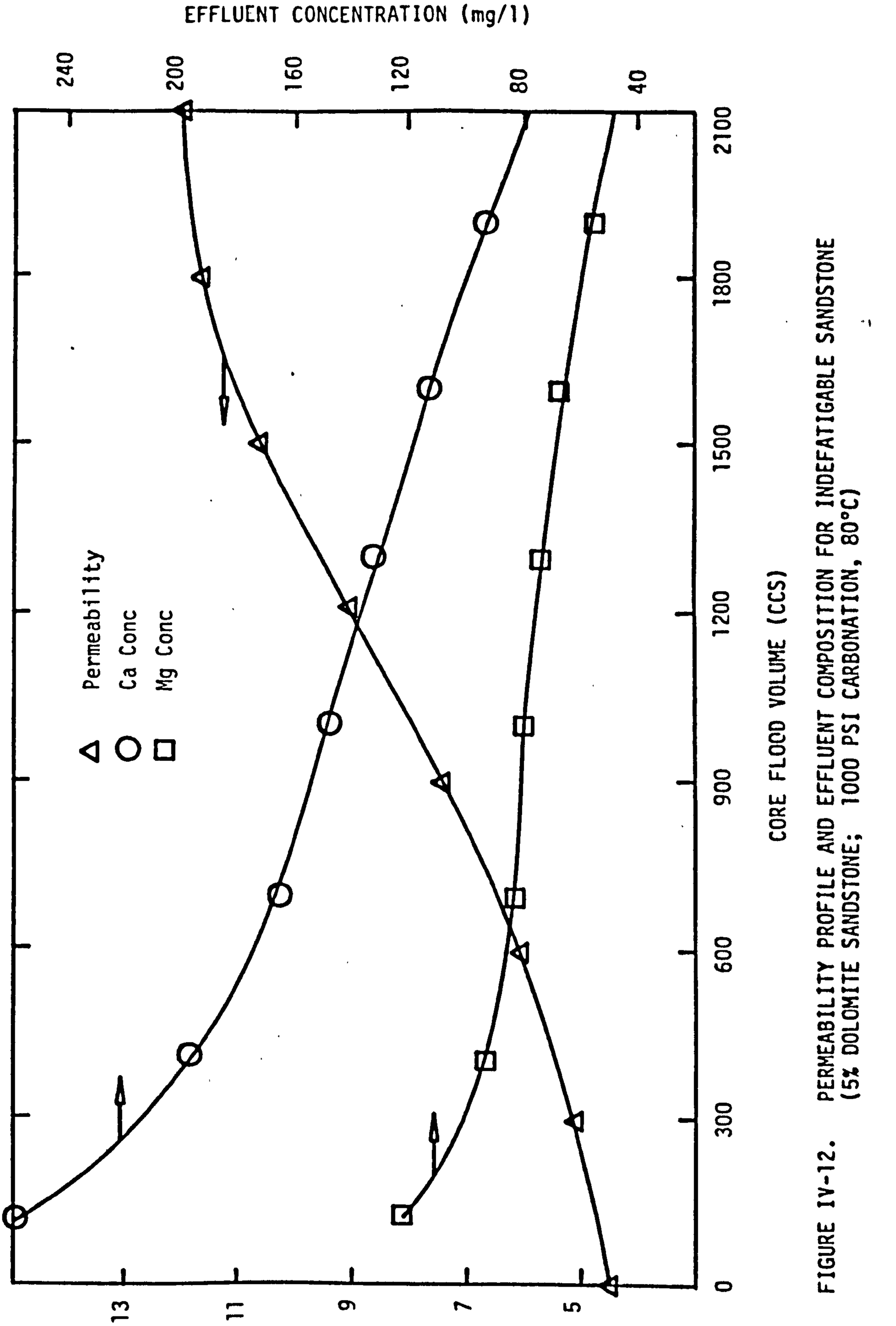

FIGURE IV-12. PERMEABILITY PROFILE AND EFFLUENT COMPOSITION FOR INDEFATIGABLE SANDSTONE
(5% DOLOMITE SANDSTONE; 1000 PSI CARBONATION, 80°C)

PLATE IV-12. PHOTOMICROGRAPH; CROSSED NICOLS, X2.5 MAGNIFICATION. INDEFATIGABLE SANDSTONE PRIOR TO 1000 PSI, 80°C CARBONATED WATER FLOOD. THE DOLOMITE OCCURS AS LARGE CRYSTALS AND MORE UNIFORMLY AS FINE PORE FILL

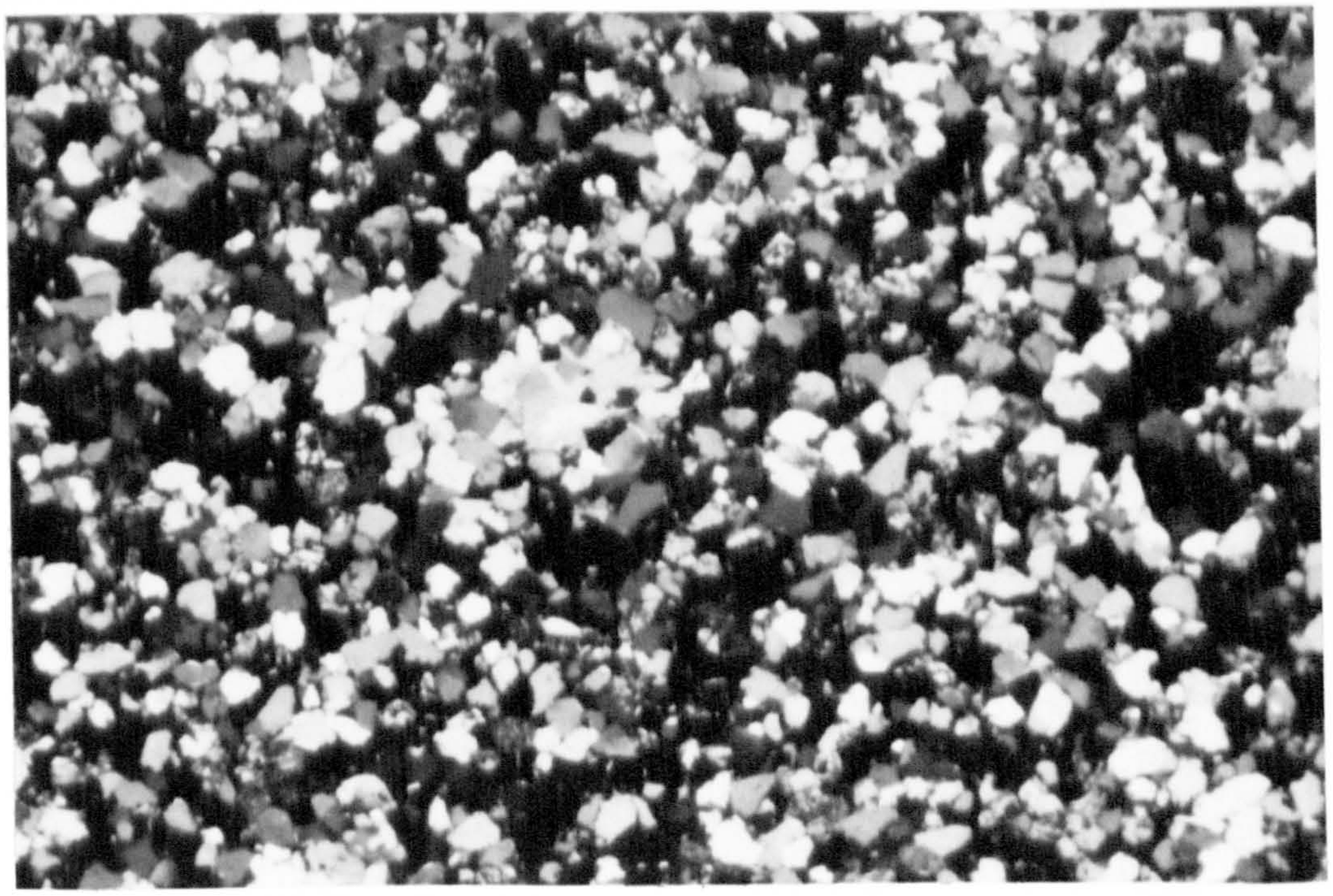

PLATE IV-13. PHOTOMICROGRAPH; CROSSED NICOLS, X3 MAGNIFICATION. INDEFATIGABLE SANDSTONE AFTER 1000 PSI, 80°C CARBONATED WATER FLOOD, SHOWING TOTAL DISSOLUTION OF FINE DOLOMITE CRYSTALS

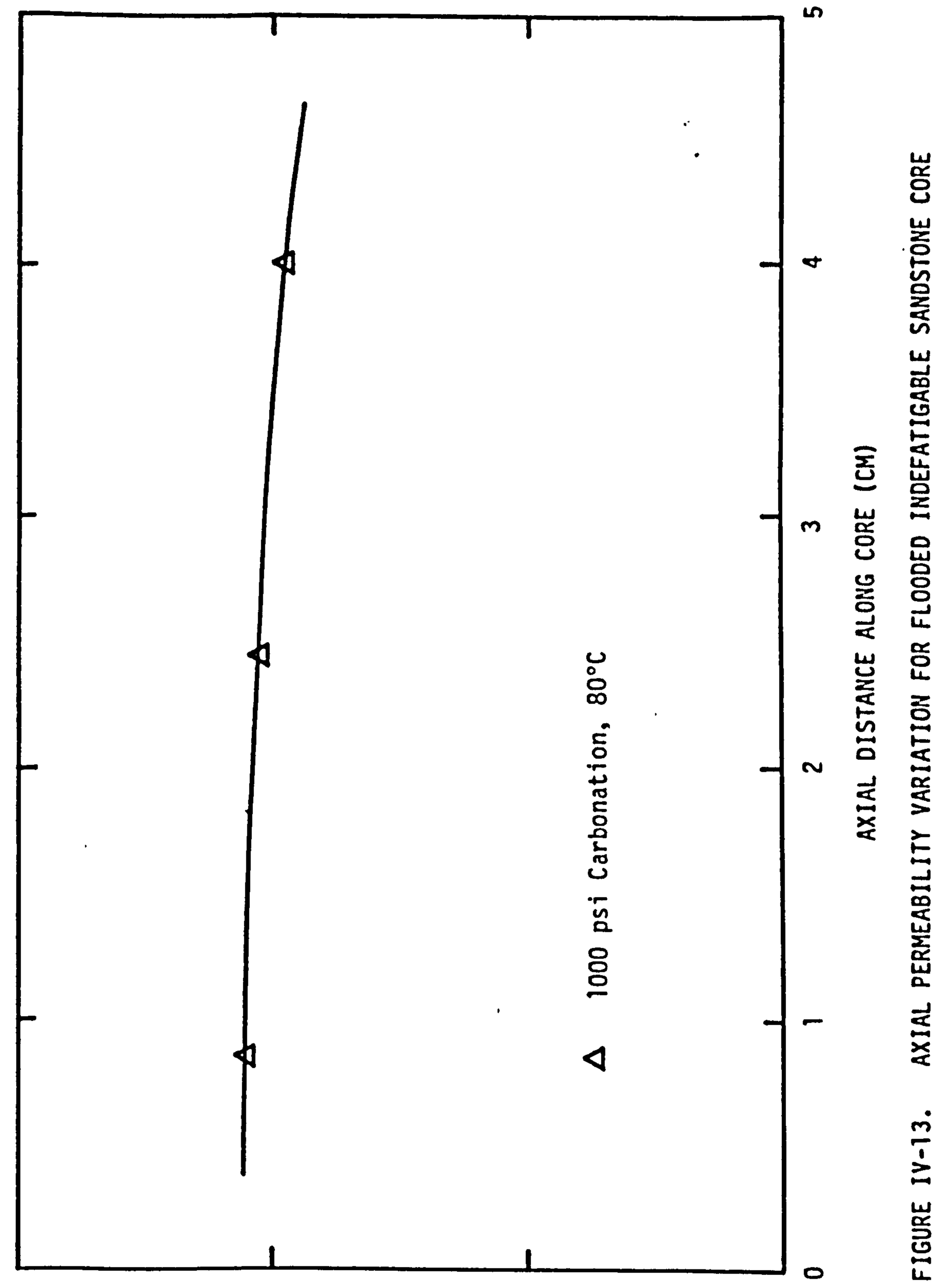

FIGURE IV-13. AXIAL PERMEABILITY VARIATION FOR FLOODED INDEFATIGABLE SANDSTONE CORE

The second test on Indefatigable material was carried out on a core from slightly higher up in the reservoir gas zone. The core contained a well defined 8 mm thick, coarse band running through the centre. It was considered that preferential dissolution would occur within this apparently permeable zone. The result of the test, carried out at an increased carbonation pressure of 2,000 psi, is presented in Figure IV-14.

Initially, the permeability rose steeply and the effluent ion concentrations were high as rapid dissolution took place. A steadily reduced dissolution effect, as indicated by the levelling of the permeability and ion concentration profiles, was then observed until breakthrough of a permeability front was reached on flowing 1,500 ccs. Examination of the flooded core showed that, as expected, preferential dissolution of the coarser band had occurred, being the likely explanation for early front breakthrough. Plates IV-14 and IV-15 were taken of the inlet core face prior to, and on completion of the test. In Plate IV-14 the coarse band is hardly visible, whereas upon preferential dissolution, in Plate IV-15 it is clearly defined.

Also, thin section comparisons of unflooded and flooded material (Plates IV-16 and IV-17) identify the preferential dissolution mechanism. The mass of crystalline dolomite cement in the fine layer on the left of the Plates is seen to be unaffected by dissolution, while as with the first test, in the coarse band the finer dolomite was removed and the large crystals left undissolved.

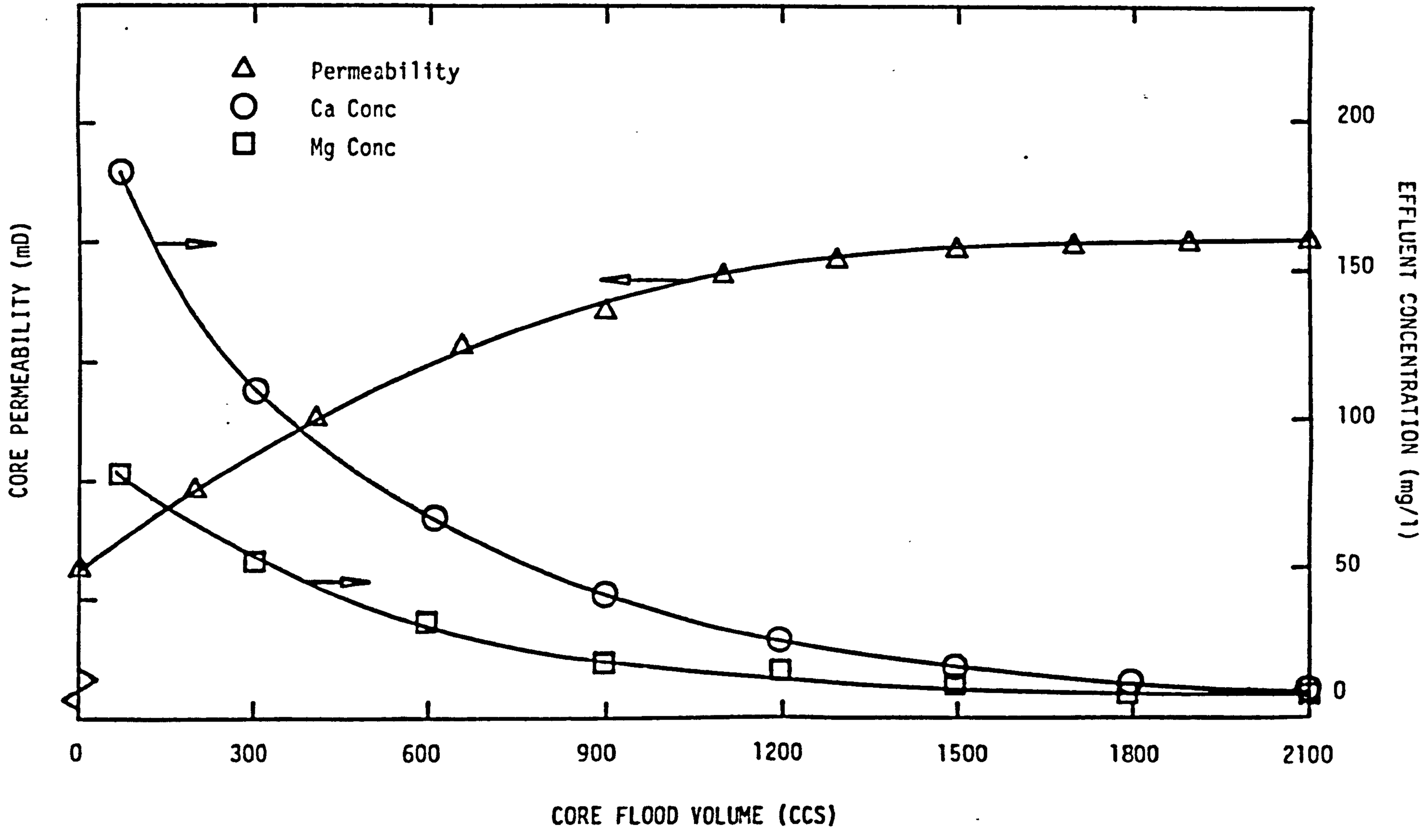

FIGURE IV-14. PERMEABILITY PROFILE AND EFFLUENT COMPOSITION FOR INDEFATIGABLE SANDSTONE (5% DOLOMITE SANDSTONE; 2000 PSI CARBONATION, 80°C)

PLATE IV-14. CLOSE-UP OF INLET CORE FACE PRIOR TO 2000 PSI, 80°C CARBONATED WATER FLOOD ON INTERLAYERED INDEFATIGABLE SANDSTONE

PLATE IV-15. INLET CORE FACE AFTER 2000 PSI, 80°C CARBONATED WATER FLOOD ON INTERLAYERED INDEFATIGABLE SANDSTONE, SHOWING CLEARLY DEFINED, PREFERENTIALLY DISSOLVED, COARSE LAYER

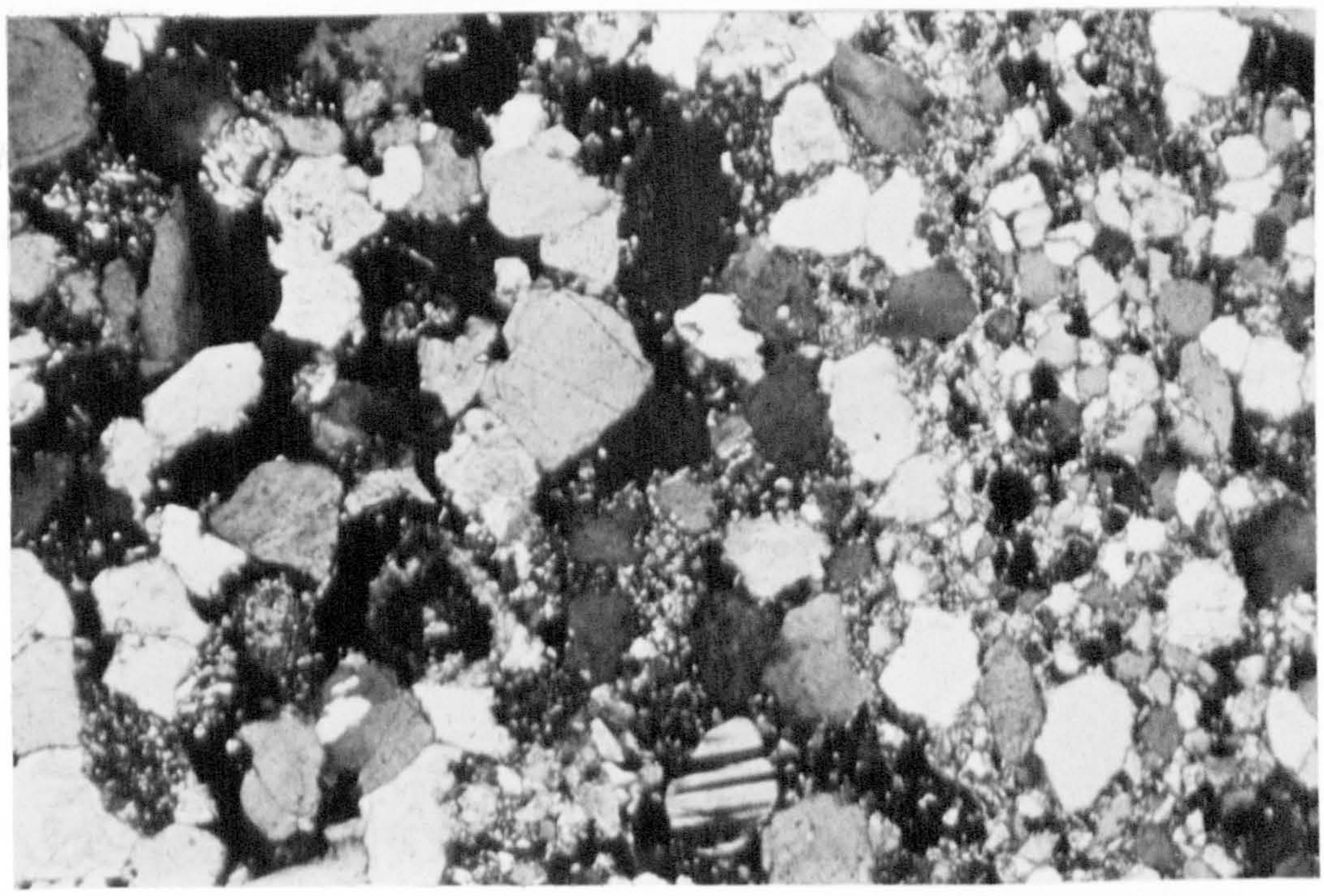

PLATE IV-16. PHOTOMICROGRAPH; CROSSED NICOLS, X4 MAGNIFICATION. INTERLAYERED INDEFATIGABLE SANDSTONE PRIOR TO 2000 PSI, 80°C CARBONATED WATER FLOOD. THE DOLOMITE OCCURS AS A UNIFORM PORE FILL IN THE FINE LAYER AND MORE SPORADICALLY AS SMALL AND LARGE CRYSTALS IN THE COARSE LAYER

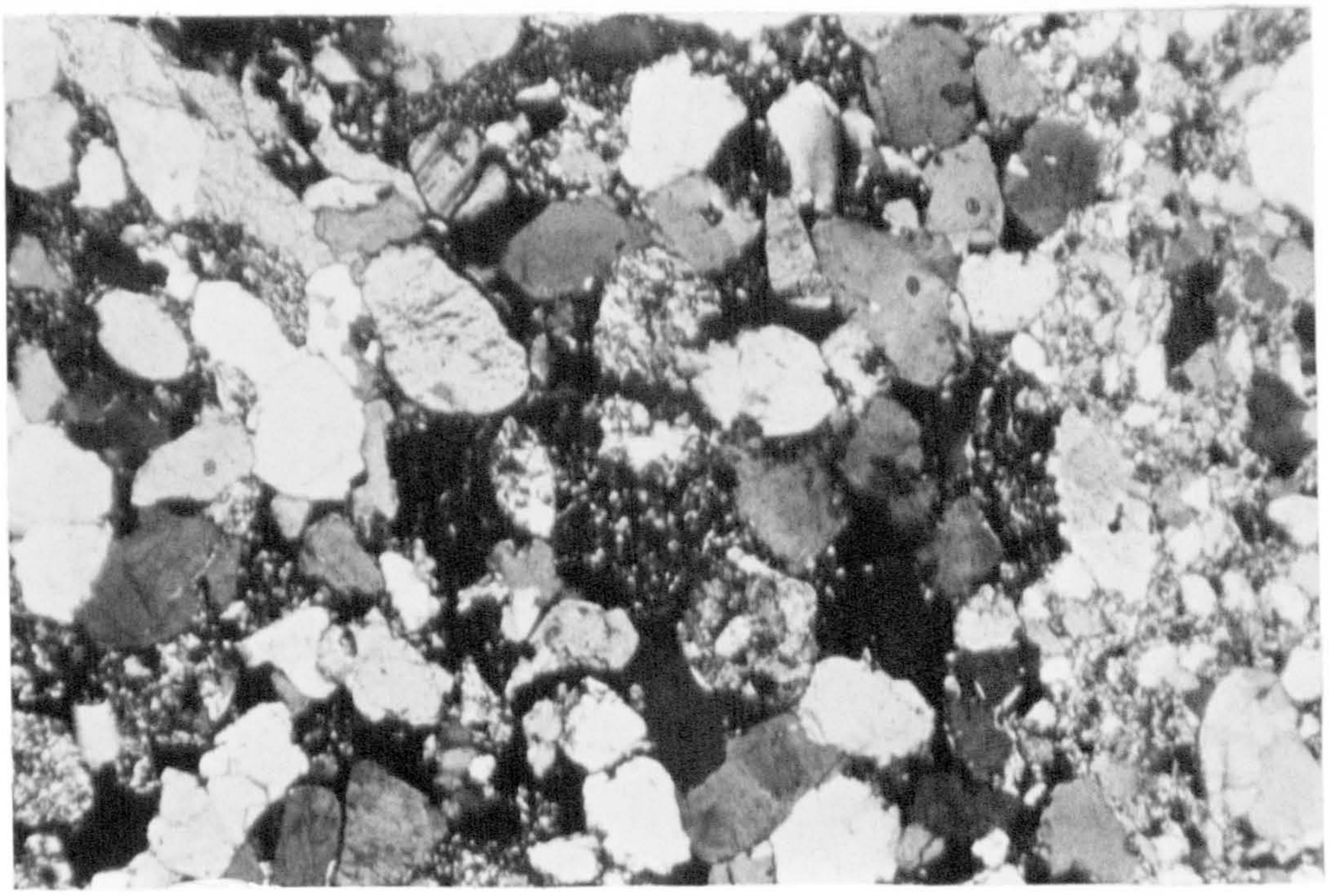

PLATE IV-17. PHOTOMICROGRAPH; CROSSED NICOLS, X4 MAGNIFICATION. INTERLAYERED INDEFATIGABLE SANDSTONE AFTER 2000 PSI, 80°C CARBONATED WATER FLOOD, SHOWING SELECTIVE REMOVAL OF SMALL DOLOMITE CRYSTALS FROM THE COARSE LAYER

For the third test on Indefatigable sandstone, core material from the base of the gas zone was selected and the carbonation pressure further increased to 3,000 psi. A similar shape of permeability profile to those from the first two tests was obtained (Figure IV-15), although a somewhat larger increase in permeability from 11.7 to 39.6 mD, was measured. Levelling off in the rate of permeability increase, or front breakthrough, was obtained upon injection of 2,300 ccs of carbonated water.

The core disintegrated on removal from the core holder, suggesting that weakening due to dissolution under the higher pressure conditions had occurred. This limited analyses of the flooded core to porosity and pore size distribution measurements on one ½ inch core section left in tact. As with the previous rock types used in the study, there was found to be little change in porosity between unflooded and flooded material, while again it was shown that selective enlargement of the large diameter pores (Figure IV-16) took place in the test.

Three tests on identical Indefatigable core materials, at 2,000 psi carbonation pressure, were then undertaken to investigate the presence of residual oil on dissolution. The aim was to determine how dissolution would progress in a poorly swept reservoir, or portion of a reservoir. The cores for these tests were extracted from the same piece of core, part of a gas condensate zone of the Indefatigable reservoir.

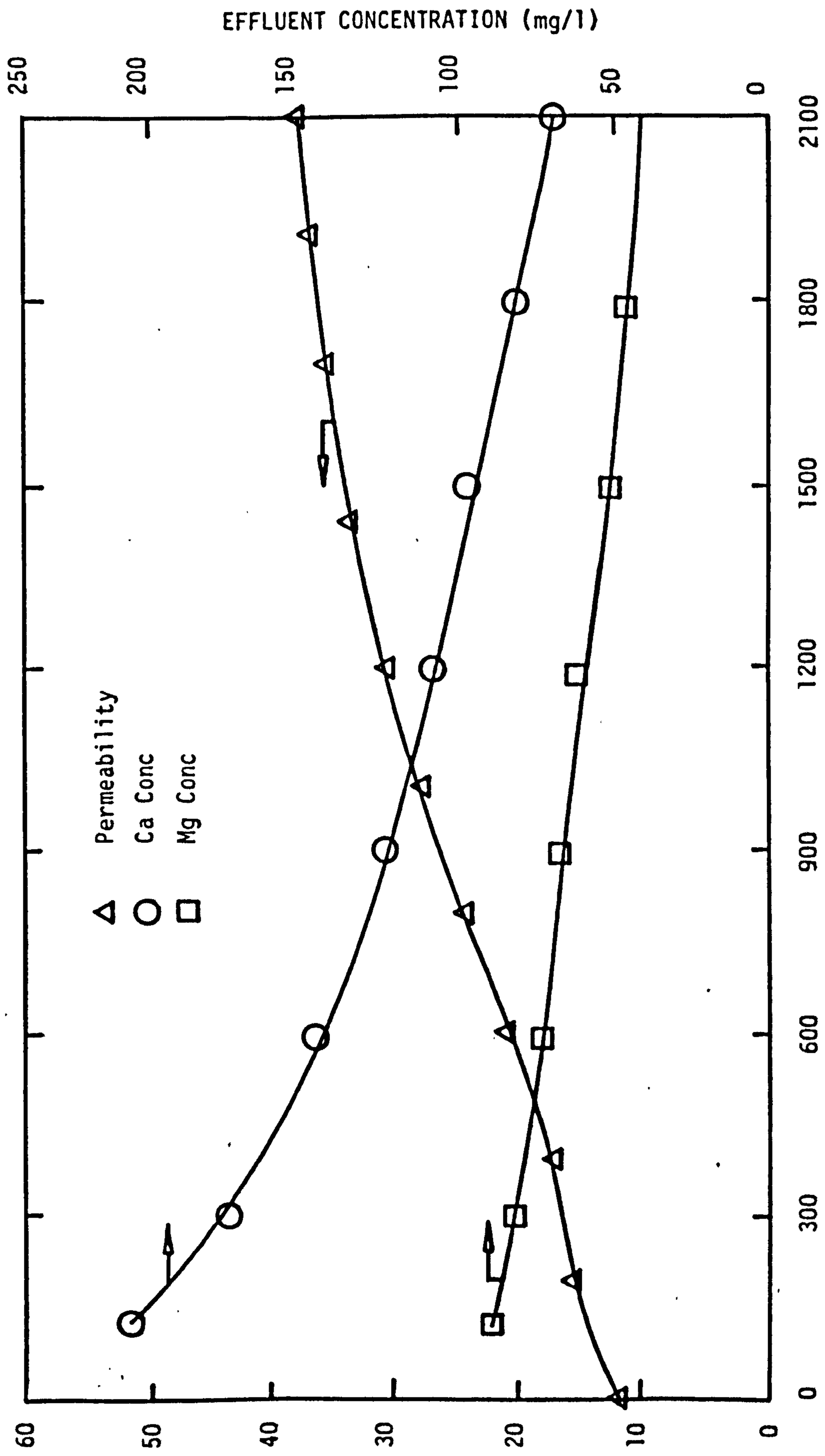

FIGURE IV-15. PERMEABILITY PROFILE AND EFFLUENT COMPOSITION FOR INDEFATIGABLE SANDSTONE (5% DOLOMITE SANDSTONE; 3000 PSI CARBONATION, 80°C)

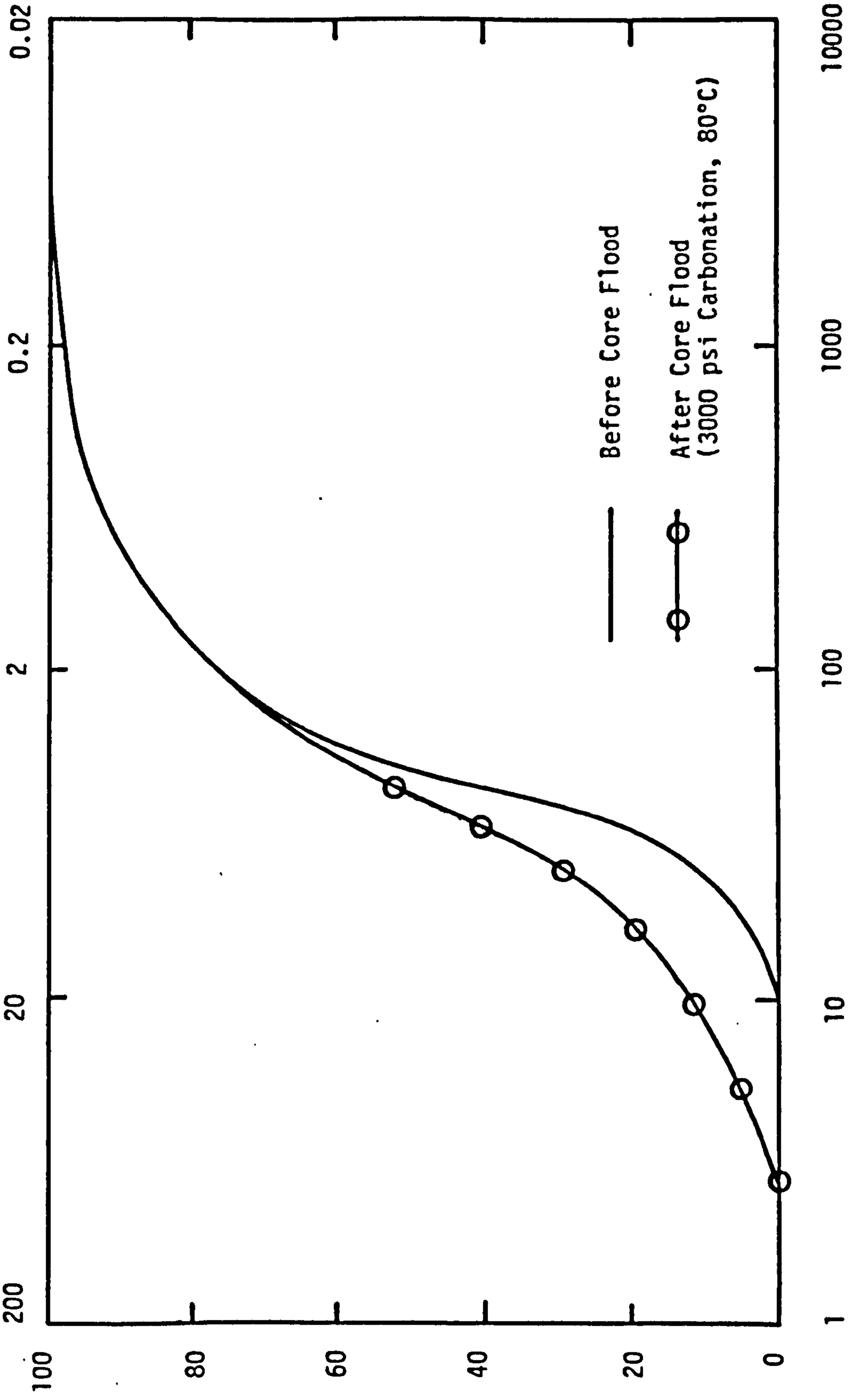

FIGURE IV-16. PORE SIZE DISTRIBUTIONS FOR INDEFATIGABLE SANDSTONE

For the first test a core was cleaned by solvent immersion to enable the dissolution mechanism under oil free conditions to be ascertained. Then for the second test the core was left containing natural gas condensate, while for the third a cleaned core, artificially saturated with crude oil to residual water-flood level, was used. The results for the clean core test are presented in Figure IV-17, the condensate containing core in Figure IV-18, and the oil containing core in Figure IV-19. Although difficult to make exact comparisons due to the differing initial permeabilities of the three cores, there are obvious similarities and differences between the results obtained.

In all three tests the permeability profile was found to increase and then level off as breakthrough of a permeability front occurred. Thin section comparisons of the sandstone cores before and after testing (Plates IV-18 and IV-19) showed that breakthrough in each case was due to total dissolution of dolomite. However, the core flood volume required to achieve breakthrough was considerably different for each test. In the clean core test breakthrough was obtained upon injection of only 1,400 ccs, while in the cores containing condensate and crude oil, 4,000 ccs and 2,500 ccs were required respectively. This, together with the low effluent calcium and magnesium concentrations measured in the early stage of the condensate and oil containing core tests, indicates that the presence of oil initially screens dissolution. On removal of the oil, presumably by CO_2 transfer and viscosity reduction, dissolution proceeded as normal.

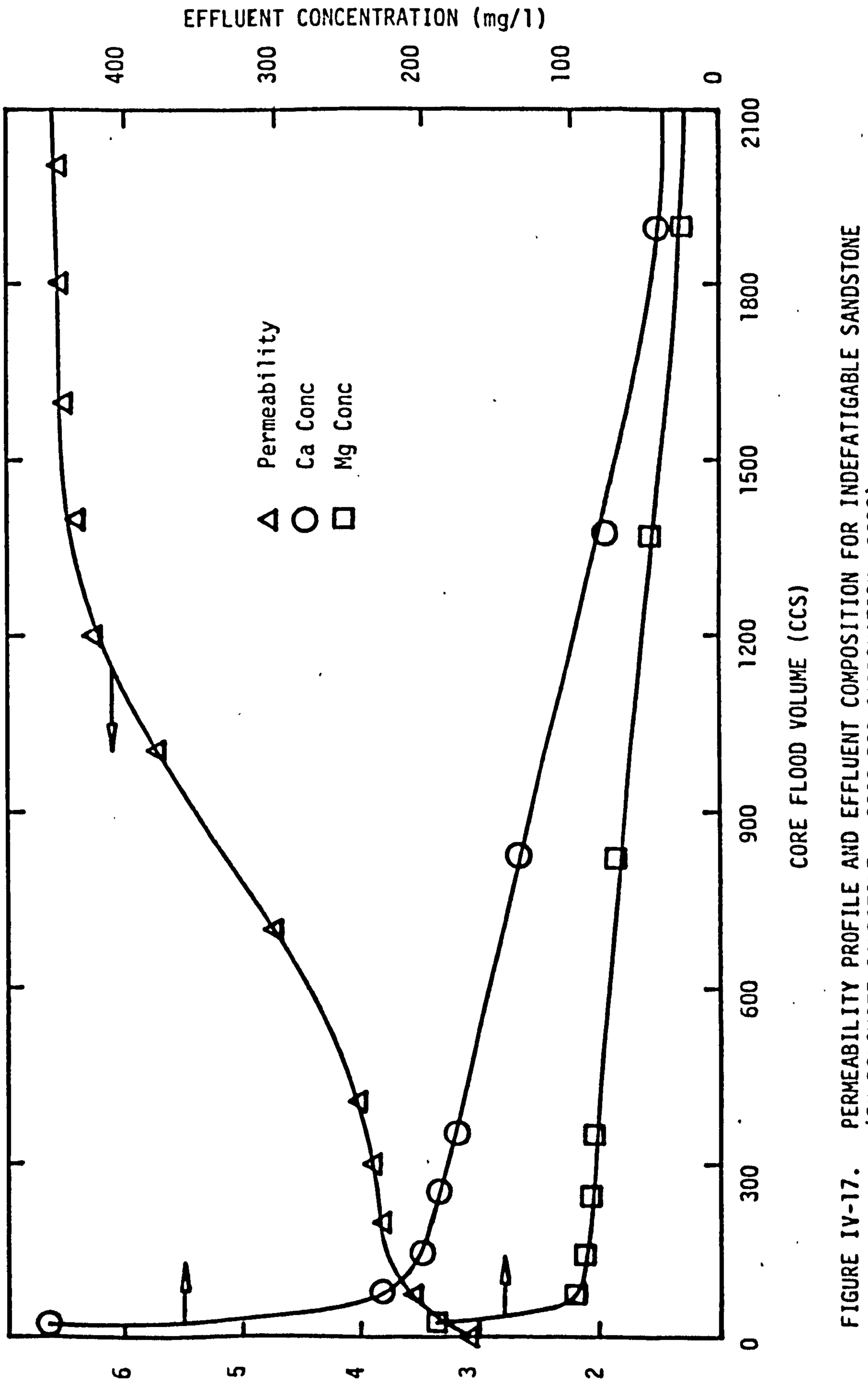

FIGURE IV-17. PERMEABILITY PROFILE AND EFFLUENT COMPOSITION FOR INDEFATIGABLE SANDSTONE (5% DOLOMITE SANDSTONE; 2000 PSI CARBONATION, 80°C)

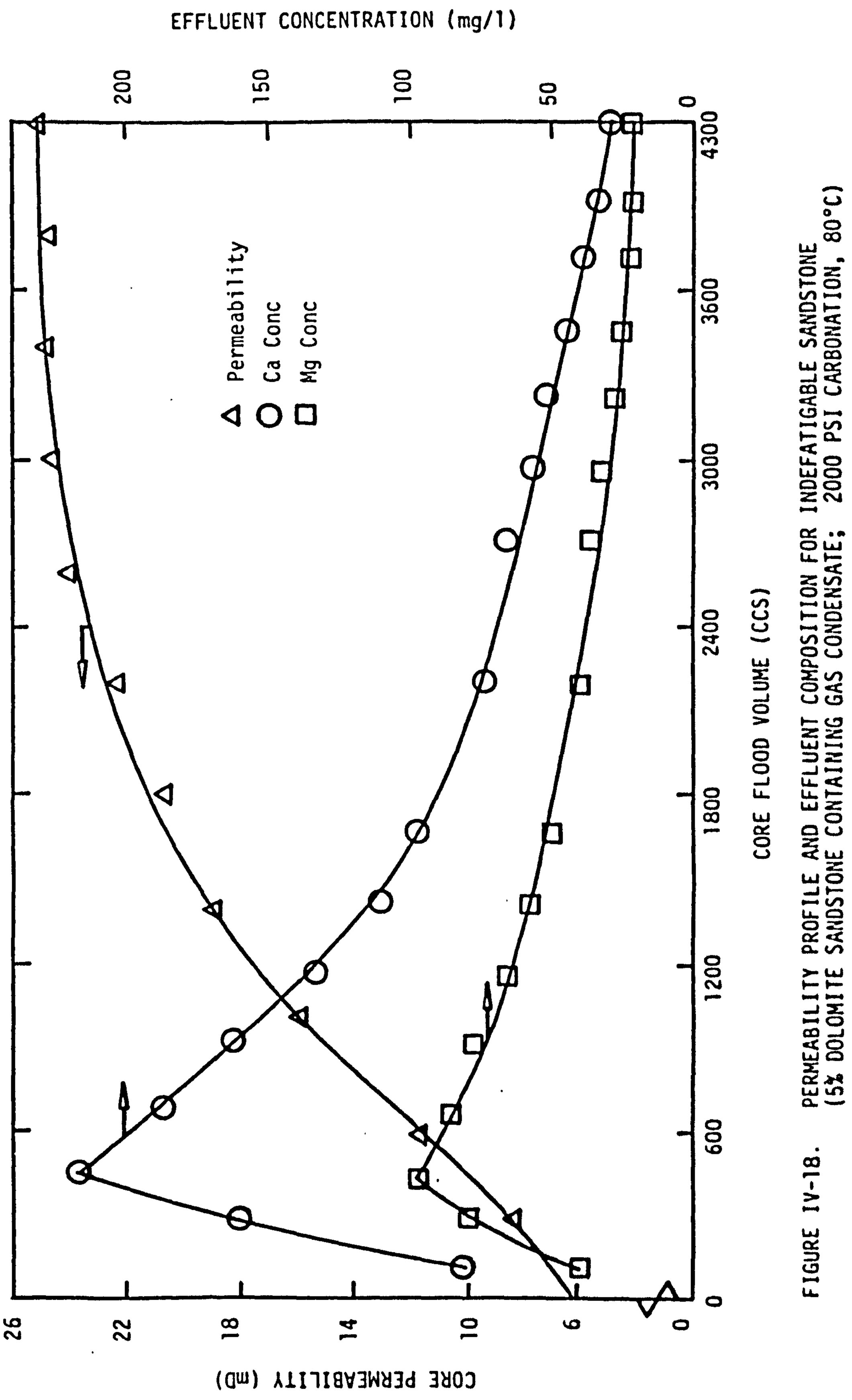

FIGURE IV-18. PERMEABILITY PROFILE AND EFFLUENT COMPOSITION FOR INDEFATIGABLE SANDSTONE
(5% DOLOMITE SANDSTONE CONTAINING GAS CONDENSATE; 2000 PSI CARBONATION, 80°C)

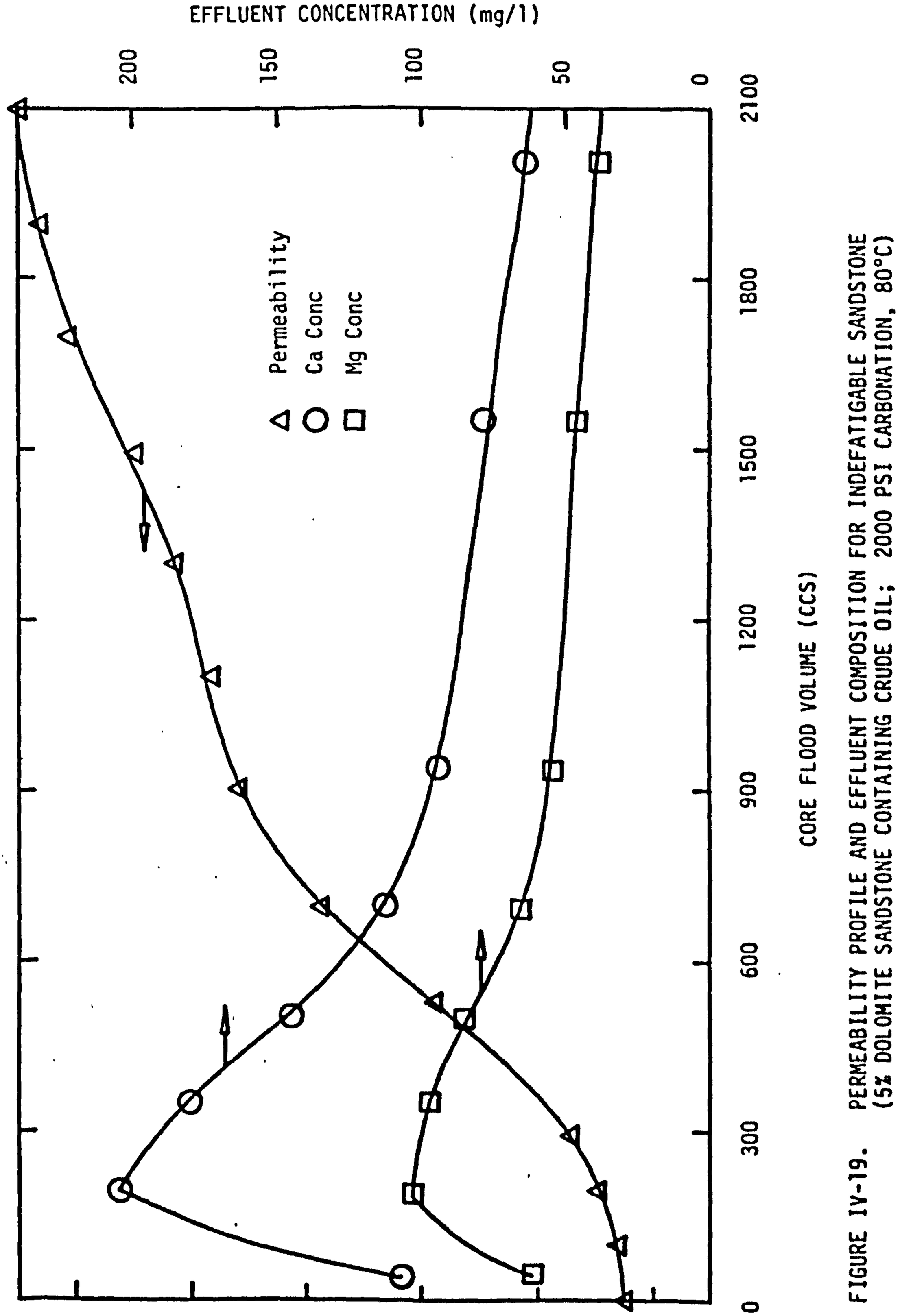

FIGURE IV-19. PERMEABILITY PROFILE AND EFFLUENT COMPOSITION FOR INDEFATIGABLE SANDSTONE (5% DOLOMITE SANDSTONE CONTAINING CRUDE OIL; 2000 PSI CARBONATION, 80°C)

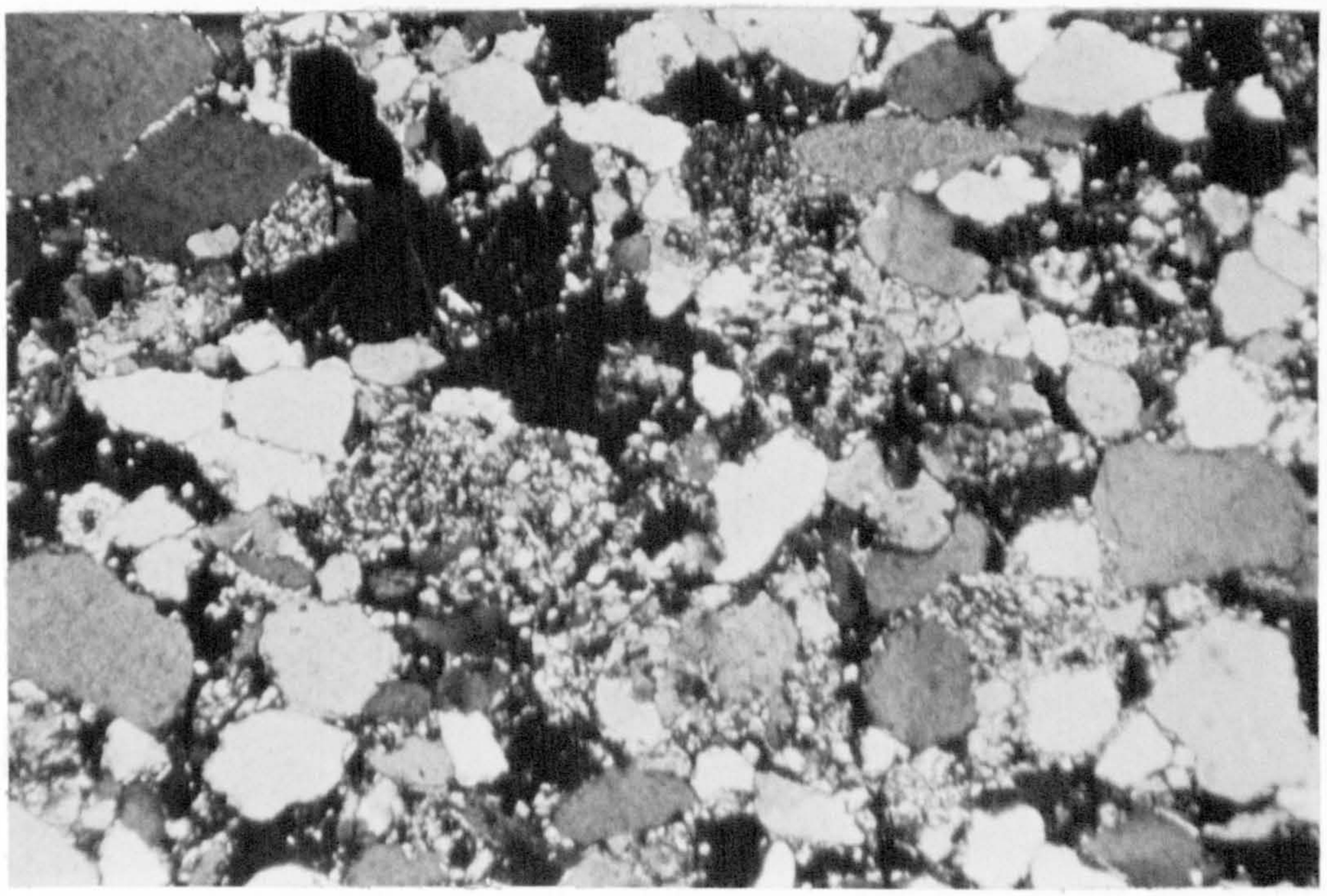

PLATE IV-18. PHOTOMICROGRAPH; CROSSED NICOLS, X4 MAGNIFICATION. CLEANED SANDSTONE FROM GAS CONDENSATE ZONE OF INDEFATIGABLE FIELD. ABUNDANT DOLOMITE OCCURS MAINLY AS FINE CRYSTALS BUT ALSO AS SCATTERED LARGER CRYSTALS

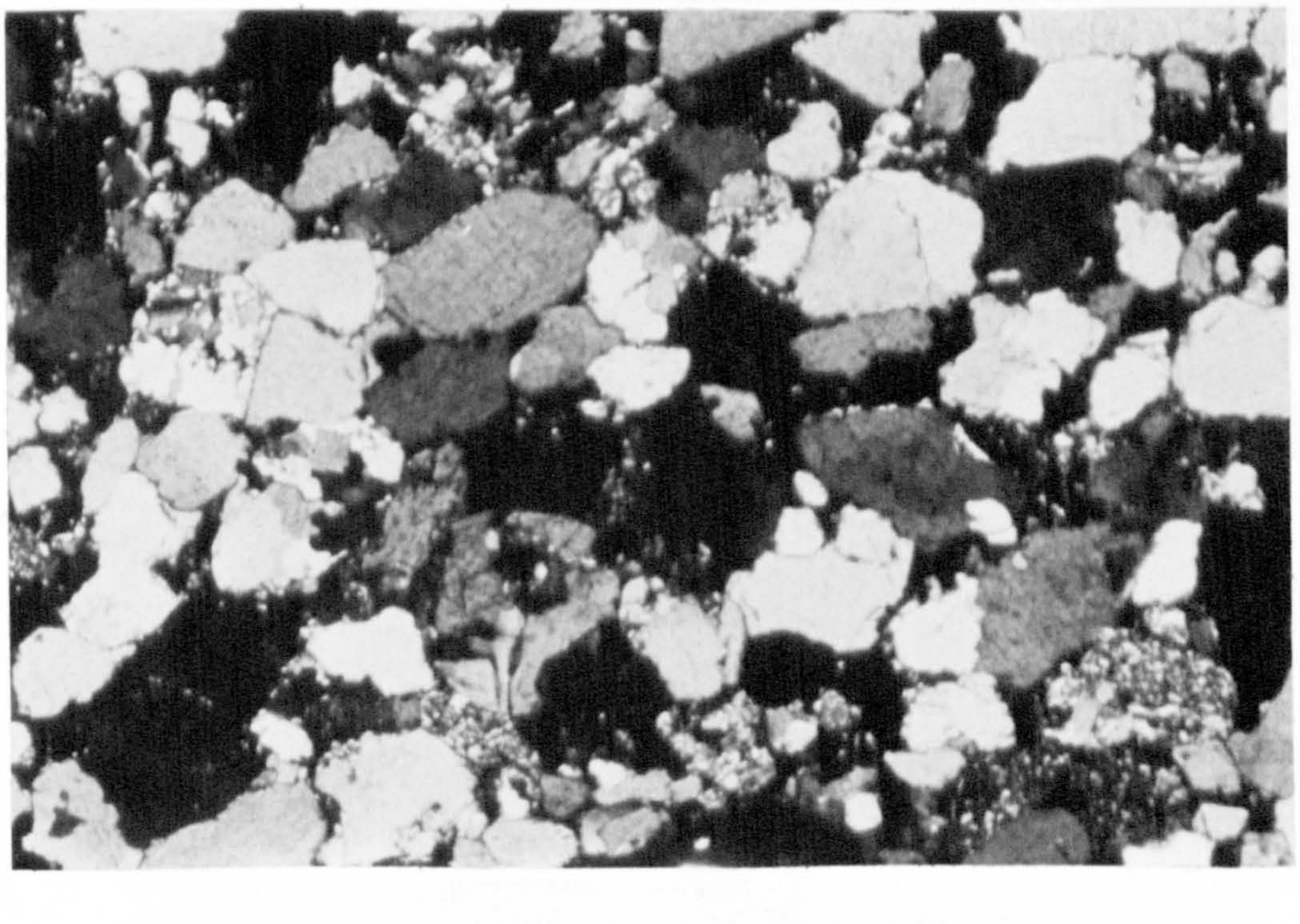

PLATE IV-19. PHOTOMICROGRAPH; CROSSED NICOLS, X4 MAGNIFICATION. CLEANED SANDSTONE FROM GAS CONDENSATE ZONE OF INDEFATIGABLE FIELD AFTER 2000 PSI, 80°C CARBONATED WATER FLOOD, SHOWING COMPLETE DISSOLUTION OF DOLOMITE

The slower breakthrough in the condensate containing core than in the artificially oil saturated core was considered due to the wettability difference between the two. In the uncleaned core the condensate appeared very viscous, adhering to the sandstone minerals, while the oil containing core was purposely prepared water wet. It would appear that the condensate was more "resistant" to the carbonated flood water.

4.8 Oxfordshire Jurassic Limestone

A single core test at 1,500 psi carbonation pressure and 80°C was run on a fossiliferous limestone from the Oxfordshire Jurassic, the permeability profile of which is presented in Figure IV-20. A very dramatic increase in permeability was obtained, with the differential pressure across the core falling to almost zero at maximum flow rate, upon injection of only 300 ccs or 50 pore volumes.

Examination of the flooded core revealed that the rapid permeability increase was due to the formation of two large "wormholes" of roughly circular cross section. One of the wormholes, varying in diameter from 0.5 mm to 1.5 mm, was found to be continuous over the length of the core, while the other was smaller and appeared to taper out half-way along the core. In Plate IV-20 a typical limestone core, together with the divided flooded core containing wormholes is shown. An additional photograph, taken through a camera bellows attachment, of the larger wormhole (Plate IV-21), shows that the material surrounding the main channel had become very porous and would almost

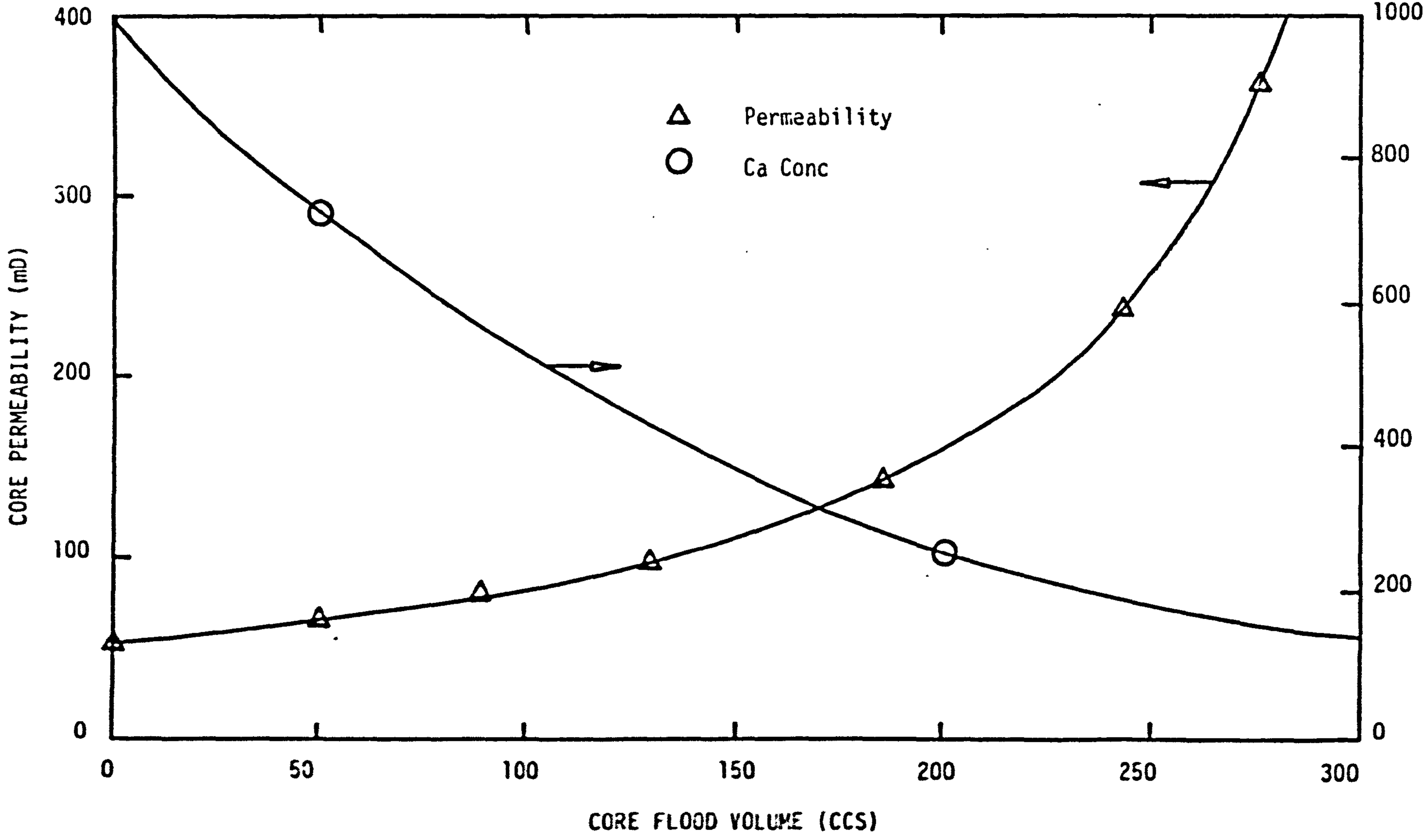

FIGURE IV-20. PERMEABILITY PROFILE AND EFFLUENT COMPOSITION FOR OXFORDS JURASSIC LIMESTONE (90% CALCITE LIMESTONE; 1500 PSI CARBONATION, 80°C)

PLATE IV-20. UNFLOODED LIMESTONE CORE ON LEFT WITH DIVIDED, WORMHOLED LIMESTONE CORE ON RIGHT

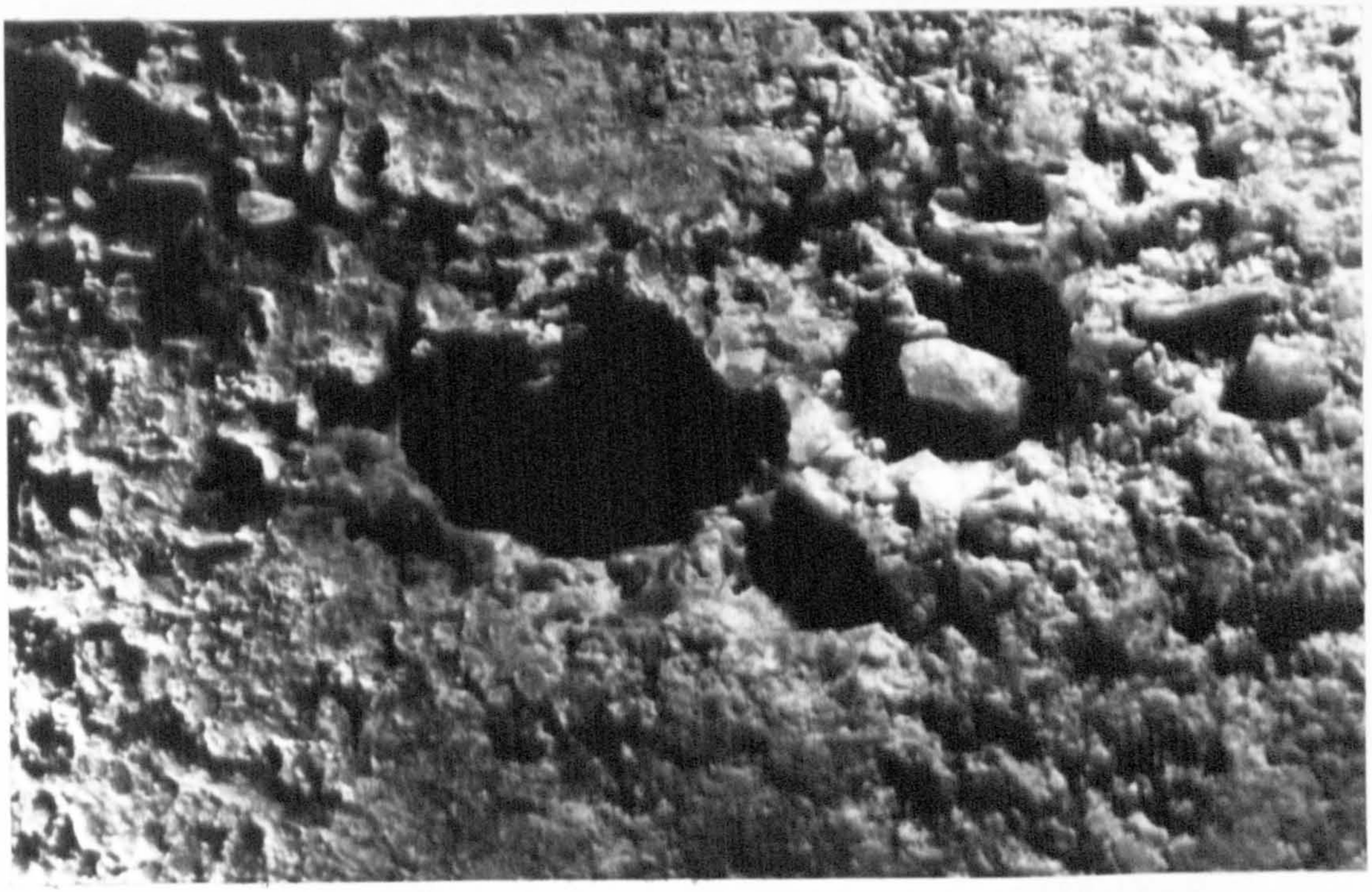

PLATE IV-21. CLOSE-UP OF LARGE WORMHOLE AND FRIABLE SURROUNDS FORMED IN OXFORDS JURASSIC LIMESTONE DURING 1500 PSI, 80°C CARBONATED WATER FLOOD

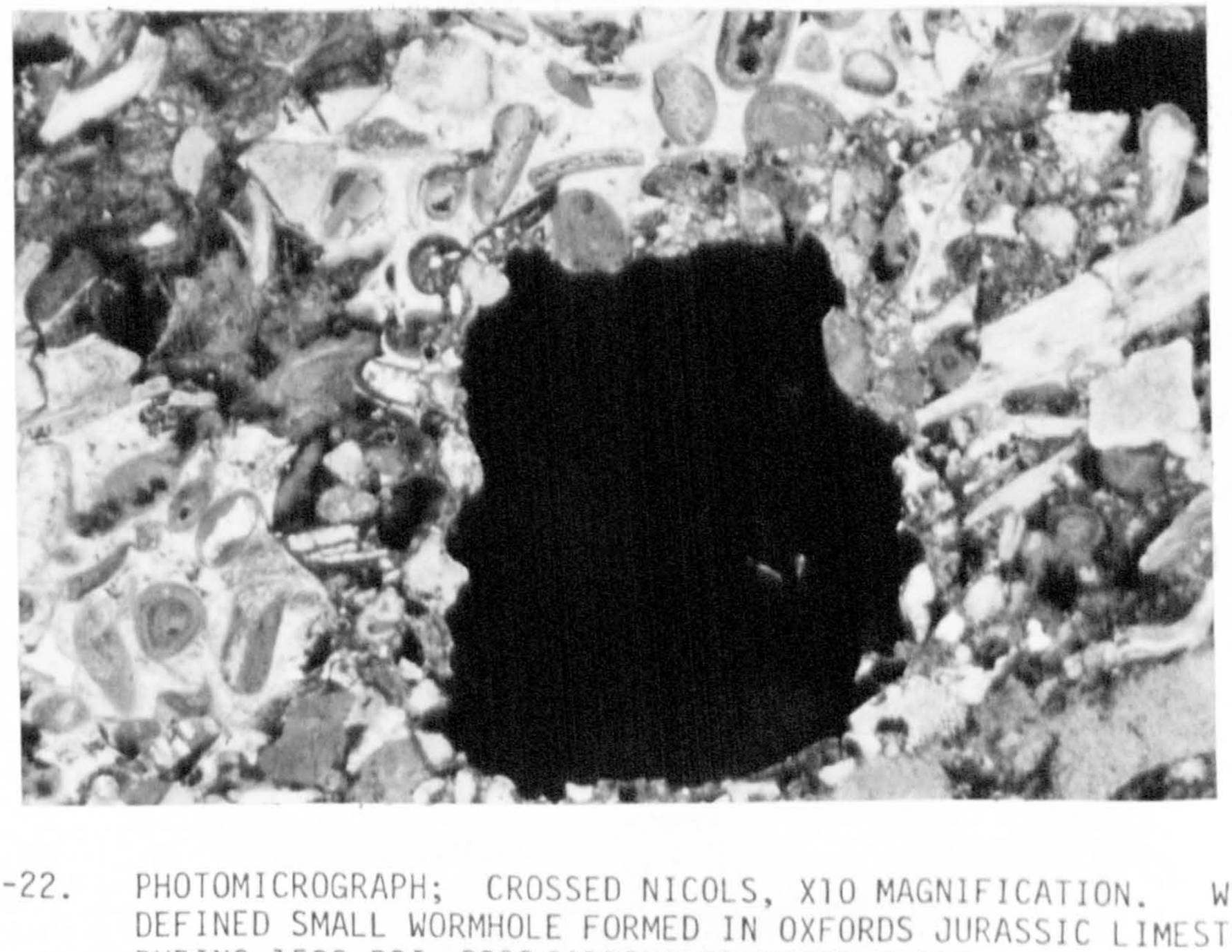

PLATE IV-22. PHOTOMICROGRAPH; CROSSED NICOLS, X10 MAGNIFICATION. WELL DEFINED SMALL WORMHOLE FORMED IN OXFORDS JURASSIC LIMESTONE DURING 1500 PSI, 80°C CARBONATED WATER FLOOD

certainly have collapsed had the test been continued. On the other hand, the smaller wormhole, as shown in thin section in Plate IV-22, appeared to be very well defined.

Flow channels in carbonate rocks generally exist as factures or vugs, with the result that wormholing is a common phenomenon in acidisation of carbonates. The result of the carbonated water flood, although very dramatic, was therefore not unexpected and suggests that dissolution would be a substantial aid to recovery in CO_2 flooding of carbonate rocks.

4.9 Summary of Results

1) For the most part large increases in core permeability due to carbonate dissolution were obtained in the experiments, with as expected, the more dramatic results from the high pressure runs. However, no conclusive results were obtained from tests on unconsolidated materials, where fines migration and plugging on dissolution would have been a possibility.

2) Where increases in permeability were experienced, a characteristic permeability profile was obtained if the test continued long enough. Typically, a rise in permeability followed by levelling off and attainment of a constant value was obtained, as depletion of carbonate or channel formation progressed to completion.

3) Five types of dissolution effect were identified in the tests:

a) uniform dissolution,

b) single channel dissolution,

c) multiple channel dissolution,

d) selective dissolution of smaller carbonate crystals,

e) a combination of b) and d)

The type obtained was largely dependent on the mineralogical framework within the sandstone core under test. Where mineralogical inhomogeneities were present, channel or selective dissolution effects were generally experienced, while in more homogeneous cores, uniform effects were normal.

4) Permeability measurements on flooded core segments showed that dissolution of carbonate from cores produced a change in local permeability which travelled as a front through the cylindrical core.

5) The small change in porosity between unflooded and flooded cores, in conjunction with pore size distribution comparisons, showed that the dramatic increase in permeability of a core during a carbonated water flood was probably due to the removal of constrictions and selective dissolution of the larger pores.

6) The presence of residual oil was found to initially screen dissolution and delay permeability front migration.

CHAPTER V

THEORETICAL CONSIDERATIONS

5.1 Introduction

5.2 Schechter-Gidley Model

5.3 Lund-Fogler-McCune Model

5.4 Discussion of the Two Models and Their Applicability to Carbonate Dissolution in Carbonated Water

5.5 Dissolution Rate Data Requirements

5.1 Introduction

It was shown in Chapter IV that the movements of dissolution permeability fronts through cores are seldom governed by uniform carbonate dissolution, but rather are more often determined by inhomogeneities in the rock framework. As a result predictive mathematical modelling of carbonate dissolution in carbonated water is likely to be very difficult and of little practical value for most rock types.

At present there are only two primary models that describe the dissolution of a porous matrix by a flowing medium: the Schechter-Gidley Acidisation Model and the Lund-Fogler-McCune Acidisation Model. Both suppose that a uniform dissolution occurs over the entire rock framework during stimulation, which is probably valid for high concentration acidisation, but as has been demonstrated is rare during a carbonated water flood. Such factors as mineralogical layering, local carbonate concentrations and the preferential dissolution of fine grained material (outlined in Chapter IV), which generally control the rate of permeability front migration in a carbonated water flood, cannot be accounted for with either model. Thus, applicability of predictive modelling to carbonated water flooding is effectively limited to homogeneous rocks with uniform grain size and mineral distribution.

Although clearly very restricted in their use, the Schechter-Gidley and Lund-Fogler-McCune models, together with their applicability to carbonate dissolution in carbonated flood water are discussed in subsequent sections of this chapter.

5.2 Schechter-Gidley Model

Schechter, Gidley and co-workers (52-56) have developed a "microscopic" model for the process of matrix acidisation, in which the porous matrix is represented by a collection of randomly distributed capillaries possessing a variety of cross-sectional areas. In this so-called capillary model the cylindrical pores in the matrix are assumed to be interconnected so that fluid can flow through the matrix under the influence of a pressure gradient.

The pore structure is characterised by a pore size distribution function $\eta(A,x,t)$ where $\eta(A,x,t)dA$ is defined as the number of pores per unit volume, with cross-sectional areas between A and A + dA. From this function it can be seen that the number of pores at any point,

$$N = \int_0^\infty \eta(A,x,t)dA \qquad (5.1)$$

and the porosity is

$$\phi = l\int_0^\infty A\eta(A,x,t)dA \qquad (5.2)$$

or

$$\frac{\phi}{\phi} = \frac{\int_0^\infty A\eta(A,x,t)dA}{\int_0^\infty A\eta(A,x,0)dA} \qquad (5.3)$$

where l is the average length of a pore.

The Schechter-Gidley model also takes Darcy's Law into account giving the permeability ratio, on simplifying, as:

$$\frac{K}{K_o} = \frac{\int_o^\infty A^2 \eta(A,x,t)dA}{\int_o^\infty A^2 \eta(A,x,0)dA} \qquad (5.4)$$

where K_o is the initial permeability of the porous matrix and K is the permeability at any time during or after acidisation.

Now, the distribution function η will change as the acid reacts within the matrix and the pores increase in size. There are two fundamental processes that cause a change in the pore size:

1) reaction with the walls of a pore, and
2) interconnection (or collision) or pores when the solid separating the flow channels is dissolved.

An equation, called the evolution equation, describing the behaviour of the pore size distribution function based on the theory of capillary growth with collision has been derived and is as follows:

$$\frac{\partial n}{\partial t} + \frac{\partial(u\eta)}{\partial A} = 1\left[\int_o^A \eta(A-A^1,x,t)\eta(A^1,x,t)u(A^1,x,t)dA^1 - \int_o^\infty [\, u(A,x,t) + u(A^1,x,t)\,]\ \eta(A,x,t)\eta(A^1,x,t)dA^1\right] \qquad (5.5)$$

where A is the cross-sectional area of a pore, $\eta(A,x,t)$ is the pore size distribution function and $u(A,x,t)$ is the pore growth function, defined as:

$$u(A,x,t) = \frac{dA}{dt} \qquad (5.6)$$

The quantity u represents the rate of growth of the area of a single pore having an area A, and is thus largely dependent upon the nature of the dissolution reaction within that pore. The overall rate of reaction is in turn determined by both the rate of mass transfer and the rate of surface reaction, so that pore geometry, flow rate and many other factors enter into the determination of u. Reaction rate data for use in this theory were obtained from experiments where acid was injected through short cores and effluent concentration measured using an ionometric electrode technique (57). In addition, however, an approximate kinetic-hydrodynamic model was developed to theoretically evaluate the growth function reaction rate data. The model is fully discussed in a Ph.D. thesis by Guin (53) and is not presented here.

Equations 5.3 and 5.4 relate the porosity and permeability to integrals of the pore size distribution. Thus, by solving Equation 5.5 for the pore size distribution as a function of time, the changes in permeability and porosity may be calculated.

In summary, the pore growth function contains the reaction rate and determines the change in the distribution function η with respect to time and position. The pore size distribution in turn determines the local porosity and permeability.

5.3 Lund-Fogler-McCune Model

More recently Lund, Fogler, McCune and co-workers (51, 58, 59) have developed a "macroscopic" model for sandstone acidisation.

The model combines information about the geometry, the flow and the reactions within a sandstone matrix, to predict the movements of acid and permeability fronts through linear cores as a function of acid concentration and flow rate.

The assumption is made that the main mineral constituent of sandstone, quartz, is unreactive and acts only as a supporting matrix for the more soluble minerals. . The reactivity of the acid soluble minerals (mainly felspars and clays) for their part, is assumed to be approximated by a single rate law and a single overall relationship, W, the stoichiometric coefficient (the number of moles of acid required to dissolve 1 mole of minerals combined as a single reactive species).

The formulation of the fundamental model equations is based on two differential material balance equations; one for the acid flowing axially through the core and another for the minerals in the core. A mass balance on the acid yields the equation:

$$\frac{\partial(\emptyset C)}{\partial t} + V \frac{\partial C}{\partial x} = R_s \qquad (5.7)$$

where $\emptyset$ = porosity, x = axial distance along core,
C = acid concentration, t = time,
V = superficial velocity, R_s = heterogeneous reaction rate of acid with rock.

Similarly a differential mass balance for the solid phase yields:

$$\frac{\partial\left[(1-\emptyset)C_M\right]}{\partial t} = r_a \qquad (5.8)$$

where C_M = lumped concentration of all minerals other than quartz in sandstone

r_a = reaction rate of lumped dissolvable minerals

The heterogeneous reaction rate of the liquid phase acid and the reaction rate of the minerals are interconnected by the stoichiometric coefficient, so that:

$$R_s = Wr_a \tag{5.9}$$

Assuming the lumped dissolvable minerals to obey a single reaction equation (60), then the rate law for their dissolution may be expressed as:

$$R_s = k_r C(C_M - C_{M1}) \tag{5.10}$$

where k_r = reaction rate constant

C_{M1} = irreducible dissolvable mineral concentration

If it is further assumed that the porosity change in the sandstone during acidisation is small and slow compared to the change in acid concentration (61, 62), Equations 5.7 and 5.8 can be simplified, by letting $\emptyset = \emptyset_o$, the initial porosity. Then by substituting the stoichiometric coefficient and the rate law into Equations 5.7 and 5.8, these equations can be solved (51) to yield the acid concentration and dissolvable mineral distributions in the core during acidisation. For simplification the resulting equations are expressed in terms of the following dimensionless groups:

$$\text{time, } t_D = \frac{tV}{\phi_o L} \tag{5.11}$$

$$\text{axial distance, } x_D = \frac{x}{L} \tag{5.12}$$

$$\text{acid concentration, } C_D = \frac{C}{C_o} \tag{5.13}$$

$$\text{dissolvable mineral content, } C_{MD} = \frac{C_M - C_{M1}}{C_{MO} - C_{M1}} \tag{5.14}$$

$$\text{Damkohler number, } Da = \frac{k_r (C_{MO} - C_{M1}) L}{V} \tag{5.15}$$

(ratio of the rate at which the acid reacts to the rate at which the acid moves through the sandstone)

$$\text{Acid capacity number, } Ac = \frac{\phi_o C_o}{W(1-\phi_o)(C_{MO}-C_{M1})} \tag{5.16}$$

(molar ratio of acid present in pore space to the acid required to dissolve all the mineral accessible to reaction)

where L = core length

C_o = initial acid concentration

C_{MO} = initial dissolvable mineral concentration

The resulting equations are:

$$C_D = \frac{1}{1 + EXP\left[DaAc\left((1 + 1/Ac)x_D - t_D\right)\right]} - EXP\left[DaAc(x_D - t_D)\right] \tag{5.17}$$

$$C_{MD} = \frac{1}{1 + EXP\left[-DaAc\left((1 + 1/Ac)x_D - t_D\right)\right]} - EXP\left[-Dax_D\right] \tag{5.18}$$

Although the porosity change was assumed minimal to solve the mass balance differential equations, it can now be computed through the relation:

$$\Delta\phi = \phi - \phi_o = (1-C_{MD})\Delta\phi_{max} \qquad (5.19)$$

where $\Delta\phi_{max}$ = porosity increase when all dissolvable minerals accessible to reaction have been consumed.

Also the local permeability K of a sandstone undergoing acidisation can be expressed as a function of the porosity change (58), as:

$$\frac{K}{K_o} = EXP\left[\beta \frac{\Delta\phi}{\Delta\phi_{max}}\right] = EXP\left[B(1-C_{MD})\right] \qquad (5.20)$$

where β = experimentally determined parameter which depends on sandstone type

K_o = initial core permeability

Now by integrating the local permeability over the length of the core, the overall (or average) permeability can be determined:

$$\frac{K_a}{K_o} = \frac{L}{\int_o^L \frac{dx}{K/K_o}} \qquad (5.21)$$

where K_a = average core permeability

Provided the dimensionless groups Da and Ac are known, Equations 5.19 and 5.20 can be substituted into Equation 5.21 to provide the overall permeability as a function of acid injection time.

For accuracy it is best that Da and Ac are determined experimentally from measurements during core flood experiments. However, if an adequately sized sample of the sandstone in question is not available, then Da and Ac can be estimated from a porosity and a mineralogical content analysis on the sandstone (63).

In summary, the solutions to the differential mass balance equations (i.e. Equations 5.17 and 5.18) together with Equations 5.19 and 5.20 describe the change in acid concentration, porosity and permeability as a function of the axial position in the core and the acid injection time.

5.4 Discussion of the Two Models and Their Applicability to Carbonate Dissolution in Carbonated Water

It is feasible that for a homogeneous porous matrix, both the Schechter-Gidley and the Lund-Fogler-McCune models could be used to model carbonate dissolution in carbonated water. Both have proved reasonably successful in predicting results of core flood acidisation experiments (59, 64), and could quite easily be used to model a carbonated water flood, providing appropriate dissolution rate data were to be obtained.

The basic problem of the capillary model lies in the description of the pore geometry. It is assumed that the length to diameter ratio of the pores is large, that the pores all have a similar geometric shape, and that this shape does not change during stimulation. Furthermore, a one dimensional pore size distribution function is

used to describe the complex geometry of a three dimensional porous media pore space. Clearly these assumptions have limited validity, effectively restricting any correlation between the evolution of the model matrix and the changes in an actual porous medium. For example, it would not be possible to predict the absolute value of some property of a real porous medium from some other property using the model. Thus, use of the Schechter-Gidley capillary model is somewhat limited in that all quantities of interest have to be taken in the form of ratios.

The Lund-Fogler-McCune model has advantages over the capillary model in this respect, in that it forgoes any attempt to relate macroscopic and microscopic properties. However, it tends to be less widely applicable than the capillary model. This is due to the assumption being made that the porosity change during stimulation is negligible (to enable solution of the mass balance equations), preventing extension of the model to sandstones having large carbonate contents or a greater percentage of dissolvable material than inert material.

As mentioned earlier, both the Lund et al and Schechter-Gidley models have produced reasonably good predictive results for core flood acidisation tests. The capillary model was developed using well ordered porous media with a narrow pore size distribution (manufactured porous material) while the microscopic model was developed using one particular sandstone type (a felspathic quartzite). It was generally found that although the models worked well in predic-

ting minor experimental variations, error was obtained as the experimental variables were made to differ. This behaviour suggests that the models may have to be refined in order to handle more divergent problems.

As far as dissolution in sandstone reservoir rocks during a CO_2 flood is concerned, it is safe to assume that the only mineral constituents likely to be significantly altered will be the carbonates. Therefore, it is unlikely that there would be any drastic change in the pore framework as there often is in matrix acidisation. For a homogeneous matrix, both the Schechter-Gidley and the Lund-Fogler-McCune models should then be effective in predicting the comparatively minor stimulation results obtained from carbonate dissolution in carbonated flood water.

Use of the Lund et al model would, however, be preferable in that it has been tested successfully on natural sandstone. As was shown in Chapter IV, dissolution of carbonate in carbonated water from typical reservoir sandstone may give rise to fairly dramatic increases in permeability, although only minimal increases in porosity are normal. Thus, there should be no difficulty neglecting porosity increase in use of the macroscopic model. If however, predictive calculations were required for sandstones with fairly high carbonate contents, where large porosity increases would be likely, then only the Schechter-Gidley capillary model could be used.

5.5 Dissolution Rate Data Requirements

Before either the capillary or macroscopic models can be applied to carbonate dissolution in carbonated water, the dissolution rates of the individual carbonate minerals in the rock must be known. At present, only limited information on carbonate reaction rates is available, making further kinetic studies imperative if any useful modelling is to be carried out. Moreover, the required rate data must be obtained under CO_2 flood field conditions if the model is to be fully representative.

The rate of dissolution of any mineral is dependent upon: 1) the rate of transport of reactants and products between the mineral surface and the bulk solution, 2) the rate of heterogeneous reaction at the mineral surface, and possibly 3) the rates of homogeneous reactions within the solvent with the products from the heterogeneous reaction (65). Depending upon the fluid flow and chemical characteristics of the environment, one or all of these processes may be important in determining the dissolution rate. If the reaction rate far exceeds the transport rate, the net rate of dissolution is virtually controlled by diffusive and convective transport processes between a near-saturated fluid surface layer and a subsaturated bulk solution. If any reaction rate is slow relative to transport processes, then the rate of dissolution is essentially reaction controlled.

The system $CaCO_3$ - H_2O is of considerable scientific interest and has therefore been subject to extensive reaction rate studies in the

past. In a series of experimental studies at low pressures and temperatures it has been shown that transport processes play an important role in the rate of dissolution of calcite in solutions of carbonic acid in which the pH is less than 4 (50, 66, 67). Above pH 4, dissolution is thought to be primarily determined by the kinetics of surface reaction (65, 67-70). Dissolution rate expressions for calcite, related to the various hydrodynamic and chemical parameters under study are presented in most of the above works.

Outside the comparatively limited pressure and temperature ranges of these studies, there appears to be a complete lack of dissolution rate data for calcite. In addition, there is little data on impure forms of calcite (such as iron or magnesium calcite) and dolomite. It is clear, therefore, that if realistic modelling of carbonate dissolution in different sandstones during CO_2 flooding is to be undertaken, comprehensive reaction rate studies will have to be made. These will have to be made over quite a wide range of pressure and temperature conditions, as it is possible that dissolution proceeds by different mechanisms as the conditions vary.

The tests most often used for determining mineral reaction rates are:

1) the static reaction rate test, in which a mineral sample is contacted with unstirred solvent at a known ratio of mineral surface area to solvent volume (71),

2) flow experiments where solvent is flowed between parallel plates of mineral (72, 73),

and

3) dynamic tests where mineral specimens are rotated through an agitated solvent solution (69, 74).

The progress of the reaction in these tests is followed by chemical analysis of regularly taken liquid samples. In general, the tests model some aspects of the reaction process such as area to volume ratio, or solvent flow velocity, but do not accurately model all field conditions. For example, it has been demonstrated that under static conditions, mass transfer to and from the mineral surface tends to mask the functionally of the reaction rate at the mineral surface.

For the purpose of determining carbonate dissolution rate data under CO_2 flood conditions, either flow or dynamic experiments could be used. Flow experiments would, however, be preferable at this stage as they could be carried out with little modification to the carbonated water permeameter already in operation. If a dynamic set-up were to be used, completely new apparatus would have to be designed and constructed.

Reaction rate studies are to be undertaken in the next phase of the research programme (75), so full discussion of the "pros and cons" of flow and dynamic type measurement systems will be deferred until then. Suffice to say for the present, that the most important

aspect of reaction rate work is to develop mechanistic explanations for dissolution over a complete range of pressure, temperature and hydrodynamic conditions (76). Only when the mechanisms of dissolution are known can rate expressions be obtained to fit in predictive models.

CHAPTER VI

CONCLUSIONS AND RECOMMENDATIONS

6.1 Conclusions

6.2 Recommendations

6.1 Conclusions

The following conclusions were drawn from the results of this investigation:

1. The high pressure, high temperature carbonated water permeameter constructed to investigate carbonate dissolution effects on carbon dioxide flooding was successful in providing new insight into the variables that control the dissolution process.

2. No significant reduction in permeability or evidence for fines migration was obtained in any of the experiments, although it was found impossible to flood friable reservoir material using the present core holder set-up. Thus, carbonate dissolution is not envisaged as providing any well injectivity decline problems for a CO_2 flood in a competent reservoir formation.

3. Substantial increases in permeability due to carbonate dissolution were experienced in most rock types tested. Moreover, a zone or front of increasing permeability was found to travel through the core from inlet to outlet face, suggesting that in a CO_2 flood situation, a permeability front would also be produced and move forward into the reservoir from the injection well. The velocity and continuity of front migration would depend on numerous factors. Reservoir properties such as temperature, permeability, rock homogeneity and the composition-concentration-distribution of carbonate minerals, together with the CO_2 flood characteristics such as slug regime and flow rate, would all contribute.

4. Cores containing mineralogical inhomogeneities or permeable zones were found to promote selective dissolution and channel formation. In a reservoir situation such an occurrence would clearly enhance imhomogeneities already present and further their associated problems. A major problem could be carbonated water breaking through the CO_2 slugs.

5. The presence of residual oil was found to initially inhibit carbonate dissolution owing to transfer of CO_2 from the carbonated water to the oil. This may be significant in a poorly swept reservoir with high residual oil content, in reducing or eliminating any expected stimulation effect.

6. Existing mathematical models are unlikely to prove successful for most rock types in predicting carbonated water - carbonate mineral dissolution effects.

6.2 Recommendations

The following recommendations are made for future studies:

1. Further carbonated water floods should be carried out on unconsolidated reservoir sandstones to determine whether fines release and plugging is at all likely. To prevent core collapse the cores should be encased in thick resin, rather than mounted in a rubber sleeve, requiring that a new core holder be designed and constructed. In addition, if a series of differential pressure tappings could be connected at various points along the core, the advance rate of any

permeability front would be rapidly discernible. This would avoid having to carry out time consuming core segment permeability analyses, but would require extra pressure transducers and recording facilities.

2. A piston displacement cell would be preferable to the transfer barrier, in that the barrier rubber membranes were found to last fairly limited periods before bursting. Both nitrile and butyl rubber membranes in contact with CO_2 were found unsatisfactory in terms of "life expectancy".

3. A better and more accurately controllable back pressure regulator is required to combat the fluctuations in differential pressure obtained in the core tests. The present regulator was found to generate system pressure build up followed by sudden release, causing a wave pattern to the core differential pressure trace. A dome load regulator as opposed to the present spring load type is recommended.

4. Tests on cores longer than three inches should be carried out to more fully evaluate permeability front advance phenomena. This may not, however, be possible with typically four inch diameter reservoir core.

5. Dissolution reaction rate data for carbonate minerals in carbonated water should be determined to enable mathematical predictions at least to be attempted. The data would also be useful in determining whether dissolution was likely to occur in or immediately adjacent to the injection wellbore, or if it was to occur less intensively over a wider radius.

APPENDICES

APPENDIX 1

CARBONATED WATER CORE FLOODING PROCEDURE

CARBONATED WATER CORE FLOODING PROCEDURE

To eliminate possible error at high pressure each of the valves on the permeameter were numbered (Figure A1-1) and an ordered experimental procedure adhered to. The procedure is outlined in subsequent sections.

A1.1 Core Mounting

The core is first mounted inside a rubber sleeve in the core holder cell and a selected confining pressure (generally 50 percent greater than the test injection pressure) then applied to the core by pressuring the rubber sleeve with water. Valve 28 is opened, the system purged of air through valve 27, and the desired water pressure, as shown by the 0-600 bar gauge, obtained via a manual hydraulic pump system. Valve 28 is then closed.

For unconsolidated core materials the confining pressure and core pressure have to be raised simultaneously to prevent core collapse. The core pressure is applied by the CO_2 gas booster in this operation, whilst the hydraulic pump is used to generate the confining pressure.

A1.2 Temperature Control

At this stage the transfer barrier and core holder heaters are switched on and adjusted to establish constant system temperature. The time required to produce the desired operating temperature may be as long as five hours, due to the large thermal capacities of the systems and consequent slow response.

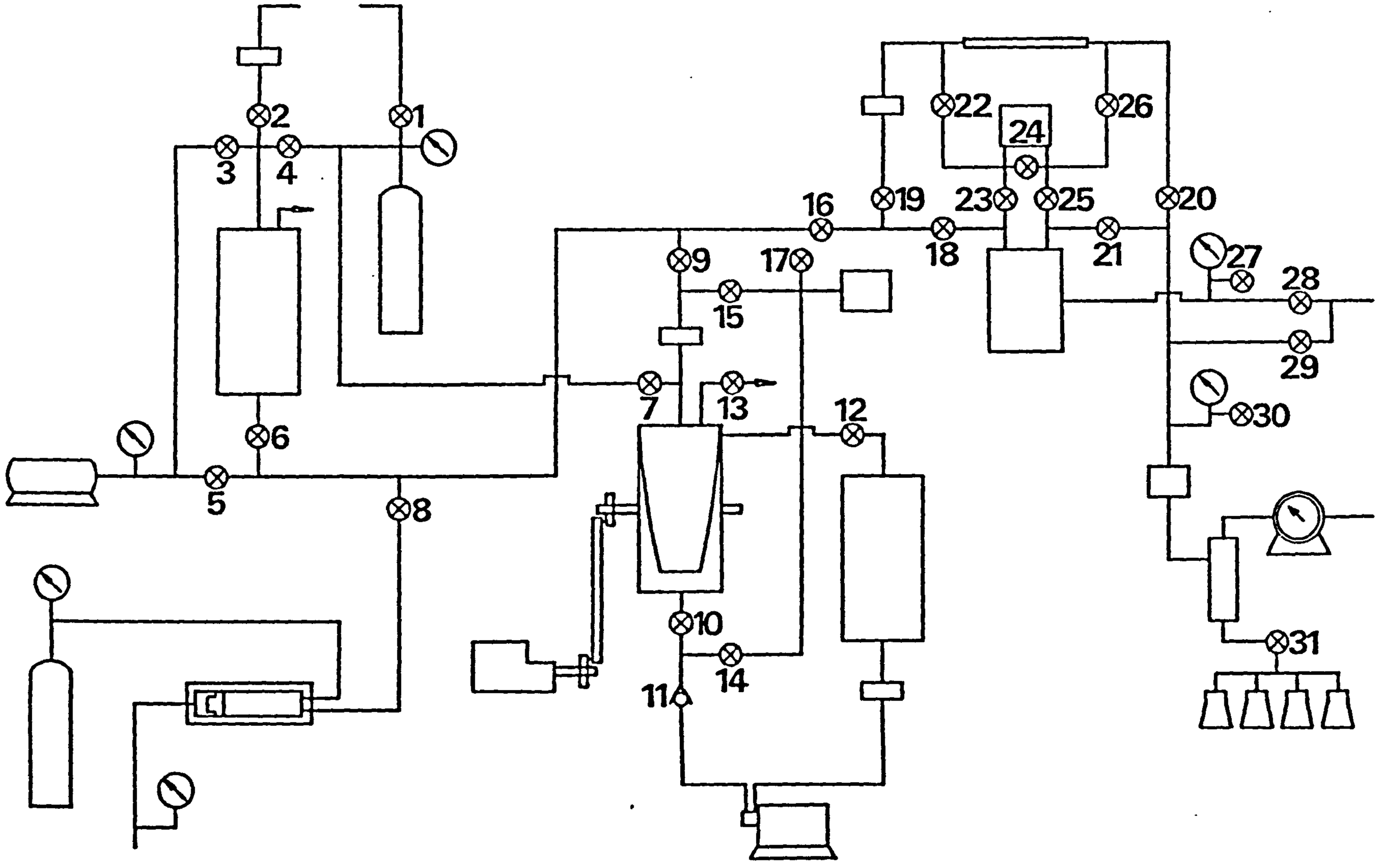

FIGURE A1-1. SCHEMATIC DIAGRAM OF CARBONATED WATER PERMEAMETER WITH VALVES NUMBERED

Whilst heating is in progress, evacuation, core saturation and transfer barrier charging are carried out.

A1.3 Evacuation

A possible variation in the dissolved salts content with an unknown effect on CO_2 solubility was eliminated by using synthetic sea water in all experiments. The desired quantity of brine is mixed in a preparation vessel, then driven by carbon dioxide pressure through a 0.25 micron filter and valve 2 to the brine reservoir in the permeameter.

The laboratory vacuum pump is then switched on and evacuation of the flow system conducted by the following procedure:

1. With valves 2 and 4 closed, valve 3 is opened to deaerate the brine in the brine reservoir. Valve 3 is then closed.
2. With the transfer barrier in the vertical position, valve 9 is opened to evacuate the inside of the rubber membrane. Valve 9 is then closed.
3. Valves 16, 18, 19, 22, 23, 24, 25 and 26 are opened to evacuate the core, viscometer and the lines to the differential pressure transducer. Valve 5 is then closed and the vacuum pump switched off.

A1.4 Core Saturation and Transfer Barrier Charging

1. Air is removed from the lines to the low pressure carbon dioxide supply by breaking the tube fittings upstream of valves

4 and 7, and purging with CO_2. The fittings are then reassembled.

2. The brine reservoir is pressurised through valve 4 by 10 to 20 psi carbon dioxide pressure. Valve 6 is opened and the core, viscometer and lines to the differential pressure saturated with deaerated brine. Valves 16, 19, 22 and 26 are then closed.

3. Valves 9 and 13 are opened and the rubber membrane in the transfer barrier filled with brine. Valves 4, 6, 9 and 13 are then closed.

4. The Eldex pump is started and valves 10 and 12 opened to purge residual air from the oil circuit. Completion of purging is judged visually by observing oil return to the top of the oil reservoir. Valve 12 is then closed.

5. Valves 14 and 17 are opened to purge the oil line to the 0 - 5,000 psi transducer. Valve 17 is then closed and the pump switched off.

A1.5 Back Pressuring

Valve 29 and purge valve 30 are opened, and water from the hydraulic pump forced through the back pressure regulator. Valve 30 is then closed and the pressure set to the desired level by hand adjustment of the control on the regulator. The pressure is read from the 0 - 400 bar precision gauge on the instrument panel. Valve 29 is then closed.

A1.6 Brine Flooding

1. The pump is started and the pressure in the transfer barrier raised to the flow test level (slightly below the system back pressure). The pressure is read from the digital display connected to the 0 - 5,000 psi transducer.
2. Valves 9 and 16 are opened and the pressure again raised to the test level.
3. Valve 21 is opened to equalise the system pressure, and valve 24 carefully closed to initiate flow of brine through the core. The differential pressure across the core is continuously monitored on the strip chart recorder.
4. The temperatures of the core and the brine throughout the flow system are periodically checked and recorded.
5. Liquid effluent from the separator is collected in flasks from the start of core flooding. It is directed by way of valve 31 to one of four different outlets.
6. Brine flooding is carried out until such a time as a reference (stabilised) permeability value is attained.
7. The pump is switched off, valve 24 opened, and valves 16, 18, 21, 23 and 25 closed.
8. Valve 12 is slowly opened to reduce the pressure in the transfer barrier to atmospheric.
9. Valves 9, 10 and 14 are then closed.

A1.7 Recharging

1. Valve 7 is opened and the membrane in the transfer barrier reshaped by low pressure CO_2 gas. Valves 7 and 12 are then closed.

2. Valves 4, 6, 9 and 13 are opened and the rubber membrane in the transfer barrier filled with brine. Valves 4, 6 and 13 are then closed and the low pressure CO_2 supply turned off.

A1.8 CO_2 Pressuring and Equilibrium Attainment

Carbon dioxide gas is introduced periodically from the gas intensifier to the brine on the inside of the membrane in the transfer barrier. Equilibrium between the gas and liquid phases is obtained by bringing them into intimate contact by oscillation of the transfer barrier vessel. In the early stages the gas pressure has to be increased by the addition of more CO_2, to compensate for the pressure decrease caused by the gas going into solution. Equilibrium is determined by observing no pressure change for a considerable time.

The precise procedure is as follows:

1. The 0 - 2,000 psi CO_2 regulator is opened and set to around 20 psi.
2. Air is purged from the high pressure CO_2 line from the gas booster by breaking the tube fittings upstream of valve 8. The fittings are then reassembled.
3. Valves 8, 15 and 17 are opened to purge oil from the lines to the 0 - 5,000 psi pressure transducer. Valve 17 is then closed.
4. The 0 - 2,000 psi CO_2 regulator is slowly opened to around 600 psi (gas booster supply pressure must exceed 500 psi).

5. The mechanical rocking assembly is engaged and started. Its appropriate cycle is adjusted by the manual control from the Kopp variator.
6. The gas booster is started and the CO_2 discharge pressure adjusted via the compressed air supply regulator.
7. The brine in the transfer barrier is pressurised periodically by opening and closing valve 9. It takes 4 to 8 hours to bring the carbonated water solution to equilibrium, depending upon the temperature and the desired equilibrium pressure. When equilibrium is attained, agitation of the transfer barrier vessel is stopped, valve 8 is closed and the CO_2 gas and air supplies turned off.
8. The transfer barrier is disengaged from the rocking mechanism and set in the vertical position.
9. Valve 15 is closed and valve 17 slowly opened to reduce the CO_2 pressure in the lines to the 0 - 5,000 psi transducer to atmospheric.

A1.9 Gas Flow and Viscosity Determination

1. The pump is started and valve 14 opened to oil purge all air and CO_2 from the lines to the 0 - 5,000 psi transducer.
2. Valve 17 is closed and the oil pressure raised to a level slightly above the transfer barrier pressure.
3. Valves 10, 16, 19, 22, 26 and 20 are opened in turn and all excess CO_2 gas pumped through the viscometer. The CO_2 flows through the wet gas meter, saturating the water in the meter, to vent.

4. As soon as continuous flow of carbonated water into the gas-liquid separator is observed, valve 24 is closed and the carbonated water viscosity measurement carried out. Valve 24 is then reopened and valves 19, 20, 22 and 26 closed.

A1.10 Carbonated Water Core Flooding

1. Valves 18, 21, 23 and 25 are opened, valve 24 slowly closed and carbonated water flowed through the core. The differential pressure across the core is continuously monitored on the strip chart recorder.
2. Temperatures throughout the flow system are periodically checked and recorded.
3. Liquid effluent from the separator is collected in flasks from the start of core flooding, and the volume of CO_2 gas produced from the core effluent solution is measured by the revolution counter on the wet gas meter.

A1.11 Close Down

1. After the desired volume of carbonated water has been pumped through the core and collected, the pump is switched off and valves 8, 19 and 24 opened. The back pressure regulator is then slowly adjusted to reduce the flow system pressure to atmospheric. Valve 8 is then closed.
2. The heating systems are switched off.

3. Valve 9 is closed, valves 7 and 12 opened, and the rubber membrane in the transfer barrier reshaped by low presssure CO_2. Valves 7 and 12 are then closed.
4. Valve 21 is closed, valve 5 opened and the vacuum pump switched on to evacuate the core and associated pipework. Evacuation is continued for two to three hours during cooling. Valve 5 is then closed and the vacuum pump switched off.
5. The core sleeve confining pressure is reduced by slowly opening valve 27, and the sleeved core removed from the core holder cell.
6. All liquid flow lines are flushed clean. The lines upstream of the core holder are flushed with distilled water while the downstream lines are flushed with citric acid to remove any carbonate precipitate.

A1.12 Analyses

Following a core test a series of different analyses are performed on the core, and the effluent analysis for calcium and magnesium is completed. The core is divided into segments, and the permeability, porosity, pore size distribution and concentration of minerals in the core segments are then measured (Chapter III).

APPENDIX 2

PETROGRAPHIC DESCRIPTIONS AND PHOTOMICROGRAPHS OF ROCKS USED IN CORE TESTS

A2.1 Yorkshire Jurassic Sandstone

Calcarenaceous sandstone consisting of subrounded detrital quartz and detrital carbonate debris cemented by micritic ferroan calcite (Plate A2-1). The detrital carbonate comprises for the most part of elongate fibrous calcite shell fragments (Plate A2-2), often with a central pocket of sparry calcite cavity-fill crystals, and scattered large twinned calcite intraclasts. The shell fragments are orientated parallel to the bedding in an interlayered quartz (sandy) and carbonate (limey) framework.

Plates A2-3 and A2-4 show S.E.M. views of the sandstone. With the advantages over light microscopy of depth of focus and high magnification, the shape and contacts between the quartz grains are clearly visible. Also apparent are the micritic calcite cement, seen in Plate A2-4 coating a quartz grain, and some relatively large diameter pores.

Sand Grain Shape:	subrounded
Coarseness:	fine (average quartz grain diameter 0.25mm with shell fragment lengths up to 7 mm)
Sorting:	good
Grain Contact:	point to short line

PLATE A2-1. PHOTOMICROGRAPH; CROSSED NICOLS, X4 MAGNIFICATION. YORKS JURASSIC SANDSTONE SHOWING QUARTZ GRAINS (WHITE, GREY AND BLACK) AND SHELL FRAGMENTS (DARK BROWN) CEMENTED BY CALCITE (LIGHT BROWN)

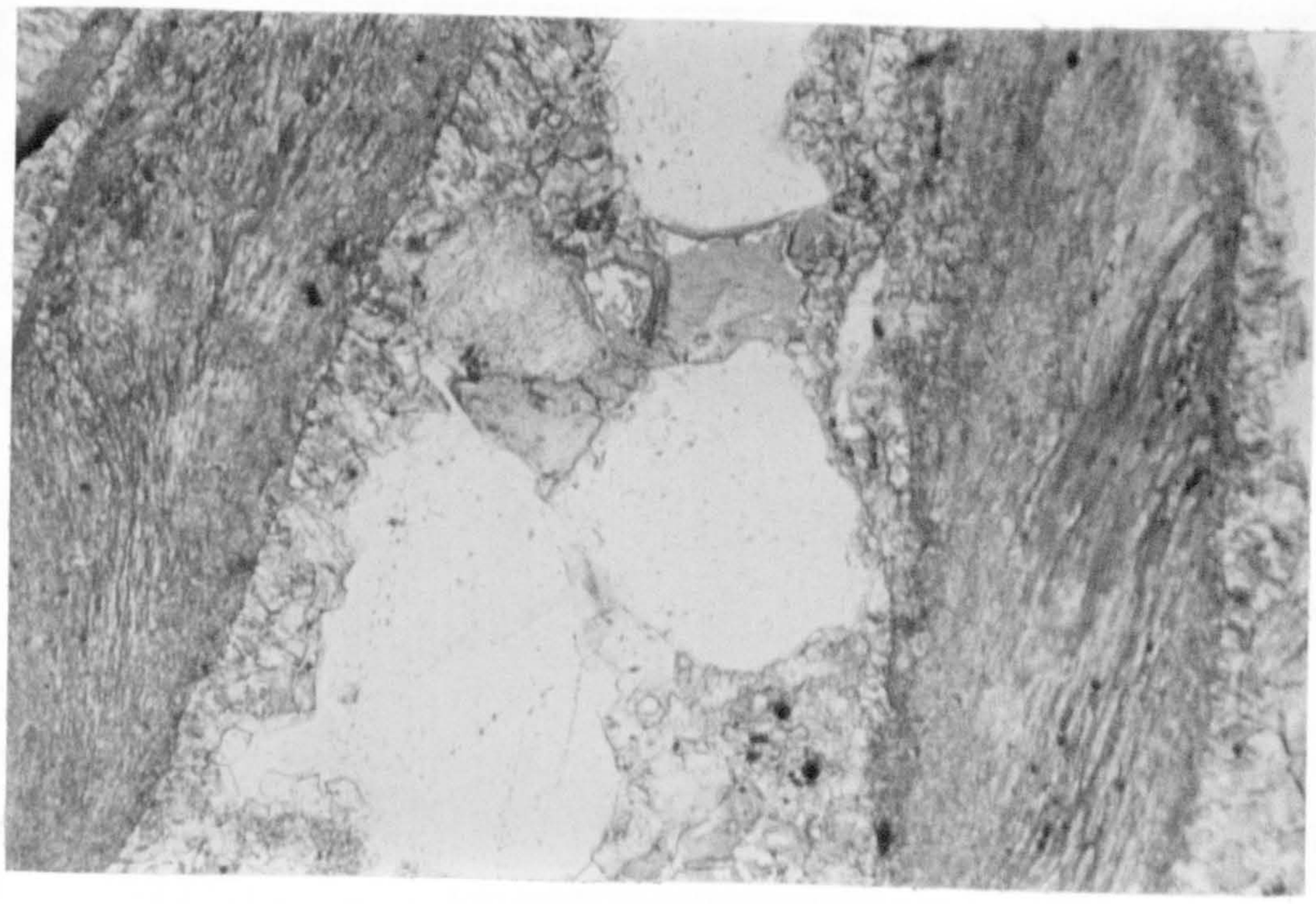

PLATE A2-2. PHOTOMICROGRAPH; PLAIN LIGHT, X10 MAGNIFICATION. YORKS JURASSIC SANDSTONE STAINED FOR CALCITE USING ALIZARIN RED S. THE DETRITAL SHELL FRAGMENTS HAVE STAINED RED INDICATING PURE CALCITE COMPOSITION, WHILE THE MICRITIC FERROAN CALCITE SURROUNDING THE SHELLS AND QUARTZ GRAINS (WHITE) HAS STAINED BLUE

PLATE A2-3. S.E.M. VIEW OF YORKS JURASSIC SANDSTONE (X 122 MAGNIFICATION) SHOWING DETRITAL QUARTZ GRAINS WITH MICRITIC CALCITE PORE FILL

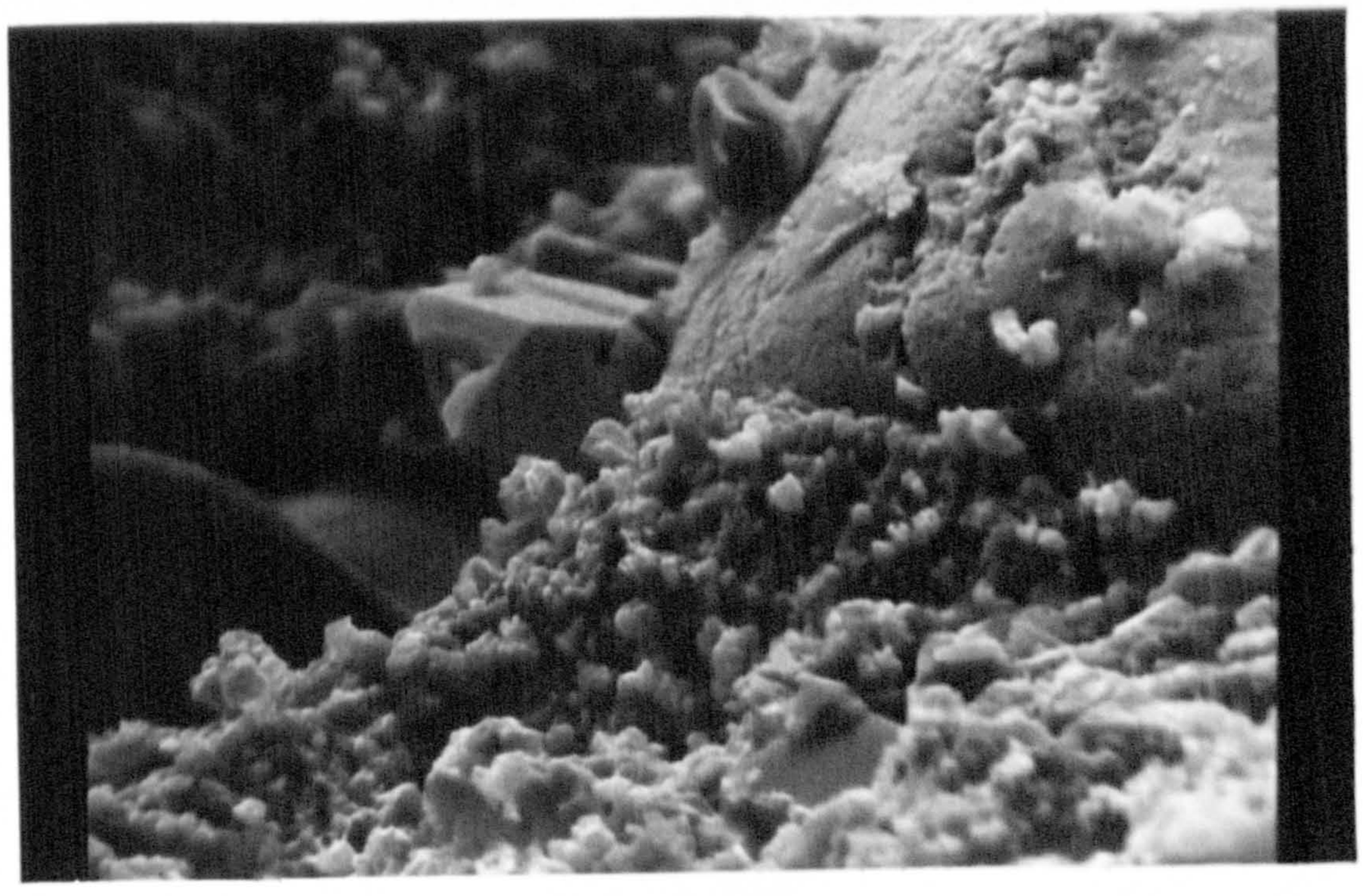

PLATE A2-4. S.E.M. VIEW OF YORKS JURASSIC SANDSTONE (X 570 MAGNIFICATION) SHOWING MICRITIC CALCITE CEMENT COATING A QUARTZ GRAIN. THE CLEARLY DEFINED CRYSTAL IN THE CENTRE OF THE PICTURE IS QUARTZ WHICH HAS FORMED DIAGENETIC OVERGROWTH

A2.2 Fife Carboniferous Sandstone (A)

Dolomitic submature/mature quartzarenite composed for the most part of subangular to rounded quartz grains partially cemented by secondary ferroan dolomite (Plate A2-5). The dolomite is relatively evenly distributed in a compacted detrital matrix, occurring as rhomb shaped crystals and less commonly as crystalline masses in the voids between sand grains (Plate A2-6). The size of the dolomite rhombs is closely related to the size of the detrital grains and hence to the resulting pore spaces.

Coarseness:	fine (average quartz grain diameter 0.2mm)
Sorting:	moderate
Grain Contact:	line to concave-convex

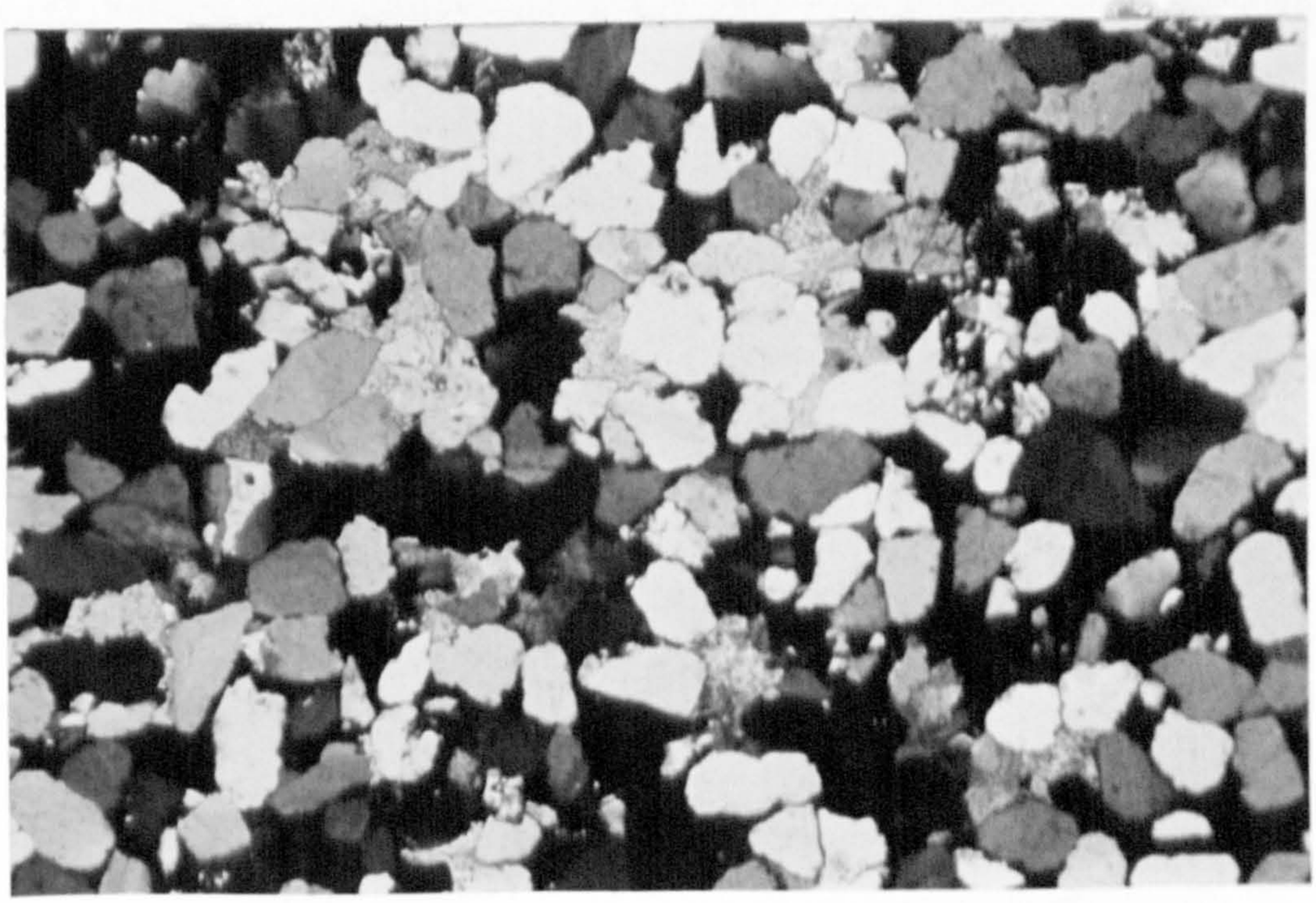

PLATE A2-5. PHOTOMICROGRAPH; CROSSED NICOLS, X4 MAGNIFICATION. FIFE CARBONIFEROUS SANDSTONE (A) COMPOSED OF DETRITAL QUARTZ GRAINS, PARTIALLY CEMENTED BY SECONDARY DOLOMITE (YELLOW/ ORANGE)

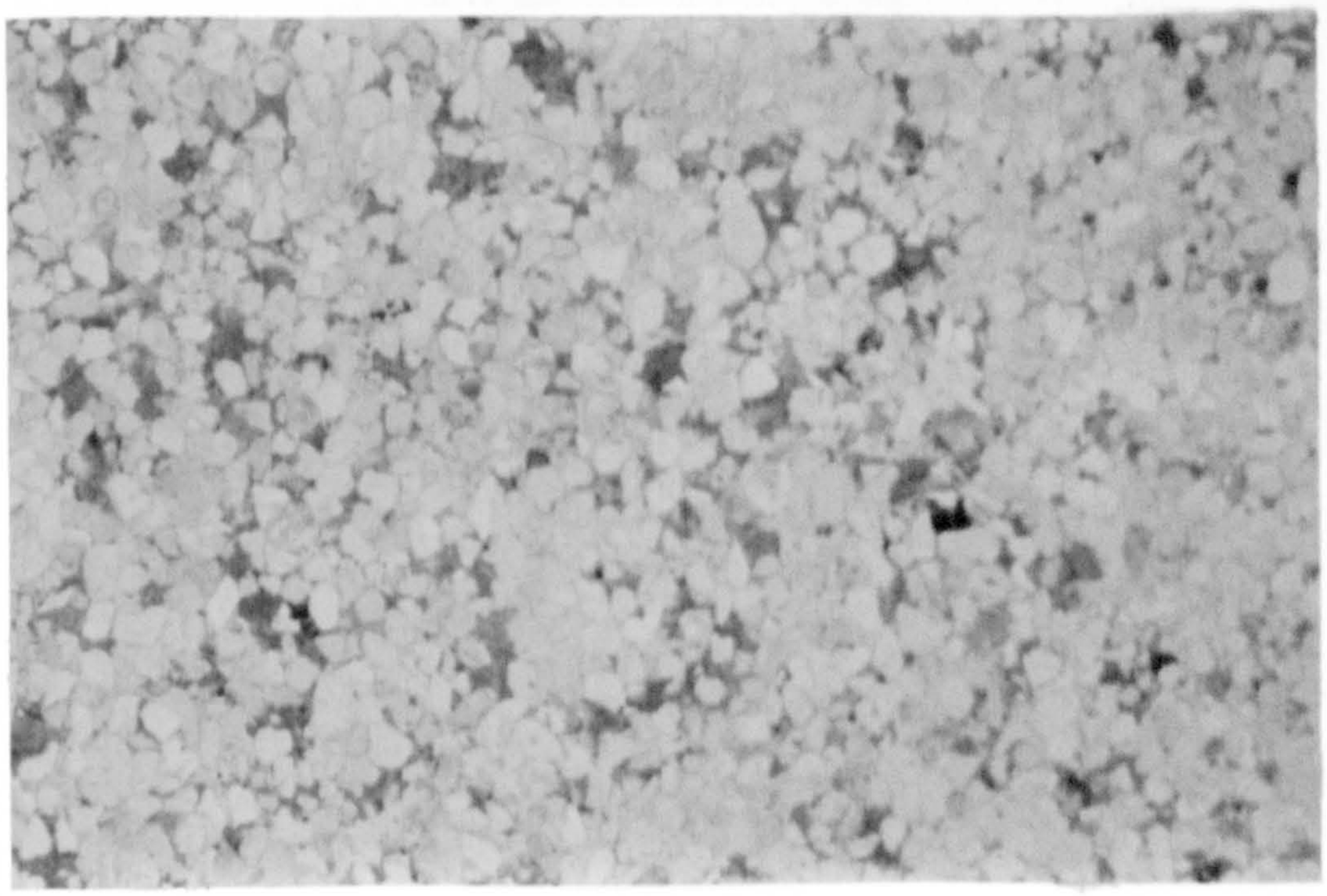

PLATE A2-6. PHOTOMICROGRAPH; PLAIN LIGHT, X2 MAGNIFICATION. SHOWS THE EVEN DISTRIBUTION OF FERROAN DOLOMITE (STAINED BLUE USING POTASSIUM FERRICYANIDE) IN FIFE CARBONIFEROUS SANDSTONE (A).

A2.3 Fife Carboniferous Sandstone (B)

Dolomitic submature quartzarenite composed of tightly packed sub-rounded quartz grains with minor amounts of interstitial dolomite and clay. Compaction was well advanced prior to carbonate precipitation, limiting the dolomite occurrence to scattered crystals and aggregates, often filling two or three adjacent pores (Plate IV-9).

Coarseness :	very fine (average quartz grain diameter 0.08 mm)
Sorting :	moderate
Grain Contact :	long line to concave-convex

A2.4 Rotliegende Sandstone from Southern North Sea

Poorly consolidated, calcitic, submature quartzarenite consisting of subrounded grains and rock fragments partially cemented by calcite (Plate A2-7). The calcite occurs as large scattered crystals approaching the size of the detrital grains while many of the quartz grains have thin clay coatings.

Coarseness :	very fine to medium
Sorting :	poor
Grain Contact :	point to point

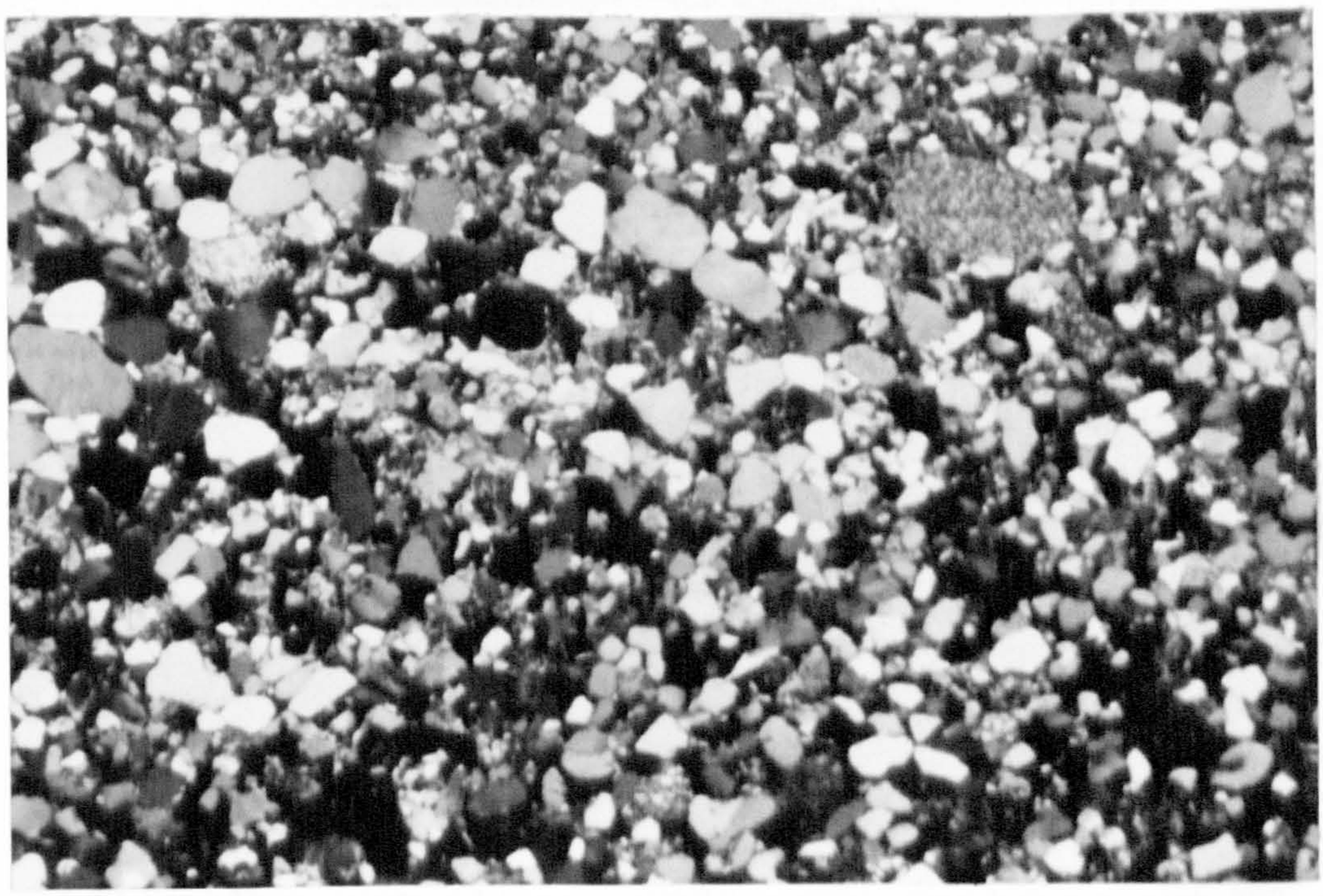

PLATE A2-7. PHOTOMICROGRAPH; CROSSED NICOLS, X3 MAGNIFICATION. ROTLIEGENDE SANDSTONE FROM SOUTHERN NORTH SEA COMPOSED OF DETRITAL QUARTZ GRAINS (WHITE, GREY, BLACK) WITH PARTIAL CALCITE PORE FILL (LIGHT BROWN)

A2.5 Jurassic Sandstone from Northern North Sea

Very poorly consolidated, dolomitic, submature subarkose composed of angular to subangular quartz and felspar grains cemented by dolomite. A photomicrograph of typical material is presented in Plate A2-8. The dolomite occurs as small crystals of the same order of size as the sand grains. Cementation clearly took place prior to any significant compaction of the detrital matrix.

Coarseness :	medium (average sand grain diameter 0.3 mm)
Sorting :	poor
Grain Contact :	short line to point

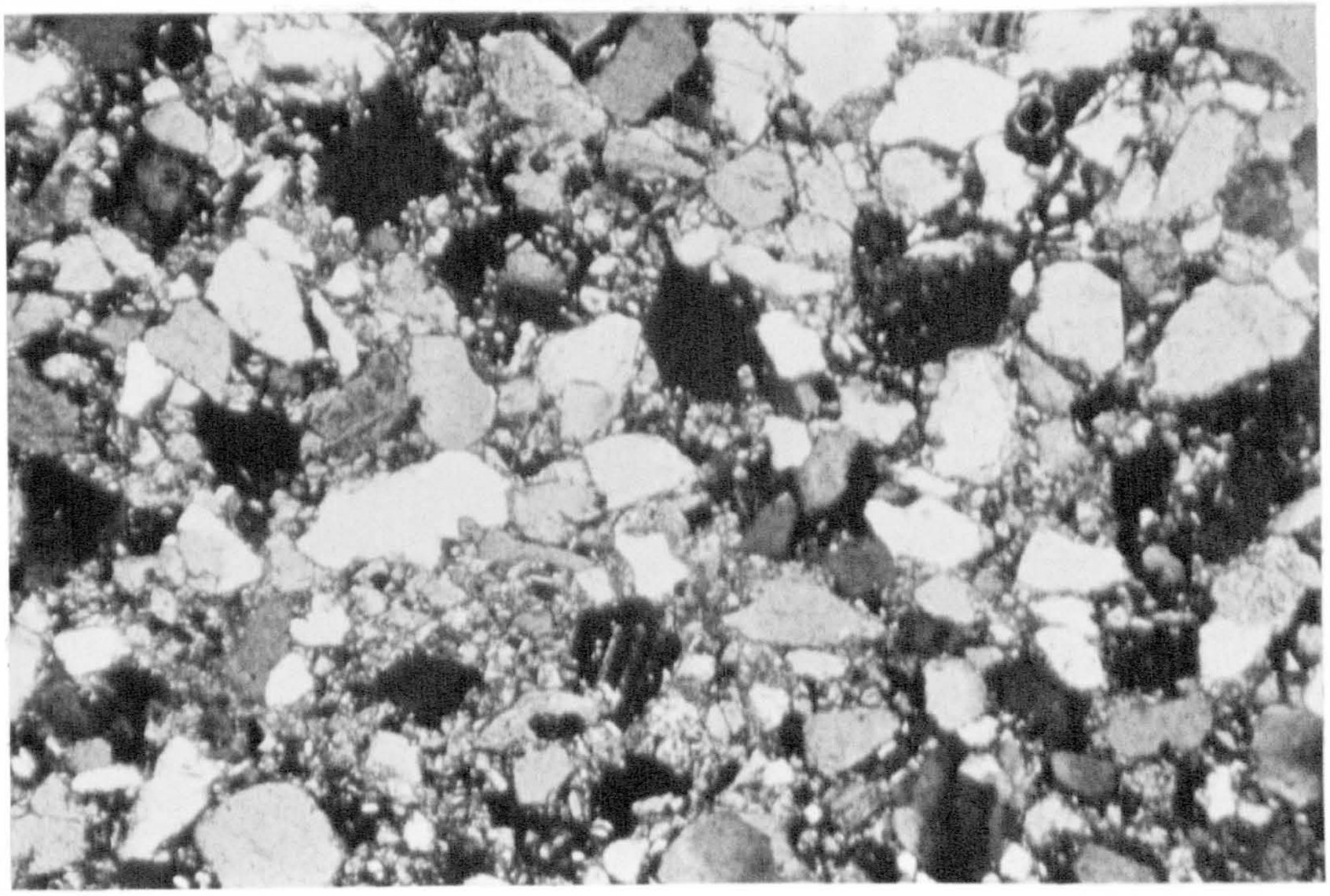

PLATE A2-8. PHOTOMICROGRAPH; CROSSED NICOLS, X4 MAGNIFICATION. JURASSIC SANDSTONE FROM NORTHERN NORTH SEA SHOWING POORLY CONSOLIDATED DETRITAL GRAINS CEMENTED BY FINELY CRYSTALLINE DOLOMITE

A2.6 Jurassic Sandstone from Indefatigable Field

Dolomitic submature quartzarenite composed mostly of subangular to subrounded quartz grains and rock fragments partially cemented by dolomite. Small amounts of detrital and pore-fill clay are also present, the pore-fill appearing to have formed by recrystallisation of the detrital material. The dolomite occurs as scattered crystalline masses totally cementing the detrital grains, and more uniformly as finely crystalline pore-fill (Plate A2-9). In areas that are totally cemented the detrital grains are held by single dolomite crystals, obliterating porosity.

Although for the most part the sandstone is relatively homogeneous, some horizons contain interlayered coarser and finer bands as shown in Plate IV-16.

Coarseness:	very fine to medium (average sand grain diameter 0.1 mm)
Sorting:	very poor
Grain Contact:	short line to concave-convex

PLATE A2-9. PHOTOMICROGRAPH; CROSSED NICOLS, X4 MAGNIFICATION. INDEFATIGABLE FIELD SANDSTONE

A2.7 Oxfordshire Jurassic Limestone

Poorly washed biosparite composed of shell fragments and ooliths cemented by calcite spar (Plate A2-10). Minor amounts of intraclasts and subrounded detrital quartz grains are also present. The shell fragments are normally elongate (generally in the order of 0.4 mm long but up to 1.5 cm), orientated parallel to the bedding. They, along with the quartz grains, often have a superficial oolitic envelope.

Some minor interlayering of tightly packed carbonate detritus with only a small proportion of cement, and less consolidated material with a much higher proportion of cement, occurs in an otherwise homogeneous framework.

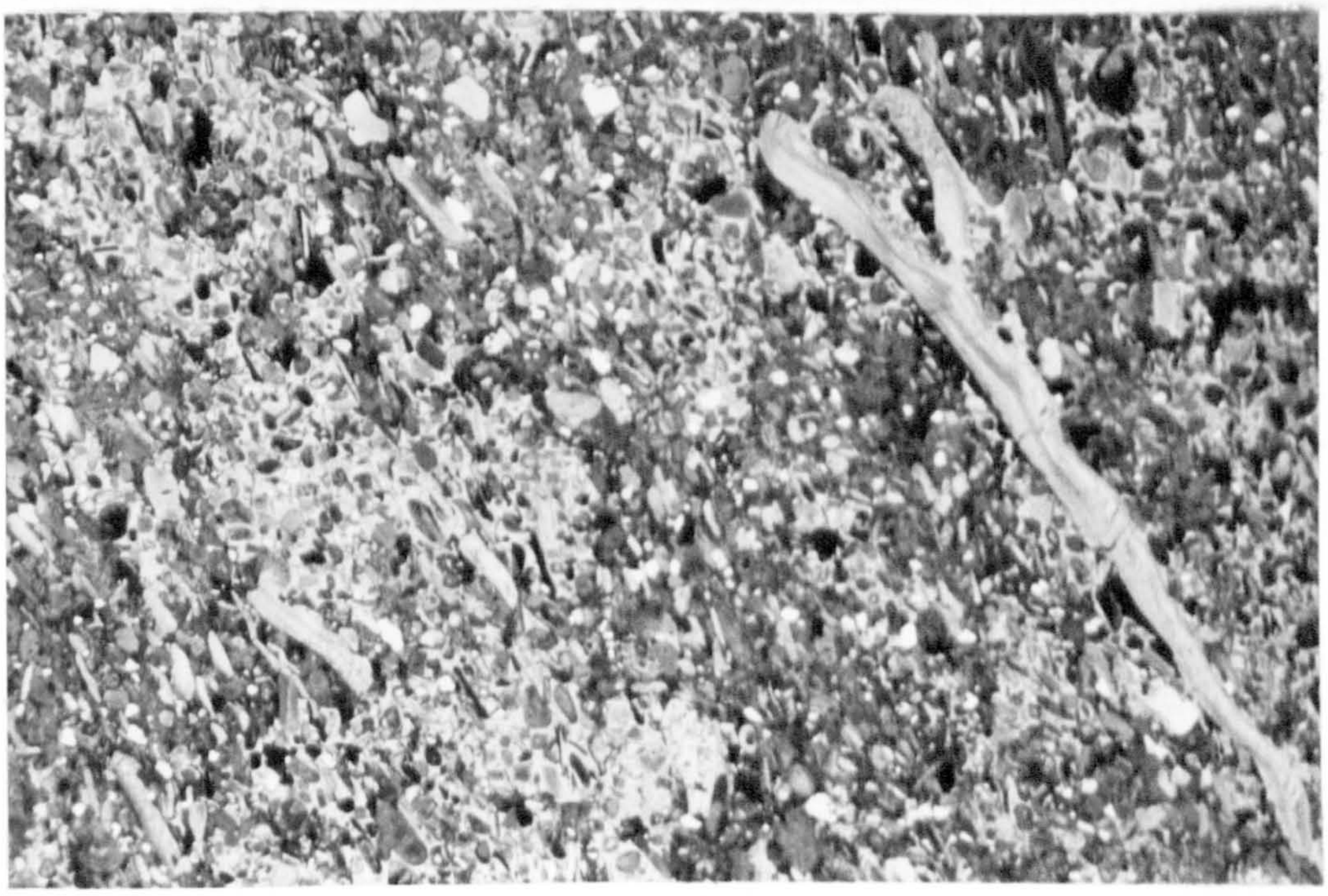

PLATE A2-10. PHOTOMICROGRAPH; CROSSED NICOLS, X2 MAGNIFICATION. OXFORDS JURASSIC LIMESTONE SHOWING SHELL FRAGMENTS, OOLITHS AND QUARTZ GRAINS CEMENTED BY CALCITE SPAR

APPENDIX 3

STAINING PROCEDURE FOR CARBONATE MINERAL IDENTIFICATION

CARBONATE STAINING PROCEDURE

The following three organic dye staining solutions were used:

a) Solution of 0.2 g alizarin red S dissolved in 100 ml 1.5% hydrochloric acid.

b) Solution of 2 g potassium ferricyanide dissolved in 100 ml 1.5% hydrochloric acid.

c) Mixture of 3 parts (a) to 2 parts (b).

The complete procedure for preparing stained thin sections was as follows:

1. Prepare a finely polished thin section.
2. Etch section in 1.5% HCl for 30 seconds.
3. Stain section for 60 seconds in the staining solution.
4. Wash section quickly in distilled water.
5. Dry section and then cover slip.

The stain colours produced are given below in Table A3-1.

CARBONATE MINERAL	ALIZARIN RED S	POTASSIUM FERRICYANIDE	MIXTURE
Calcite	pink to red	-	pink to red
Ferroan Calcite	pink to red	blue	mauve to blue
Dolomite	-	-	-
Ferroan Dolomite	-	blue	turquoise

TABLE A3-1. CARBONATE MINERAL STAIN COLOURS

APPENDIX 4

DETERMINATION PROCEDURES FOR CALCIUM AND MAGNESIUM ION CONCENTRATIONS BY EDTA TITRATION

ANALYSIS FOR CALCIUM AND MAGNESIUM BY EDTA TITRATION

HHSNNA indicator permits the determination of calcium ion concentration in the presence of magnesium ions. It produces a sharp colour change from wine red to pure blue when calcium is titrated with EDTA at pH values above 10 (77).

For the joint determination of calcium and magnesium Eriochrome Black T is generally used as an indicator (78). On titration with EDTA at pH 10 the red colour of the indicator changes sharply to blue at the end point.

A4.1 Procedure for Calcium

1. Pipette two 25 ml portions of the mixed solution into two separate conical flasks and dilute each with 25 ml of distilled water.
2. Acidify each sample with a few drops of hydrochloric acid to ensure solution of all carbonate.
3. To the first flask add 4 ml of 8M-potassium hydroxide solution and allow to stand for 3 - 5 minutes with occasional swirling. This brings the pH of the solution up into the required range.
4. Add 30 mg each of potassium cyanide and hydroxylammonium chloride and swirl the contents of the flask until the crystals dissolve. These additives mask the effects of interfering elements on the titration.
5. Add 0.2 g of HHSNNA indicator and titrate with 0.01M-EDTA solution until the colour changes from red to blue. The volume of titre (x ml) is noted.

6. To the second flask run x-1 ml of the EDTA solution.

7. Add 4 ml of 8M-potassium hydroxide, then 30 mg each of potassium cyanide and hydroxlammonium chloride. Swirl the flask until the crystals dissolve.

8. Add 0.2 g of HHSNNA indicator and complete the titration. Note the volume of titre (y ml).

9. From the relation:

$$1 \text{ ml } 0.01\text{M-EDTA} = 0.4008 \text{ mg Ca}$$

the calcium ion concentration (Ca^{2+}) is computed as:

$$Ca^{2+} = \frac{y \times 0.4008 \times 1000}{25.0} \quad \text{mg/l}$$

A4.2 Procedure for Total Calcium and Magnesium

1. Pipette 25 ml of the mixed solution into a conical flask and dilute with 25 ml of distilled water.

2. Acidify the sample with a few drops of hydrochloric acid.

3. Buffer the solution to pH 10 by adding 5 ml of monoethanolamine-hydrochloric acid and mixing.

4. Add 30 mg each of potassium cyanide and hydroxylammonium chloride and swirl the contents of the flask until the crystals dissolve.

5. Add 0.2 g of Eriochrome Black T indicator and titrate with 0.01M-EDTA to a pure blue end point. The volume of titre (z ml) is noted.

6. From the relation:

$$1 \text{ ml } 0.01\text{M-EDTA} = 0.2432 \text{ mg Mg}$$

the magnesium ion concentration (Mg^{2+}) is computed as:

$$Mg^{2+} = \frac{(z - y)\ 0.2432 \times 1000}{25.0} \quad mg/l$$

APPENDIX 5

CORE FLOOD FLOW RATES

TEST CONDITION	FLOW RATE (CCS/MINUTE)	CUMULATIVE CORE FLOOD VOLUME (CCS)	PERMEABILITY (mD)
Distilled Water, 1000 psi, 20°C	1.06	250	16.6
	1.53	800	27.5
	2.87	2100	49.1
Brine, 1000 psi, 20°C	4.06	2100	248.0
Carbonated Brine, 1000 psi, 20°C	2.40	1050	385.5
	4.06	2100	755.0
Carbonated Brine, 1000 psi, 80°C	4.06	2100	810.6
Carbonated Brine, 3000 psi, 80°C	3.84	2100	580.0
Core Containing Crude Oil; Carbonated Brine, 3000 psi, 80°C	0.40	50	5.1
	1.75	150	12.3
	2.18	250	29.9
	3.84	2100	130.0

TABLE A5-1. FLOW RATES USED IN TESTS ON YORKS JURASSIC SANDSTONE.

TEST CONDITION	FLOW RATE (CCS/MINUTE)	CUMULATIVE CORE FLOOD VOLUME (CCS)	PERMEABILITY (mD)
Carbonated Brine, 1000 psi, 20°C	4.06	2100	180.0
Carbonated Brine, 2500 psi, 80°C	3.87	2100	720.0

TABLE A5-2. FLOW RATES USED IN TESTS ON FIFE CARBONIFEROUS SANDSTONE (A).

TEST CONDITION	FLOW RATE (CCS/MINUTE)	CUMULATIVE CORE FLOOD VOLUME (CCS)	PERMEABILITY (mD)
Carbonated Brine, 1000 psi, 80°C	2.85	250	5.0
	3.30	500	5.8
	3.70	750	6.7
	4.06	2100	12.4
Carbonated Brine, 2000 psi, 80°C	1.85	400	6.5
	2.85	1100	7.8
	2.92	2100	8.0
Carbonated Brine, 3000 psi, 80°C	3.80	2100	39.6
Cleaned Core for Comparison with Gas Condensate and Oil Containing Cores; Carbonated Brine, 2000 psi, 80°C	0.50	50	3.0
	1.43	1250	6.4
	2.30	2100	6.6
Core Containing Gas Condensate; Carbonated Brine, 2000 psi, 80°C	2.30	300	8.3
	3.95	4200	24.6
Core containing Crude Oil; Carbonated Brine, 2000 psi, 80°C	0.50	400	2.1
	1.43	1050	4.8
	2.30	2100	6.6

TABLE A5-3. FLOW RATES USED IN TESTS ON INDEFATIGABLE FIELD SANDSTONE

TEST CONDITION	FLOW RATE (CCS/MINUTE)	CUMULATIVE CORE FLOOD VOLUME (CCS)	PERMEABILITY (mD)
Carbonated Brine, 1500 psi, 80°C	1.48	50	72.4
	2.38	100	91.6
	4.02	250	269.7

TABLE A5-4. FLOW RATES USED IN TEST ON OXFORDS JURASSIC LIMESTONE.

LIST OF REFERENCES

1. Bernard, G.G., Holm, L.W. and Harvey, C.P.: "Use of Surfactant to Reduce CO_2 Mobility in Oil Displacement", Soc. Pet. Eng. J. (Aug. 1980) 281-292.

2. Shelton, J.L. and Schneider, F.N.: "The Effects of Water Injection on Miscible Flooding Methods Using Hydrocarbons and Carbon Dioxide", Soc. Pet. Eng. J. (June 1975) 217-226.

3. Kane, A.V.: "Performance Review of a Large Scale CO_2 WAG Enhanced Recovery Project, SACROC Unit, Kelly-Snyder Field", J. Pet. Tech. (Feb. 1979) 217-231.

4. Holm, L.W.: "Status of CO_2 and Hydrocarbon Miscible Oil Recovery Methods", J. Pet. Tech. (Jan. 1976) 76-84.

5. Newton, L.E., Jr., and McClay, R.A.: "Corrosion and Operation Problems, CO_2 Project, SACROC Unit", paper SPE 6391 presented at the SPE-AIME Permian Basin Oil and Gas Recovery Conference, Midland, Texas, March 10-11, 1977.

6. Pontious, S.B. and Tham, M.J.: "North Cross (Devonian) Unit CO_2 Flood-Review of Flood Performance and Numerical Simulation Model", paper SPE 6390 presented at the SPE-AIME Permian Basin Oil and Gas Recovery Conference, Midland, Texas, March 10-11, 1977.

7. Hansen, P.W.: "A CO_2 Tertiary Recovery Pilot, Little Creek Field, Mississippi", paper SPE 6747 presented at the SPE-AIME 52nd Annual Fall Technical Conference and Exhibition, Denver, Oct. 9-12, 1977.

8. Doscher, T.M. and Kuuskraa, V.A.: "Carbon Dioxide for Enhanced Recovery of Crude Oil", paper presented at the European Symposium on Enhanced Oil Recovery, Edinburgh, July 5-7, 1978.

9. Cameron, J.T.: "SACROC Carbon Dioxide Injection - A Progress Report", paper presented at the API Production Department Annual Meeting, Los Angeles, April, 1976.

10. Kuuskraa, V.A. and Doscher, T.M.: "Economics of North Sea Enhanced Oil Recovery", paper presented at the European Symposium on Enhanced Oil Recovery, Edinburgh, July 5-7, 1978.

11. Crawford, H.R., Neill, G.H., Bucy, B.J. and Crawford, P.B.: "Carbon Dioxide - A Multipurpose Additive for Effective Well Stimulation", J. Pet. Tech. (March, 1963) 237-242.

12. Dodds, W.S., Stutzman, L.F. and Sollami, B.J.: "Carbon Dioxide Solubility in Water", Chem. Eng. Data Series (1956) 1, 92-95.

13. Miller, J.P.: "A Portion of the System $CaCO_3$-CO_2-H_2O with Geological Implications", Am. Jour. Sci. (March 1952) 250, 161-203.

14. Segnit, E.R., Holland, H.B. and Biscardi, C.J.: "The Solubility of Calcite in Aqueous Solutions", Geochim. et Cosmochim. Acta (1962) 26, 1301-1331.

15. Ellis, A.J.: "The Solubility of Calcite in Carbon Dioxide Solutions", Am. Jour. Sci. (May 1959) 257, 354-365.

16. Sharp, W.E.: "The System $CaO-CO_2-H_2O$ in the Two Phase Region Calcite and Aqueous Solution", Ph.D. Thesis, Univ. of California (1964).

17. Sharp, W.E. and Kennedy, G.C.: "The system $CaO-CO_2-H_2O$ in the Two Phase Region Calcite and Aqueous Solution", Jour. of Geol. (1965) 73, 391-403.

18. Berendsen, P.: "The Solubility of Calcite in CO_2-H_2O Solutions and Geologic Applications", Ph.D. Thesis, Univ. of California (1971).

19. Holm, L.W.: "CO_2 Slug and Carbonated Water Oil Recovery Process", Prod. Monthly (Sept. 1963) 6-28.

20. Holm, L.W. and Josendal, V.A.: "Mechanisms of Oil Displacement by Carbon Dioxide", J. Pet. Tech. (Dec. 1974) 1427-1436.

21. Stright, D.H. Jr., Aziz, K., Settari, A., and Starratt, F.E.: "Carbon Dioxide Injection into Undersaturated Viscous Oil Reservoirs - Simulation and Field Application", J. Pet. Tech. (Oct. 1977) 1248-1258.

22. "Secondary and Tertiary Oil Recovery Processes", Interstate Oil Compact Commission, Oklahoma City (Sept. 1974).

23. Henry, R.L.: "A Laboratory Study of CO_2 and H_2S Miscible Injection in an Oil Filled Porous media", Ph.D. Thesis, Univ. of Missouri-Rolla (1977).

24. Staples, M.: "Permeability Reduction in CO_2 Injection Projects due to Carbonate Dissolution", M.Eng. Thesis, Heriot-Watt Univ. (1978).

25. Conner, W.D.: "Tertiary Oil Recovery by CO_2 Injection", report to the US Energy Research and Development Administration (Oct. 1977).

26. Martin, J.W.: "Additional Oil Production Through Flooding with Carbonated Water", Prod. Monthly (July 1951) 15, 18-22.

27. Holm, L.W.: "Carbon Dioxide Solvent Flooding for Increased Oil Recovery", Trans. AIME (1959) 216, 225-231.

28. Johnson, W.E., Macfarlane, R.M., Breston, J.N. and Neil, D.C.: "Laboratory Experiments with Carbonated Water and Liquid Carbon Dioxide as Oil Recovery Agents", Prod. Monthly (Nov. 1952) 17, 15.

29. Reed, M.G.: "Formation Permeability Damage by Mica Alteration and Carbonate Dissolution", paper SPE 6009 presented at the SPE-AIME 51st Annual Fall Technical Conference and Exhibition, New Orleans, Oct. 3-6, 1976.

30. Mungan, N.: "Permeability Reduction Through Changes in pH and Salinity", J. Pet. Tech. (Dec. 1965) 1449-1453.

31. Martin, J.W.: "Operation of Orco Process Near Richburg", Oil and Gas Jour. (Dec. 1951) 82-86.

32. Powell, J.P.: "Orco Process, K. and S. Project", Prod. Monthly (May 1959) 36-39.

33. Scott, J.O., and Forrester, C.E.: "Performance of Domes Unit Carbonated Water Flood", J. Pet. Tech. (Dec. 1965) 1379-1384.

34. De Nevers, N.: "Carbonated Waterflooding. Is it a Lab. Success and a Field Failure", World Oil (Sept. 1966) 93-96.

35. Holm, L.W.: "Modified Water Floods Can Improve Ultimate Recovery", World Oil (Oct. 1969) 126-132.

36. Alsinbili, M.B.: "An Experimental and Theoretical Investigation on Oil Recovery by High Pressure Carbon Dioxide Injection", Ph.D. Thesis, Univ. of Oklahoma (1972).

37. White, R.W.: "Oil Recovery by CO_2 - Past and Future", Petroleum Engineer (Dec. 1971) 58-60.

38. Reeson, D.M. and Ortloff, G.D.: "Laboratory Investigation of the Water-Driven Carbon Dioxide Process for Oil Recovery", Trans., AIME (1959) 216, 388-391.

39. Holm, L.W.: "Comparison of Propane and CO_2 Solvent Flooding Processes", AIChE Jour. (1961) 2, 179-184.

40. Rathnell, J.J., Stalkup, F.I. and Hassinger, R.C.: "A Laboratory Investigation of Miscible Displacement by Carbon Dioxide", paper SPE 3483 presented at SPE-AIME 46th Annual Fall Meeting, New Orleans, Oct. 3-6, 1971.

41. Kumar, N. and Von Gonten, W.D.: "An Investigation of Oil Recovery by Injecting CO_2 and LPG Mixtures", paper SPE 4581 presented at the SPE-AIME 48th Annual Fall Meeting, Las Vegas, Sept. 30 - Oct. 3, 1973.

42. Huang, T.S.E. and Tracht, J.H.: "The Displacement of Residual Oil by Carbon Dioxide", paper SPE 4735 presented at the SPE-AIME Improved Oil Recovery Symposium, Tulsa, April 22-24, 1974.

43. Stalkup, F.I.: "Carbon Dioxide Miscible Flooding: Past, Present and Outlook for the Future", J. Pet. Tech. (Aug. 1978) 1102-1112.

44. Frey, R.P.: "West Texas Unit Reponds to CO_2 Flood", paper presented to Southwestern Petroleum Short Course, Texas Tech. University, Lubbock, April 1975.

45. Harvey, M.T., Shelton, J.L. and Kelm, C.H.: "Field Injectivity Experiences with Miscible Recovery Projects using Alternate Rich Gas and Water Injection", paper SPE 4738 presented at the SPE-AIME Improved Oil Recovery Symposium, Tulsa, April 22-24, 1974.

46. Lindsay, D.M.: "An Experimental Study of Sandstone Acidising", M.Sc. Thesis,Univ. of Texas (1976).

47. Dickson, J.A.D.: "Carbonate Identification and Genesis as Revealed by Staining", Jour. Sed. Pet. (June 1966) 36, 491-505.

48. "API Recommended Practice for Analysis of Oil Field Waters", American Petroleum Institute, Dallas, Texas (Nov. 1968).

49. Sippel, R.F. and Glover, E.D.: "The Solution Alteration of Carbonate Rocks", Geochim. et Cosmochim. Acta (1964) 28, 1401-1471.

50. Weyl, P.K.: "The Solution Kinetics of Calcite", Jour. Geol. (1958) 66, 163-176.

51. Lund, K.: "The Acidisation of Sandstone", Ph.D. Thesis, Univ. of Michigan (1974).

52. Schechter, R.S. and Gidley, J.L.: "The Change in Pore Size Distributions from Surface Reactions in Porous Media", AIChE Jour.(May 1969) 339-350.

53. Guin, J.A.: "Chemically Induced Changed in Porous Media", Ph.D. Thesis, Univ. of Texas (1969).

54. Guin, J.A. and Schechter, R.S.: "Matrix Acidisation with Highly Reactive Acids", Soc. Pet. Eng. J. (Dec. 1971) 11, 390-398.

55. Sinex, W.E. Jr.,: "Dissolution of a Porous Matrix by Slowly Reacting Flowing Acids", M.Sc. Thesis, Univ. of Texas (1970).

56. Sinex, W.E. Jr., Schechter, R.S. and Silberberg, I.H.: "Dissolution of a Porous Matrix by Slowly Reacting Flowing Acids", Ind. Eng. Chem. Fundam. (May 1972) 205-209.

57. Williams, B.B., and Whiteley, M.E.: "Hydrofluoric Acid Reaction with a Porous Sandstone", Soc. Pet. Eng. J. (Sept. 1971) 306-314; Trans., AIME, 251.

58. McCune, C.C., Fogler, H.S., Lund, K., Cunningham, J.R., and Ault, J.W.: "A New Model of the Physical and Chemical Changes in Sandstone During Acidising", Soc. Pet. Eng. J. (Oct. 1975) 361-370.

59. Lund, K. and Fogler, H.S.: "Acidisation . V.On the Prediction of the Movement of Acid and Permeability Fronts in Porous Media", Chem. Eng. Sci. (1976) 31, 381-392.

60. Lund, K., Fogler, H.S. and McCune, C.C.: "Predicting the Flow and Reaction of HCl/HF Acid Mixtures in Porous Sandstone Cores", Soc. Pet. Eng. J. (Oct. 1976) 248-260; Trans., AIME, 261.

61. McCune, C.C. and Fogler, H.S.: "An Experimental Technique for Obtaining Permeability - Porosity Relationships in Acidisation", paper 52e presented at 74th National Meeting AIChE, New Orleans, March 11-15, 1973.

62. McCune, C.C., Fogler, H.S., and Kline, W.E.: "An Experimental Technique for Obtaining Permeability - Porosity Relationships in Acidised Porous Media", I.E.C. Fundamentals (1979) 18, 188-191.

63. Fogler, H.S. and McCune, C.C.: "On the Extension of the Model of Matrix Acid Stimulation to Different Sandstones", AIChE Jour. (1976) 22, 799-805.

64. Lund, K., Fogler, H.S., McCune, C.C. and Ault, J.W.: "Acidisation. IV. Experimental Correlations and Techniques for the Acidisation of Sandstone Cores", Chem. Eng. Sci. (1976) 31, 373-380.

65. Plummer, L.N.: "Rates of Mineral-Aqueous Solution Reactions", Ph.D. Thesis, North-Western Univ. (1972).

66. Kaye, C.A.: "The Effect of Solvent Motion on Limestone Solution", Jour. Geol. (1957) 65, 35-46.

67. Berner, R.A. and Morse, J.W.: "Dissolution Kinetics of $CaCO_3$ in Sea Water", Am. Jour. Sci. (1974) 274, 108-134.

68. Erga, O. and Terjesen, S.G.: "Kinetics of the Heterogeneous Reaction of Calcium Bicarbonate Formation", Acta Chem. Scand.," (1956) 10, 872-874.

69. Terjesen, S.G., Erga, O., Thorsen, G. and Ve, A.: "Phase Boundary Processes as Rate Determining Steps in Reactions between Solids and Liquids", Chem. Eng. Sci. (1960) 14, 277-289.

70. Plummer, L.N. and Wigley, T.M.L.: "The Dissolution of Calcite in CO_2 Saturated Solutions at 25^{o}C and 1 Atmosphere Total Pressure", Geochim. et Cosmochim. Acta (1976) 40, 191-202.

71. Nierode, D.E. and Williams, B.B.: "Characteristics of Acid Reaction in Limestone Formations", Soc. Pet. Eng. J. (Dec. 1971) 406-418.

72. Barron, A.N., Hendrickson, A.R. and Wieland, B.R.: "The Effect of Flow on Acid Reactivity in a Carbonate Fracture", J. Pet. Tech. (April 1962) 409-415.

73. Williams, B.B., Gidley, J.L., Guin, J.A. and Schechter, R.S.: "Hydrochloric Acid - Calcium Carbonate Reaction", Ind. Eng. Chem. Fundam. (1970) 9, 589-596.

74. Boomer, D.R., McCune, C.C. and Fogler, H.S.: "Rotating Disc Apparatus for Reaction Rate Studies in Corrosive Liquid Environments", Review of Scientific Instruments (Feb. 1972) 43, 225-229.

75. Will, G.: Ph.D. Thesis, Heriot-Watt Univ. (to be completed Oct. 1984).

76. Wigley, T.M.L.: Private Communication, Univ. of East Anglia (Oct. 1979).

77. Vogel, A.I.: "A Text Book of Quantitative Inorganic Analysis", Longmans (1961).

78. Banks, J.: "The Volumetric Determination of Calcium and Magnesium by Ethylenediamine Tetra-Acetate Method", Analyst (1952) 77, 484-489.